A Geometric Approach Towards Momentum Conservation

Deepesh Toshniwal

Master of Science Thesis

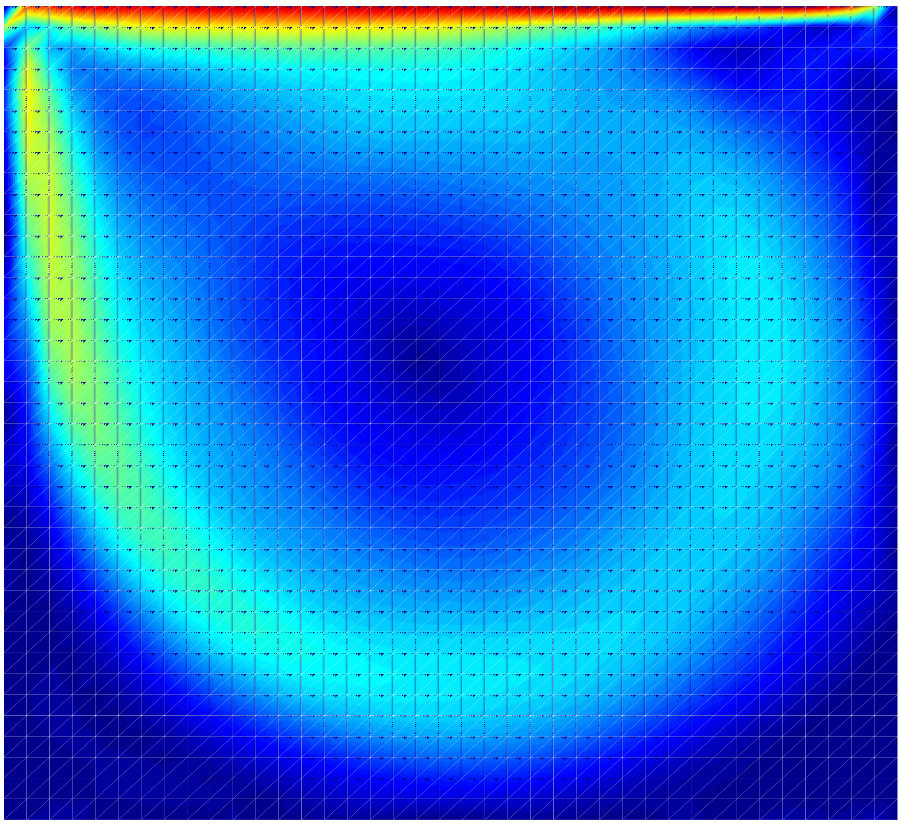

TU Delft Delft University of Technology

Marine Technology

A Geometric Approach Towards Momentum Conservation

Master of Science Thesis

For obtaining the degree of Master of Science in Marine Technology at Delft University of Technology

Deepesh Toshniwal

August 2, 2012

Faculty of Mechanical, Maritime and Materials Engineering · Delft University of Technology

Delft University of Technology
Department of Marine Technology

The undersigned hereby certify that they have read and recommend to the Faculty of Mechanical, Maritime and Materials Engineering for acceptance a thesis entitled

A Geometric Approach Towards Momentum Conservation

by

Deepesh Toshniwal

in partial fulfillment of the requirements for the degree of

Master of Science.

Dated: August 2, 2012

Supervisor(s):

Prof.Dr.Ir. R.H.M. Huijsmans

Dr.Ir. M.I. Gerritsma

Reader(s):

Dr.Ir. H.J. de Koning Gans

Dr.Ir.S.J. Hulshoff

Ir. Artur Palha

Abstract

The equations governing fluid-flow are a set of partial differential equations, as is the case for a host of other continuous field problems. Analytical solutions to these problems are not always available and computers are unable to handle continuous representations of variables. This makes a finite-dimensional projection mandatory for all variables and this may result in a loss of information. At the same time, invoking the inherent association between physical field variables and geometric quantities, as seen in [1, 2, 3], it is known that stable discretisation schemes can be constructed. In this spirit, mimetic discretization strategies are based on minimizing the loss of information in going from a continuous to a discrete setting by making a clear distinction between exact/topological and approximate/constitutive relations in a physical law, and then focussing on an exact representation of the former and a suitable approximation of the latter. For further reading, please see [4, 5, 6, 7].

The Navier-Stokes equations of fluid-flow, for incompressible flows, can be written as follows in vector calculus notation, where the symbols have their usual meaning.

$$\begin{aligned} \frac{\partial \boldsymbol{v}}{\partial t} + (\boldsymbol{v}.\nabla)\boldsymbol{v} = -\frac{1}{\rho}\nabla p + \nu\nabla^2\boldsymbol{v} \quad &\text{in} \quad \Omega\,, \\ \nabla.\boldsymbol{v} = 0 \quad &\text{in} \quad \Omega \end{aligned}$$

In this work, a geometric approach towards the solution of these equations is explored. The framework presented so far in [7] did not contain all the ingredients needed to resolve the geometric nature of momentum and other associated quantities. In this sense, this work is an extension of the framework employed in [7, 8] with conservation of momentum as its focus. The resulting scheme satisfies mass and momentum conservation laws exactly, and resembles a staggered-mesh finite-volume method. In addition, a generalized-conservation law is derived that could possibly lead to the conservation of a large set of secondary variables as well (kinetic energy, enstrophy *etc*). This still needs to be numerically verified in a future work. The discretization for momentum conservation presented in this work is tested numerically for Kovasznay flow, and lid-driven cavity flow.

Table of Contents

List of Figures

List of Tables

Acknowledgements

I've received fantastic support from Dr. Marc Gerritsma during the course of my thesis and for this I'm immensely grateful. His incredible patience in dealing with my questions and his availability for discussions at all times is deeply appreciated, and I am aware that his invaluable input has been the most important factor in shaping this work to its present form. I'd also like to express my heartfelt thanks towards Prof. Rene Huijsmans for allowing me the freedom to pursue this slightly esoteric line of work. Without his complete support this work would not have been possible.

I cannot thank Prof. Antonio Pascoal enough for all the help and support that he has given me over the last few years. It has been absolutely wonderful knowing him, and everyone else at ISR.

I spent the first three months practically working from Artur's desk. I'm thankful to him for his patience, and in awe of how easy his master-plan made it for me to learn and implement all the concepts. In the same vein, I'd also like to thank Jasper and the entire mimetic-group for their help and support. A special thanks to Pedro, Peter, Rene and Francois for the Doerak sessions; excellent and in-depth review of my work; and for all the quote unquote fantastic discussions. The time spent with Giovanni, Steve and Amit will not be forgotten.

Naru, Kaua, Hridya and Murthy have been the best friends one could hope for. They kept me grounded throughout, and made it easy for me to carry on through thick and thin. Amit and Gokul have been simply brilliant, and I'm grateful for all the time that we've spent together. Magaly has really been a sanctuary for me over the last year and has shared all my highs and lows, and I'm thankful to have met her. Lastly, I'd like to thank my parents and my little sister, Omna, for their unwavering support and unconditional love. This work is dedicated to them.

"I don't know anything, but I do know that everything is interesting if you go into it deeply enough." — *Richard Feynman*

Chapter 1

Introduction

The equations governing fluid-flow are represented as a set of partial differential equations, as is the case for a host of other continuous field problems. In order to perform an analysis of physical problems, solving these equations is necessary and there are several ways available of performing this analysis. With respect to fluid-flow, one could choose an Eulerian or a Lagrangian framework, and within these frameworks, the range of methods available for solving the governing equations is immense. Some of these methods are the finite-volume, finite-element, and finite-difference methods. In this work, *mimetic* discretization schemes have been employed, and these aim at preserving symmetries associated with the physical phenomenon. This begs the question that why is preserving these symmetries so important?

Emmy Noether's theorem associates symmetry properties of a system (defined by a Lagrangian or/and a Hamiltonian) to conserved quantities in time. This theorem is so fundamental to physical conservation laws that it fades in the background, unfortunately. The whole point of mimetic methods is to respect the symmetries that a physical system has. This is attempted by trying to conserve important quantities (linear-momentum, kinetic energy, for instance) related to these symmetries. For example, for the symmetry related to translation in space, it can be proven using the principle of least action that momentum should be conserved [10]. The conservation properties are achieved in this work by invoking an often ignored association between geometric objects and physical quantities. The focus of this thesis is on constructing a method that adheres to the conservation properties for momentum and mass which form the basic building blocks for fluid-flow analysis. More specifically, the focus is on a geometric discretization of the incompressible Navier-Stokes equations (see Chapter 5).

The first part of this introductory chapter is spent introducing this association between geometry and physics, Section 1.1. Subsequently, in Section 1.2, a brief introduction to the fundamentals of mimetic methods and the prevalent literature is provided. Thereafter, at the end of this chapter an outline of the entire thesis would be given in Section 1.3.

Figure 1-1: A typical brick with a nonzero volume and a nonzero mass displaying the association of mass (density) with volumes. The density integrates on the entire volume to give mass which is eventually measured.

1.1 Geometry and Physics

For an intuitive sense of the inherent association between Geometry and Physics, consider the mass of an object. For instance, the brick shown in Figure 1-1. We notice that the brick has a nonzero volume, and we expect that it will have a nonzero mass as well. We note that for this brick, we can calculate an average density based on its measured mass, m, and its measured volume, V.

$$\rho \approx \frac{m}{V} \tag{1-1}$$

This is, however, only a crude approximation of the density, ρ, of the brick and we see that we can get a better approximation of it by measuring the mass and volume of a smaller chunk of the brick and repeating the procedure. This will be a better estimate of the brick's density, but, nevertheless, an *estimate*. Of course, a *mathematically-exact* value of the density, can be obtained by the following limit where the mass, dm, inside an infinitesimally small volume, dV, is measured.

$$\rho = \lim_{dV \to 0} \frac{dm}{dV} \tag{1-2}$$

However, does the above mathematically-exact density make sense physically? As stated in [11],

> *The quantity of matter is the measure of the same, arising from its density and bulk conjunctly.*

The conjunction of density and an objects bulk, or volume, is obviously the most important part of the above statement. Therefore, if we let the volume, dV, of the piece of the brick to become zero, it is equivalent to removing the bulk of the object from the relation entirely. Since a zero-volume would contain no mass, the above mathematically-exact definition of the brick's density becomes just that: a mathematical concept. On the other hand, if the above is framed in the following way,

$$m = \int_V \rho \, dV \tag{1-3}$$

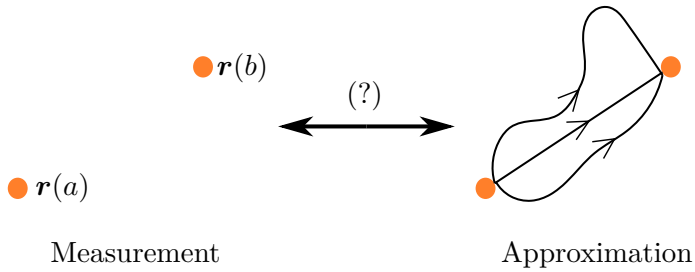

Figure 1-2: A particle undergoing displacement during a finite time-interval, t. There is no preferred path which the particle must take in a general situation, and the only thing that can be said with certainty is that velocities should naturally integrate on time-intervals to give the measured displacement as per Eq. (1-6).

where V is the chunk of the brick that we are interested in, we know that the above relation will be *exact* for all volumes, no matter how big. Moreover, the physical nature of the relation is maintained.

Similarly, consider a particle undergoing displacement $\boldsymbol{s}$ during a time-interval Δt moving from position $\boldsymbol{r}(a)$ to $\boldsymbol{r}(b)$ as shown in Figure 1-2. An estimate of the particle's velocity can be obtained by the following relation.

$$\boldsymbol{v} = \frac{\boldsymbol{s}}{\Delta t} = \frac{\boldsymbol{r}(b) - \boldsymbol{r}(a)}{\Delta t} \tag{1-4}$$

The above assumes a straight-line trajectory for the particle when there is no reason why it should be so. For a curved trajectory of the particle, it seems obvious that the above is going to be a very crude estimate of the velocity and we can improve on it by selecting smaller and smaller time-intervals. In the mathematical limit, for an infinitesimally small displacement $d\boldsymbol{s}$ in an infinitesimally small time-interval, dt, we have the velocity given by the following.

$$\boldsymbol{v} = \lim_{dt \to 0} \frac{d\boldsymbol{s}}{dt} \tag{1-5}$$

Again, it is noted that if the time-interval is allowed to go to 0 as per the above limit, the particle would not move at all, and hence the above would transform into a $\frac{0}{0}$ limit, another mathematical concept with little relation to the physics that it claims to represent. On the other hand, if we reframe the above equation in the following form,

$$\boldsymbol{s} = \int_T \boldsymbol{v}\, dt \tag{1-6}$$

we expect it to be true for time-intervals, T, of any size irrespective of the nature of the particle's trajectory. The above relation depends only on the initial and final displacements, $\boldsymbol{r}(a)$ and $\boldsymbol{r}(b)$, and not on whether the particle's trajectory between these points is a straight line of a curved line. Relations between quantities which display such properties are called topological/metric-free. Representation of such laws in numerical schemes, as will be seen later in this thesis, can be done exactly.

Not all laws are topological, of course. On the other end of the spectrum we have certain laws which are only approximate models of the behavior of real-world systems. For example,

with respect to fluids, the Newtonian assumption that stresses, τ, are linearly proportional to strains, ϵ, is an empirical law whose sole purpose is to *close* the fluid-flow model by making certain assumptions. The constant of proportionality is the viscosity, of course.

$$\tau = \mu\epsilon \tag{1-7}$$

These kinds of laws can be represented only approximately in numerical schemes and these we will call material/metric-dependent/constitutive relations.

If we ignore the question of metric-free/metric-dependent relations for now, it is evident that there exists certain natural associations between physical variables and geometric objects:

- mass-densities and volumes
- velocities and time-lines

This idea of associating physics with geometry is not new and has been around for multiple centuries, at least. The conjunction between mass-density and bulk as stated in [11] is only one such example. Maxwell, for example, remarked in [12]

> But it is evident that all analogies of this kind depend on principles of a more fundamental nature; and that, if we had a true mathematical classification of quantities, we should be able at once to detect the analogy between any system of quantities presented to us and other systems of quantities in known sciences, so that we should lose no time in availing ourselves of the mathematical labors of those who had already solved problems essentially the same.
>
> [...]
>
> At the same time, I think that the progress of science, both in the way of discovery, and in the way of diffusion, would be greatly aided if more attention were paid in a direct way to the classification of quantities.

More recently, Nobel-prize winning Physicist, Richard Feynman remarked in [13]:

> Why are the equations from different phenomena so similar? We might say: "It is the underlying unity of nature." But what does that mean? What could such a statement mean? It could mean simply that the equations are similar for different phenomena; but then, of course, we have given no explanation. The underlying unity might mean that everything is made out of the same stuff, and therefore obeys the same equations. That sounds like a good explanation, but let us think. The electrostatic potential, the diffusion of neutrons, heat flow - are we really dealing with the same stuff? Can we really imagine that the electrostatic potential is physically identical to the temperature, or to the density of particles? Certainly is not exactly the same as the thermal energy of particles. The displacement of a membrane is certainly not like a temperature. Why, then, is there an underlying unity?

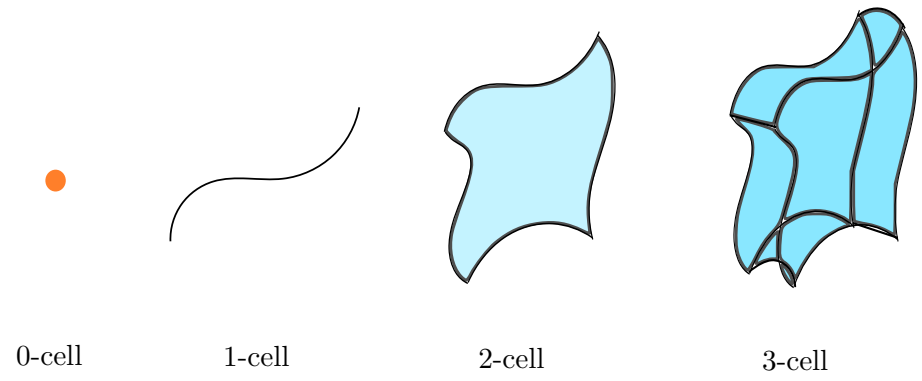

Figure 1-3: The different geometric objects that one can encounter in a 3D space.

> [...]
> Is it possible that this is the clue? That the thing which is common to all the phenomena is the space the framework into which the physics is put?

This association was rigorously investigated first by [1, 14], and then in [3, 15]. A first step in the analysis of any physical phenomenon should be to consider the natural association between the physical variables involved and geometric (and chronometric) objects: points, lines, surfaces and volumes (time instants and time intervals), as per [1, 14, 3, 15]. These geometric objects are referred to as n-dimensional cells, or n-cells, as shown in Figure 1-3.

The relation between geometric objects and physical variables also relies heavily on the orientation of these objects, and endowment of an orientation enhances their structure [3]. The objects listed above can have two types of orientation - inner and outer - and these are shown in Figure 1-4 for a 2D space, and Figure 1-5 for a 3D space. The concept of oriented geometric objects can be explained with the help of a 2-cell, for instance. Consider the inner-oriented 2-cell as shown in Figure 1-4 or Figure 1-5, and notice that the inner orientation of this cell specifies a rotation *inside* the surface. At the same time, consider the outer-oriented 2-cell as shown in Figure 1-5, and notice that this orientation specifies a *crossing*-direction *through* the 2-cell. For a detailed exposition on orientation, the reader should look up [1, 3, 4, 16]. It should be noted from Figure 1-4 and Figure 1-5 that outer orientation is determined by the geometric object in question and its embedding space's dimension. This can be best seen in Figure 1-6 where the orientation of a point, for instance, can be seen to change from a vortex sense of rotation around it for a 3-D embedding space to a direction through it for a 1-D embedding space.

To these oriented objects, physical quantities such as mass/momentum/energy fluxes (outer-oriented surfaces), velocities (inner-oriented lines) etc can be associated [1]. This 'natural' relation is mostly arrived at as a result of a heuristic analysis of the physical problem and the governing equations, as detailed in [3, 1]. An important part of this analysis is looking at the geometrical objects on which the local quantities are integrated naturally, and the fact that direct comparison can be made only between objects with the same orientation. The integrated local quantities on oriented geometric objects result in global quantities i.e.

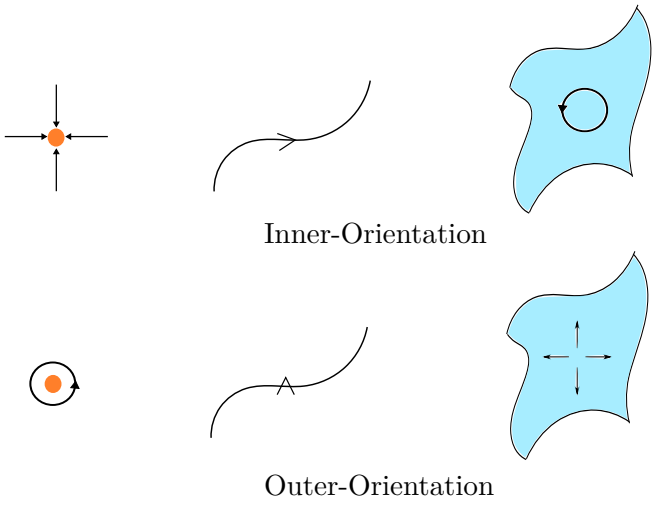

Figure 1-4: Different orientations that are possible for geometric objects in a 2D space.

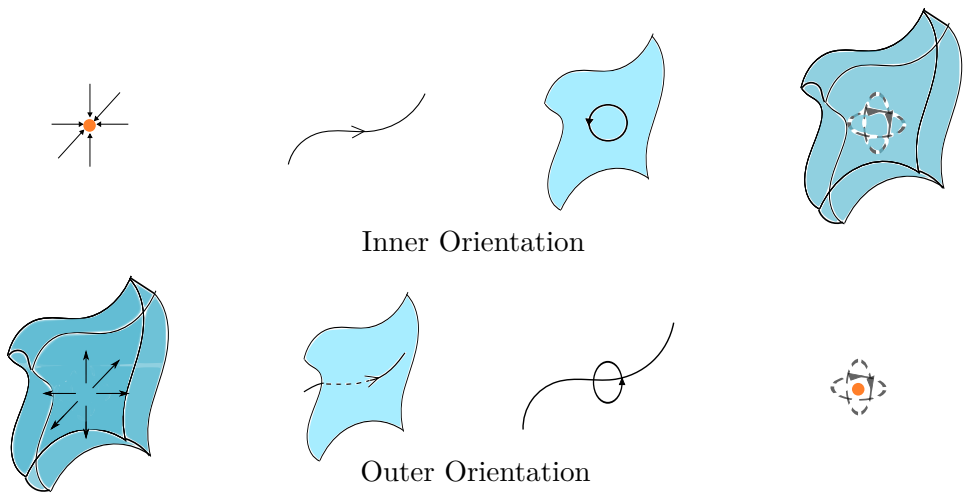

Figure 1-5: Different orientations that are possible for geometric objects in a 3D space.

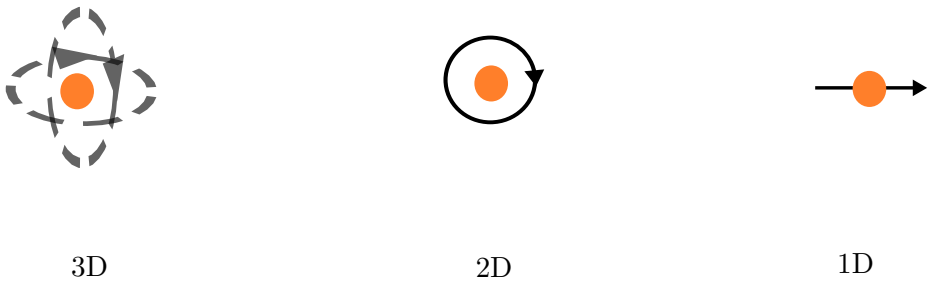

Figure 1-6: Different outer-orientations for a 0-cell depending on the dimension of the embedding space

quantities that can be measured on finite-dimensional objects. This also leads to this approach being treated as analogous to measurement processes, as highlighted in the above examples of mass and displacement.

It should be noted here that integral relations such as the ones presented above have a natural discrete representation since integrals yield discrete numbers. Moreover, by working with integral values as degrees of freedom, important theorems such as Stokes and Gauss' theorems can be easily represented even under geometric deformations (curved grids), as shown in Section 2.1.

Thus, after a suitable geometric object has been determined for every physical variable, links can be developed between them using topological relations and constitutive relations. Topological relations, as mentioned before, have an intrinsically discrete nature (metric free) that allows their exact representation in numerical schemes, and it is the constitutive laws where metric concepts (length, area, angle etc) are needed and approximations are made while discretization, chiefly because these relations are valid only in a continuous setting.

1.2 Mimetic Discretization Schemes

Analytical solutions to physical-field problems are not always available and this necessitates the use of a computer for approximating a solution. Computers, however, are unable to handle continuous representations of variables. Thus, a projection from an infinite number of degrees-of-freedom onto a finite number of degrees-of-freedom becomes mandatory (see Chapter 3). These projections *may* result in a loss of information depending on the nature of relation being discretized (topological/constitutive).

As explained in [3], conventionally, the discretization procedure is carried out starting from the governing set of partial differential equations. It consists of deriving schemes that modify the properties of the governing equations the least, and can be appropriately grouped into "numerical methods for partial differential equations". The focus of mimetic discretization strategies is based instead on "numerical methods for physical field problems": formulating the physical problem in a set of partially discrete equations, which can be subjected to suitable

analysis, with the aim of preserving, as much as possible, the physics of the problem in question.

A partially-discrete representation of the physical problem lays bare its 'structure', making clear the distinction between the topological and material relations constituting the problem, where the former can be exactly represented in a discrete setting. This distinction is at the heart of mimetic discretization schemes, also called compatible discretization schemes. As their name suggests, these schemes aim to 'mimic' the physics behind the physical problem as much as possible.

It should be noted at this point, however, that the numerical methods listed at the beginning of this chapter and mimetic-schemes are not mutually exclusive. The conservation-mimicking properties of conventional schemes as well as mimetic schemes can be found in [3], and also [17] should be seen for a nice review. The conservation-properties of these schemes are the reason why they are being explored further in this work.

Fluid-flow problems are also being looked at extensively by the Discrete Exterior Calculus group at California Institute of Technology with applications to computer graphics in mind. While [6, 18, 19] provides an excellent introduction to these methods, [20] presents geometric integration based on conserving circulation, [21] presents discrete Lie-advection, and [22] presents an approach that combines differential-geometry with a variational-calculus framework. Similar to the concepts presented in this thesis are the concepts proposed in [23, 24] where they propose a possible geometric treatment of stresses. The Finite-element Exterior Calculus presented in [25] is also built on similar concepts, and in [26] is applied to evolution problems. Diffusion related problems are treated in [27, 28]. Algebraic Topology guided numerical-schemes are also developed in [5], and their reduction-reconstruction operators have also been exploited in this work.

Closer to home, the work presented in [7] extends compatible discretization schemes to quadrilateral elements. The entire mathematical framework is explained in this paper. The works that [7] builds upon, and the ones that follow it, are [29, 30, 31], where the special edge-basis used in this work (see Chapter 3) are explained and an introduction to compatible discretization is given. Convection-diffusion problems and physically accurate advection are treated in [32, 8]. In addition to these works, [33, 34, 8, 35, 36, 37] are the students' theses published along the same lines. These have explored Hodge-decomposition, diffusion, advection, and mesh-refinement problems. The solution-representation basis used have been piecewise-polynomials as well as splines.

1.3 Thesis Outline

This thesis develops upon the concepts presented in [7] and other related work. In previous works it had been noticed that momentum conservation was not being satisfied, and the motivation behind this work is to construct a discretization scheme that adheres to this physical-symmetry that all fluid-flows must satisfy. The questions that we try to answer are:

- What is the appropriate treatment for the physical quantity *momentum*?

- Is the law of conservation of momentum like any other conservation law?
- How should bundle-valued differential-forms be implemented in the framework introduced in [7]?

Before jumping down the rabbit-hole, we introduce in some detail the mathematical framework behind this work. This is done in Chapter 2. Should the reader desire to pursue the mathematics behind this in more detail, recommended literature that should be perused would be [16, 2, 38].

Once the mathematical framework has been introduced, the discretization of our mathematical operators is explained in Chapter 3. In this chapter convergence properties related to this discretization are also investigated.

Next, using the operator discretizations developed in Chapter 3, a few physical-field problems are solved in Chapter 4. The problems that are briefly looked at are potential-flow, eletromagnetic resonant cavity, Darcy flow, and scalar and active-advection.

In Chapter 5, the geometric character of momentum (and its fluxes) is explored, and suitable discretization of the Navier-Stokes equations is done. Using this discretization, numerical-simulations are done in Chapter 6 for Kovasznay flow and Lid-driven cavity flow, Figure 1-7, and the results analysed. Some conclusions and recommendation are provided in Chapter 7.

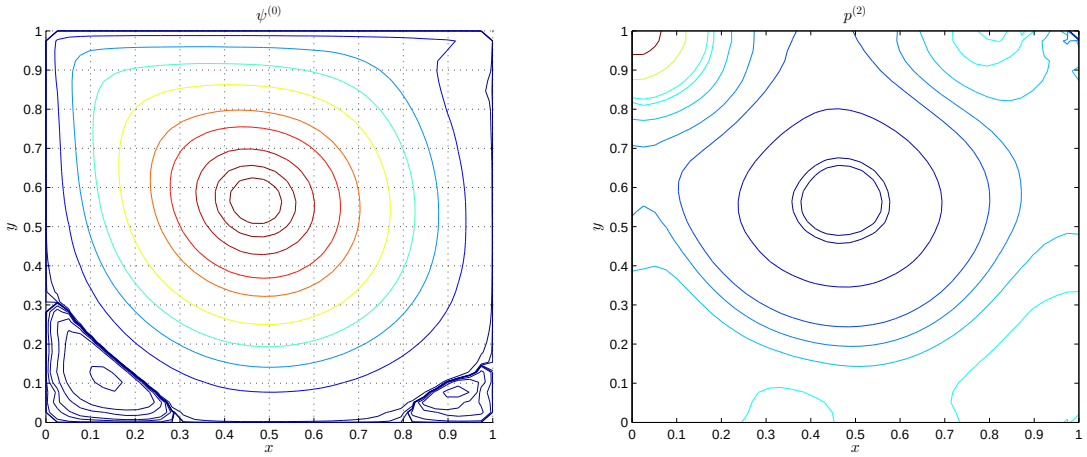

(a) Stream-function (b) Pressure

Figure 1-7: Stream-function and pressure contours plotted for the lid-driven cavity problem with a $Re = 1000$. The contours plotted are in accordance with the levels used in [9]. Mesh size is 1X1 and made up of elements of order 15.

Chapter 2

Background Theory

The mathematical framework behind mimetic discretization schemes is constructed based on an interplay between differential-geometry and algebraic-topology. These branches of mathematics are, however, unfamiliar territory with regards to a few disciplines of science/engineering. This chapter, thus, attempts to briefly introduce all the relevant concepts to the reader. For a more in-depth treatment, the text-books [16, 2, 39, 38, 40], and the papers [7, 6] are recommended.

In Section 2.1, the concepts of differential-geometry are presented with a basic overview of all the operators that are relevant to this work. Next, the concepts of algebraic-topology are presented in Section 2.2, where certain analogies with differential-geometry are pointed out to the reader. At the end, in Section 2.3, the mimetic-framework, as discussed in detail in [7], is introduced.

2.1 Differential Geometry

Translation of equations governing physical field problems in the language of differential geometry is very important because of the following reasons:

- the presence of discrete analogues of several of its concepts in algebraic topology, and
- the clear association of variables with geometric objects which reveals much of the underlying structure, and implementation-wise leads to readily obtainable global values instead of local values which are more of a mathematical abstraction

This section aims to introduce the basics of differential geometry with differential forms and some important operators acting on them. Important natural pairings between differential forms with geometric objects (points, curves, surfaces and volumes) will be seen to exist, which will pave the way to the natural pairings in a discrete setting with their discrete counterparts, cochains and chains.

2.1.1 Differential Forms

Differential forms, or exterior differential forms, are simply the objects "that one finds underneath an integral sign" [39]. In other words, a k-form is simply an object that can be naturally integrated on a k-dimensional manifold. This integration is achieved with the help of a duality pairing that exists between differential forms and tangent vectors. Before progressing further, a brief introduction to (co)tangent spaces and (co)tangent bundles is warranted. During the course of introduction of cotangent spaces, the definition of differential forms will be completed.

Tangent Spaces and Bundles

Consider a differentiable manifold $\mathcal{M}^k$. Define the tangent space, $\mathcal{M}^k_p$, to $\mathcal{M}^k$ at point p as the vector space consisting of all tangent vectors to the manifold at p. An example basis of this k-dimensional vector space is

$$\left.\frac{\partial}{\partial x^1}\right|_p, \left.\frac{\partial}{\partial x^2}\right|_p \cdots \left.\frac{\partial}{\partial x^k}\right|_p$$

if the coordinate system at p is $(x^1, x^2, \cdots x^k)$. This is the coordinate basis or the coordinate frame. Note that the symbols $\mathcal{P}, \mathcal{C}, \mathcal{S}$ and $\mathcal{V}$ are reserved for 0-, 1-, 2- and 3-dimensional manifolds (i.e. points, curves, surfaces and volumes). No dimension-specifying superscript will be used for these.

Locally, the tangent space to a n-dimensional manifold, $\mathcal{M}^n$, looks like $\mathbb{R}^n$. For each point p in $\mathcal{M}^n$ we can define a tangent space. The collection of all such tangent spaces is called the *tangent bundle* denoted by $\mathrm{T}\mathcal{M}^n$.

$$\mathrm{T}\mathcal{M}^n := \bigcup_{p \in \mathcal{M}^n} \mathcal{M}^n_p \cong \mathcal{M}^n \times \mathbb{R}^n \tag{2-1}$$

The last expression shows that the tangent bundle can (locally) be decomposed into an element of $\mathcal{M}^n$ and an element of $\mathbb{R}^n$. Such a decomposition is called a *local trivialization of the tangent bundle*. The dimension of the manifold is n and the dimension of the tangent bundle is (locally) $2n$. Using the local trivialization we can write and element of the tangent bundle as (p, X_p), i.e. the point p in M^n and the vector X_p at that point. Also note for fixed point p the sum $(p, X_p) + (p, Y_p) = (p, X_p + Y_p)$ is well-defined, since the summation takes place in $\mathbb{R}^n$, but an expression of the form $(p, X_p) + (q, Y_q)$ is not defined.

Consider the map $\pi : \mathrm{T}\mathcal{M}^n \to \mathcal{M}^n$. In terms of the local trivialization this map is given as $\pi : \mathcal{M}^n \times \mathbb{R}^n \to \mathcal{M}^n$ with $\pi(p, X_p) = p$. Then we have that $\pi^{-1}(p) \cong \mathbb{R}^n$ is called the *fiber over p*. The map $s\,; \mathcal{M}^n \to \mathrm{T}\mathcal{M}^n$ is called a *section* or a *cross section* of the tangent bundle. It assigns to each point $p \in \mathcal{M}^n$ an element $(p, X_p) \in \mathrm{T}\mathcal{M}^n$. A section of the tangent bundle $\mathrm{T}\mathcal{M}^n$ is what is commonly called a *vector field*. Of course we then have that $\pi \circ s \equiv \mathbb{I}$ is the identity over $\mathcal{M}^n$. The space of sections in $\mathrm{T}\mathcal{M}^n$ is denoted by $\Gamma(\mathrm{T}\mathcal{M}^n)$.

For the numerical methods that we will discuss, we assume that we can describe the base space M^n exactly. For very simple geometries this assumption poses no restrictions and for more complex geometries we need more advanced tools such as a NURBS representation of the manifold or a transfinite map. In a finite set of points p_i in the domain (manifold) we have the complete fiber $\pi^{-1}(p_i)$.

Cotangent Spaces, Bundles, and Differential Forms

Let E be the tangent space to a manifold $\mathcal{M}^k$ at point $x \in \mathcal{M}^k$, that is $\mathcal{M}^k_x$. This means that for a covariant tensor Q,

$$Q : E \times E \times E \times \cdots E \to \mathbb{R}$$

Here, Q is not dependent on the basis of E being used. Let $\boldsymbol{v}_i$ be vectors in E, and let the basis of E be the coordinate frame used in the introduction to tangent spaces. The dual space to this vector space is denoted by E^*, and this is called the cotangent space. The basis of this dual space is defined with the help of the following equation,

$$dx^i \left(\frac{\partial}{\partial x^j} \right) = \delta^i_j \tag{2-2}$$

where the basis of this dual space are denoted by,

$$dx^1, dx^2 \cdots dx^k$$

where δ^i_j is the Kronecker delta. Note that the use of a coordinate frame is not necessary, and in the event of a different coordinate system being used, the basis of the dual space can again be evaluated based on the above duality pairing between tangent and cotangent spaces. If the basis of the tangent space be represented by $\boldsymbol{e}_i$ in this other coordinate system, and the basis of the cotangent space be θ^i, there exists the following general pairing between these.

$$\theta^i(\boldsymbol{e}_j) = \delta^i_j \tag{2-3}$$

It can be proven that the above θ^i span a vector-space themselves, [16]. The linear-functionals (on tangent-vectors) belonging to this vector-space are then called covectors. From a physical points of view vectors can be 'seen'. For instance, a displacement $\mathbf{r}$ can be measured directly with a ruler, but covectors are invisible. One can only assess covectors by their operation on vectors. A typical example in nature is force, F. The only way we can quantify a force is to apply it to a displacement, $F(\mathbf{r})$, which equals the work done by the force over the displacement $\mathbf{r}$. This is the way force meter like a spring balance or scales work.

Now a similar construction as for the tangent space can be set up. Consider a differentiable manifold $\mathcal{M}^n$ again. With every point $p \in \mathcal{M}^n$ we associated a tangent space $\mathcal{M}^n_p$ which is spanned by n linear independent basis vectors. The dual of the vector space is $(\mathcal{M}^n_p)^*$ denoted by $\mathcal{M}^n_{p^*}$. So the fiber at p is vector space of covectors. The collection of all these fibers $(\mathcal{M}^n_p)^*$ is called the *cotangent bundle*.

$$\mathrm{T}^*\mathcal{M}^n = \bigcup_{p \in \mathcal{M}^n} \mathcal{M}^n_{p^*} \tag{2-4}$$

While a section of the tangent bundle is what is commonly called a vector field, a section of the the cotangent bundle is called a *differential* 1*-form* or a 1-form. The space of 1-forms on the manifold M^n is denoted by $\bigwedge^1 E^*$.

Differential forms then are higher-rank covectors which are multilinear real-valued functions on a collection of vectors. An exterior differential form of rank k, $\alpha \in \bigwedge^k E^*$, is then defined to be a covariant tensor of rank k that is anti-symmetric in each of its entries. Here, $\bigwedge^k E^*$ is the vector space of k-forms. The following equation elucidates the anti-symmetry of differential forms.

$$\alpha(\dots, \mathbf{v}_r \dots, \mathbf{v}_s \dots) = -\alpha(\dots, \mathbf{v}_s \dots, \mathbf{v}_r \dots) \tag{2-5}$$

The above property also implies that in n-dimensional space, if $k > n$, "there are no nontrivial k-forms on an n-manifold" [16], since a k-tuple of vectors on this n-dimensional vector space would have to be linearly dependent. This also means that this formulation of differential forms (in conjunction with the wedge product defined in the next subsection) can be useful in studying linear independence of forms.

In $\mathbb{R}^3$, we can consider 1-,2-,and 3-forms, and look at them as objects that naturally integrate on smooth curves, smooth surfaces and smooth volumes, while 0-forms are simply differentiable functions. It will be seen later, when the wedge-product is introduced, that the concept of orientation is intrinsic to differential forms and is built into their basis. For now, we can simply represent the bases of the space of p-ranked differential forms, $\bigwedge^p E^*$, as follows: $\{dx, dy, dz\}$ for $p = 1$, $\alpha^{(1)}$; $\{dydz, dzdx, dxdy\}$ for $p = 2$, $\beta^{(2)}$; and $\{dxdydz\}$ for $p = 3$, $\gamma^{(3)}$. The construction of these basis functions, and the intrinsic notion of orientation, will be explained with the help of the wedge product later..

Following the above notation, $\alpha^{(1)}$ can be written as:

$$\alpha^{(1)} = a(x, y, z)dx + b(x, y, z)dy + c(x, y, z)dz \tag{2-6}$$

In the above expression, a, b and c are functions. As is evident from the above expression, $\alpha^{(1)}$ integrates on a smooth, one-dimensional manifold, $\mathcal{C}$, and the respective natural-pairing can be shown as:

$$\left\langle \alpha^{(1)}, \mathcal{C} \right\rangle := \int_{\mathcal{C}} \alpha^{(1)} \tag{2-7}$$

As we will later see, $\alpha^{(1)}$ can be a physical variable, and the above pairing is the natural association between this physical variable and the 1D geometry. Similarly, $\beta^{(2)}$ can be expanded in terms of its basis and is seen to integrate on a smooth, two-dimensional manifold, $\mathcal{S}$, as per the following duality:

$$\left\langle \beta^{(2)}, \mathcal{S} \right\rangle := \int_{\mathcal{S}} \beta^{(2)} \tag{2-8}$$

As shown above, a general 1- or 2-form will have 3-components in a 3D space. These can be considered as the components of a vector on $\mathbb{R}^3$, and if treated as such, it is clear that their association with geometry with be lost, and so will be the structure provided by the duality-pairings in Eq. (2-7) and Eq. (2-8). Similarly, 0- and 3-forms, if only their components are considered, can be associated with scalar fields alike, but this treatment would result in the loss of their respective dualities with point objects, $\mathcal{P}$, and volume objects, $\mathcal{V}$.

Bundle-valued Differential Forms

In the process of describing momentum and other components of the momentum equation in Chapter 5, certain *exotic* variables will be encountered. These are the covector/vector-valued differential forms. These bundle-valued differential forms can be best explained as entities that map tangent/cotangent-bundles to the space of normal differential forms.

So, for instance, a covector-valued differential form would be a map from the tangent bundle, $T\mathcal{M}^n$ to the space of p-forms,

$$\alpha^{(1,p)} : T\mathcal{M}^n \to \bigwedge^p E^* \tag{2-9}$$

where $T\mathcal{M}^n$ contains all possible tangent vectors to $\mathcal{M}^n$ that can be defined at a particular point on the manifold, as was explained in the previous section.

Similarly, a vector-valued differential form would then map elements from the cotangent bundle, $T^*\mathcal{M}^n$ to the space of p-forms,

$$\alpha^{1,(p)} : T^*\mathcal{M}^n \to \bigwedge^p E^* \tag{2-10}$$

In the above equations, note that superscripts that are inside parentheses, $(\cdot)$, denote the covector-degree of the variables. Thus, $\alpha^{(1,p)}$ signifies a form that is covector-valued p-form. Those superscripts that are outside the parentheses denote vector-degree of the variables. Therefore, $\alpha^{1,(p)}$ signifies a vector-valued p-form.

The above properties are the only ones that will be used in this work, and [16, 38, 41, 42] should be perused for a more in-depth discussion.

The notation that is going to be adopted is explained as follows. The space of p-forms is going to be generally denoted by $\bigwedge^p$. However, if the physical space (manifold) with which these forms are associated is not clear from context, we will be denoting the space of p-forms by $\bigwedge^p(\Omega)$ if the manifold is Ω.

2.1.2 The Wedge Product

The space of differential k-forms, as denoted earlier by $\bigwedge^k E^*$, is constructed as follows from the space of 1-forms, E^*,

$$\bigwedge^k = E^* \wedge E^* \wedge \cdots \wedge E^* \subset \otimes^k E^* \tag{2-11}$$

The operation denoted by the symbol $\wedge$ is the wedge product, or the exterior product, and the symbol $\otimes$ denotes tensor-product. The wedge product between differential forms $\alpha^{(k)} \in \bigwedge^k$ and $\beta^{(l)} \in \bigwedge^l$ can be seen as the application of the wedge operator such that $\alpha^{(k)} \wedge \beta^{(l)}$ results in a $k+l$ exterior differential form, $\gamma^{(k+l)} \in \bigwedge^{k+l}$. Thus, the action of the operator can be represented as follows.

$$\wedge : \bigwedge^{k} \times \bigwedge^{l} E^* \rightarrow \bigwedge^{k+l} \tag{2-12}$$

The action of the wedge-product can be seen as the skew-symmetrization of the tensor product of differential forms [16]. This can be shown for the case of $\alpha^{(k)}$ and $\beta^{(l)}$ as follows, where their wedge product is seen to act on $(k+l)$-tuple of vectors $\mathbf{v}_I$, where $I = i_1, i_2, ...i_{k+l}$,

$$\alpha^{(k)} \wedge \beta^{(l)}(\mathbf{v}_I) := \sum_{\overrightarrow{K}} \sum_{\overrightarrow{J}} \delta_I^{JK} \alpha(\mathbf{v}_J)\beta(\mathbf{v}_K) \tag{2-13}$$

where $\overrightarrow{K}$ and $\overrightarrow{J}$ are 'directed' subsets of I i.e. subsets with indices arranged in ascending order, and δ_J^I is the generalized kronecker-delta defined as follows:

$$\delta_J^I := \begin{cases} 1, & \text{if } J \text{ is an even permutation of } I \\ -1, & \text{if } J \text{ is an odd permutation of } I \\ 0, & \text{if } J \text{ is not a permutation of } I \end{cases} \tag{2-14}$$

The most important properties of the wedge operator, which can be easily derived from the above, are the following:

1. Antisymmetry: $\alpha^{(k)} \wedge \beta^{(l)} = (-1)^{kl} \beta^{(l)} \wedge \alpha^{(k)}$
2. Associativity: $(\alpha^{(k)} \wedge \beta^{(l)}) \wedge \gamma^{(m)} = \alpha^{(k)} \wedge (\beta^{(l)} \wedge \gamma^{(m)})$
3. Linearity: $(\alpha^{(k)} + \beta^{(l)}) \wedge \gamma^{(m)} = \alpha^{(k)} \wedge \gamma^{(m)} + \beta^{(l)}) \wedge \gamma^{(m)}$

In particular, because of the antisymmetry of $\wedge$, for forms of odd-degree, we have

$$\alpha^{(2k+1)} \wedge \alpha^{(2k+1)} = 0 \tag{2-15}$$

Now that we have a way of constructing higher-dimensional forms using lower-dimensional exterior differential forms, we can construct the basis for 2-forms (shown in the previous subsection on Differential Forms), using the basis for 1-forms,

$$dydz = dy \wedge dz, \quad dzdx = dz \wedge dx, \quad dxdy = dx \wedge dy \tag{2-16}$$

It is clear from Eq. (2-15) earlier that basis such as $dxdx, dydy$, and $dzdz$ do not exist. Also, it can be seen that basis such as $dydx$, for instance, is simply $-dxdy$, and this is where the concept of orientation is built into these forms. For example, consider the 2-form, $\beta^{(2)}$, and integrate it on a 2-dimensional manifold, $\mathcal{S}$. The vector calculus analog of the result is going

to be $\int_{\mathcal{S}} \boldsymbol{b}.\boldsymbol{n} dS$, which is dependent on the direction of the surface normal, $\boldsymbol{n}$. The concept of the surface normal, on the other hand, doesn't need to be invoked for $\int_{\mathcal{S}} \beta^{(2)}$ because the wedge product automatically gives $\mathcal{S}$ the right orientation.

A k-form, $dx^{i_1} \wedge \cdots \wedge dx^{i_k}$, acting on a k-tuple of vectors, $(\mathbf{v}_1, \ldots, \mathbf{v}_k)$, can be geometrically seen to be $\pm$ the k-dimensional volume of the parallelopiped spanned by the projections of the vectors into the coordinate plane, with the + sign being used if the projected vectors define the same orientation as does the subset of the vector space basis, $(\partial_{i_1}, \ldots, \partial_{i_k})$ [16].

2.1.3 The Exterior Derivative

A unique operator, d, can be defined that converts p-forms to $(p+1)$-forms on the manifold $\mathcal{M}^k$,

$$\mathrm{d} : \bigwedge^{p} \rightarrow \bigwedge^{p+1} \tag{2-17}$$

with the following properties,

1. Additive: $\mathrm{d}(\alpha + \beta) = \mathrm{d}\alpha + \mathrm{d}\beta$
2. Anti-derivative: $\mathrm{d}(\alpha^{(p)} \wedge \beta^{(q)}) = \mathrm{d}\alpha^{(p)} \wedge \beta^{(q)} + (-1)^p \alpha^{(p)} \wedge \mathrm{d}\beta^{(q)}$

Note that $\mathrm{d}\alpha^{(0)}$ is defined to be the normal differential of the function $\alpha^{(0)}$,

$$\mathrm{d}\alpha^{(0)} = \frac{\partial \alpha}{\partial x} dx + \frac{\partial \alpha}{\partial y} dy + \frac{\partial \alpha}{\partial z} dz \tag{2-18}$$

where (dx, dy, dz) are the 1-form basis in a local, possibly curvilinear coordinate system. A form α is said to be exact if it is the exterior derivative of another form.

$$\alpha = \mathrm{d}\beta \tag{2-19}$$

The action of d on exact forms is as follows,

$$\mathrm{d}^2\beta := \mathrm{d}(\mathrm{d}\beta) = 0, \qquad \text{for all forms } \beta \tag{2-20}$$

In the same spirit, a closed form is defined as,

$$d\alpha = 0 \tag{2-21}$$

As is clear from the above, all exact forms are closed, but not all closed forms are exact.

The above completes the definition of the exterior derivative. From its application on 0-forms in $\mathbb{R}^3$, Eq. (2-18), it can be seen that the vector proxy of the resultant 1-form components resembles the gradient (∇) of a scalar function. Similarly, its application on a 1-form, $\alpha^{(1)}$, and a 2-form, $\beta^{(2)}$, in $\mathbb{R}^3$ gives the following, respectively,

$$\mathrm{d}\alpha^{(1)} = \left(\frac{\partial c}{\partial y} - \frac{\partial b}{\partial z}\right) dydz + \left(\frac{\partial a}{\partial z} - \frac{\partial c}{\partial x}\right) dzdx + \left(\frac{\partial b}{\partial x} - \frac{\partial a}{\partial y}\right) dxdy \tag{2-22}$$

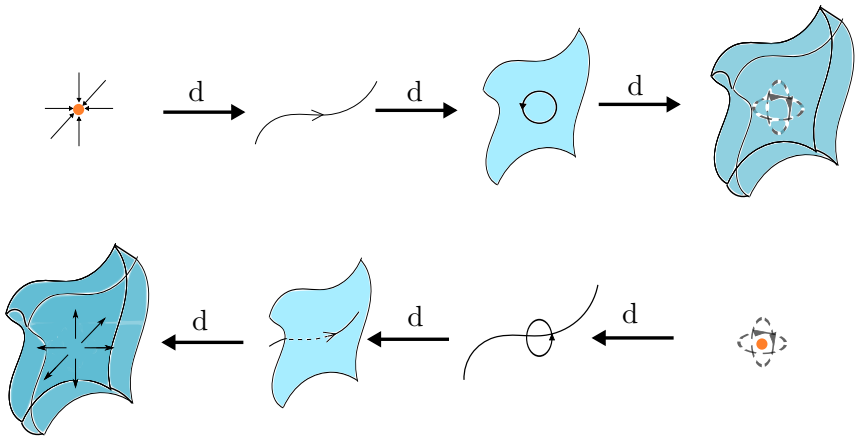

Figure 2-1: Double de Rham complex, which is a straightforward extension of Eq. (2-24). Here differential-forms of the same orientation are seen to be connected with the exterior derivative. As will be seen in Section 2.2, these relations are topological.

and,

$$\mathrm{d}\beta^{(2)} = \left(\frac{\partial a}{\partial x} + \frac{\partial b}{\partial y} + \frac{\partial c}{\partial z}\right) dxdydz \tag{2-23}$$

where (a, b, c) is the vector proxy of the components of $\alpha^{(1)}$ and $\beta^{(2)}$. It can be seen that Eq. (2-22) resembles the curl $(\nabla\times)$, and Eq. (2-23) the divergence $(\nabla.)$ of a vector in vector calculus. This means, since $\mathrm{d}^2\alpha = 0$ for all forms α from Eq. (2-20), double application of the exterior derivative resembles the following vector calculus identities,

- $\nabla \times (\nabla f) = 0$
- $\nabla \cdot (\nabla \times \boldsymbol{v}) = 0$

The exterior derivative, thus, generalizes the concept of gradient, curl and divergence, to arbitrary dimensions and curvilinear coordinates as well. It will be seen in the next subsection that the exterior derivative also helps generalize Stokes' theorem.

We can now write down the de Rham's complex shown in Eq. (2-24).

$$\mathbb{R} \longrightarrow \bigwedge^0 \xrightarrow[\textbf{grad}]{\mathrm{d}} \bigwedge^1 \xrightarrow[\textbf{curl}]{\mathrm{d}} \bigwedge^2 \xrightarrow[\textbf{div}]{\mathrm{d}} \bigwedge^3 \xrightarrow{\mathrm{d}} 0 \tag{2-24}$$

Note that the differential forms shown in Eq. (2-24) do not have an inner- or outer-orientation specified; the only requirement is that all of them should have the same orientation (i.e. inner *or* outer) for us to be able to put them in the sequence shown. Then, for different orientations, we can construct the double de Rham complex as shown in Figure 2-1. The geometric objects associated with the appropriate differential forms are shown in the figure. The horizontal links formed by d connect forms of the same orientation (p-forms with $(p+1)$-forms of the same orientation, to be specific).

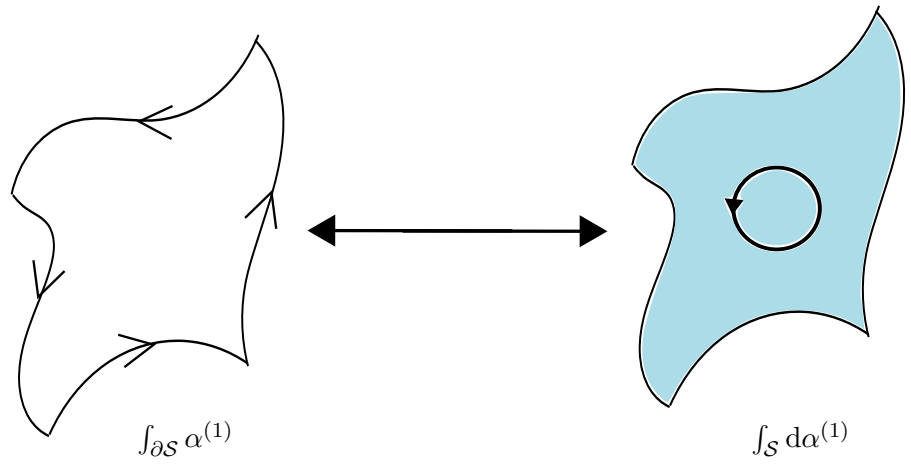

Figure 2-2: Stokes theorem demonstrated for a 2-dimensional manifold, $\mathcal{S}$. For a 2D manifold, this is equivalent to the conventional Stokes' line-integral theorem. This is easily extensible to n-dimensions, as shown in Eq. (2-25).

2.1.4 Generalized Stokes' theorem

As seen in the previous subsection, the exterior derivative is a generalization of the operators gradient, curl and divergence in vector calculus, depending on the space of differential forms, $\bigwedge^k$,on which the operator is acting, and thus results in Generalized Stokes' theorem, Eq. (2-25),

$$\int_{\mathcal{M}^{k+1}} \mathrm{d}\alpha^{(k)} = \int_{\partial\mathcal{M}^{k+1}} \alpha^{(k)} \tag{2-25}$$

which is basically,

- Fundamental theorem of Calculus for k = 0,
- Stokes' line-integral theorem for k = 1,
- Gauss' divergence theorem for k = 2.

In the above, ∂ is the boundary operator acting on the manifold $\mathcal{M}^{k+1}$. Eq. (2-25) states that the integration of the exterior derivative applied to a k-form on $\mathcal{M}^{k+1}$, which is a $(k+1)$-dimensional manifold, is the same as the integral of the k-form on the k-dimensional boundary of the manifold. Invoking the duality pairing seen in Eq. (2-7) and Eq. (2-8), we see that,

$$\left\langle \mathrm{d}\alpha^{(k)}, \mathcal{M}^{k+1} \right\rangle = \left\langle \alpha^{(k)}, \partial\mathcal{M}^{k+1} \right\rangle \tag{2-26}$$

The above states that the exterior derivative is the formal adjoint of the boundary operator. We will see later how this concept will be useful in defining the discrete exterior derivative using concepts of algebraic topology, which are to be introduced in Section 2.2.

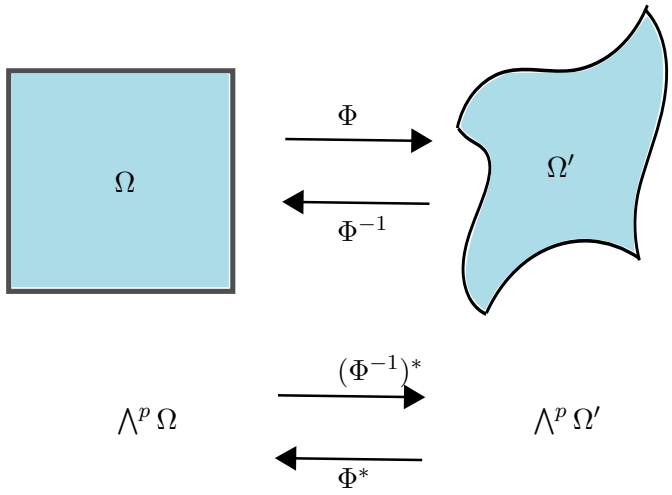

Figure 2-3: While Φ maps the domain Ω to Ω', Φ^{-1} maps differential-forms from Ω' to Ω. This is an extremely important property that makes the implementation of mimetic schemes very easy.

2.1.5 The Pullback Operator

The pullback operation is explained here keeping the implementation of our scheme in mind. In computational approaches such as the one we are talking about here, it is quite popular to have a reference element on which all analysis is done, and then use mappings to go from the simple rectangular reference element to the (usually) more complex, curvilinear physical space. In this work, Lagrange polynomials are used as the interpolation functions for the 0-form quantities and edge functions for the 1-form quantities [29, 43] in one-dimensional space. Quantities in a higher dimensional space (limited to two-dimensions here) were represented with the basis functions formed by taking appropriate tensor products of one-dimensional basis functions, since only quadrilateral elements were considered.

Since

- these functions are used for the finite-dimensional continuous representation of the field obtained as the result of a suitable projection operator [7], and
- they are all defined on simple, rectangular, reference elements

it is much easier to do all analysis on the reference element with the operators defined above. Fortunately, the language of differential geometry developed above is as easy to use in a curvilinear coordinate system as in a Cartesian one. Hence, a mapping is used between parametric and physical space. Along with this mapping comes the pullback operator and some of its very important properties that actually make the use of differential forms as easy on curved domains as on rectangular domains. This is shown in Figure 2-3

Consider a differentiable map Φ that acts on the parametric space, Ω, where the coordinates are $\boldsymbol{u}(\xi, \eta, \zeta)$, and yields the physical space, Ω', where the coordinates are $\boldsymbol{x}(x, y, z)$ - $\Phi : \Omega \rightarrow$

Ω'. Then, we have $\boldsymbol{x} = \Phi(\boldsymbol{u})$, where $\Phi(\boldsymbol{u}) = [\Phi_x(\boldsymbol{u}) \quad \Phi_y(\boldsymbol{u}) \quad \Phi_z(\boldsymbol{u})]$. The pullback operator is then defined as,

$$\Phi^* : \bigwedge^p \Omega' \to \bigwedge^p \Omega \tag{2-27}$$

and takes p-forms defined on Ω' to Ω. This is simply a change of variables applied to the differential forms defined on Ω', where all physical field variables are situated. An example is easy to demonstrate, so let $\alpha^{(1)}$ be a 1-form defined on Ω' and apply the pullback operator to this form to get a form $\beta^{(1)} = \Phi^*\alpha^{(1)})$ on Ω. If the vector proxy of the components of α is $(a(\boldsymbol{x}), b(\boldsymbol{x}), c(\boldsymbol{x}))$, we have,

$$\beta^{(1)} = \Phi^*([a(\boldsymbol{x}) \quad b(\boldsymbol{x}) \quad c(\boldsymbol{x})][dx \quad dy \quad dz]^T) \tag{2-28}$$

The pullback of 0-forms (functions), $(a(\boldsymbol{x}), b(\boldsymbol{x}), c(\boldsymbol{x}))$ is,

$$\Phi^* a(\boldsymbol{x}) = a(\Phi(\boldsymbol{u})) \tag{2-29}$$

and, thus,

$$\beta^{(1)} = [a(\Phi(\boldsymbol{u})) \quad b(\Phi(\boldsymbol{u})) \quad c(\Phi(\boldsymbol{u}))] \begin{bmatrix} \frac{\partial \Phi_x}{\partial \xi} & \frac{\partial \Phi_x}{\partial \eta} & \frac{\partial \Phi_x}{\partial \zeta} \\ \frac{\partial \Phi_y}{\partial \xi} & \frac{\partial \Phi_y}{\partial \eta} & \frac{\partial \Phi_y}{\partial \zeta} \\ \frac{\partial \Phi_z}{\partial \xi} & \frac{\partial \Phi_z}{\partial \eta} & \frac{\partial \Phi_z}{\partial \zeta} \end{bmatrix} [d\xi \quad d\eta \quad d\zeta]^T \tag{2-30}$$

As is evident from the above example and was stated earlier, the pullback is simply a change of variables applied to the differential form. Using the above property, we can rewrite the integration of a general k-form, $\alpha^{(k)}$, define on a k-dimensional manifold, $\mathcal{N}^k$, which is obtained by the mapping $\Phi : \mathcal{M}^k \to \mathcal{N}^k$, as follows,

$$\int_{\mathcal{N}^k} \alpha^{(k)} = \int_{\mathcal{M}^k} \Phi^*\alpha^{(k)} \leftrightarrow \left\langle \mathcal{N}^k, \alpha^{(k)} \right\rangle = \left\langle \mathcal{M}^k, \Phi^*\alpha^{(k)} \right\rangle \tag{2-31}$$

See also Figure 3-2. This means that instead of carrying out the integration of the form in a possibly complex physical space, it could be carried out in the rectangular parametric space with the help of Φ^*.

The pullback operator has some nice properties in that it commutes with the wedge product and the exterior derivative, which also displays their coordinate free character.

$$\Phi^*(\alpha^{(k)} \wedge \beta^{(l)}) = (\Phi^*\alpha^{(k)}) \wedge (\Phi^*\beta^{(l)}) \tag{2-32}$$

$$\Phi^* \mathrm{d}\alpha^{(k)} = \mathrm{d}\Phi^*\alpha^{(k)} \tag{2-33}$$

Using Eq. (2-33). we can also construct the following commutation diagram.

$$\begin{array}{ccc} \alpha^{(p)} & \xrightarrow{\mathrm{d}} & \beta^{(p+1)} \\ \Phi^* \downarrow & & \Phi^* \downarrow \\ \gamma^{(p)} & \xrightarrow{\mathrm{d}} & \omega^{(p+1)} \end{array} \tag{2-34}$$

Using the above properties, it is easy to see how the pullback of 2-form basis $dxdy$,for instance, can be done.

$$\begin{aligned}
\Phi^* dxdy &= \Phi^*(dx \wedge dy) \\
&= (\Phi^* dx) \wedge (\Phi^* dy) \\
&= \left(\frac{\partial \Phi_x}{\partial \xi} d\xi + \frac{\partial \Phi_x}{\partial \eta} d\eta + \frac{\partial \Phi_x}{\partial \zeta} d\zeta\right) \wedge \left(\frac{\partial \Phi_y}{\partial \xi} d\xi + \frac{\partial \Phi_y}{\partial \eta} d\eta + \frac{\partial \Phi_y}{\partial \zeta} d\zeta\right) \\
&= \left(\frac{\partial \Phi_x}{\partial \xi}\frac{\partial \Phi_y}{\partial \eta} - \frac{\partial \Phi_x}{\partial \eta}\frac{\partial \Phi_y}{\partial \xi}\right) d\xi d\eta + \left(\frac{\partial \Phi_x}{\partial \eta}\frac{\partial \Phi_y}{\partial \zeta} - \frac{\partial \Phi_x}{\partial \zeta}\frac{\partial \Phi_y}{\partial \eta}\right) d\eta d\zeta \quad \dots \\
&\quad \dots \quad + \left(\frac{\partial \Phi_x}{\partial \zeta}\frac{\partial \Phi_y}{\partial \xi} - \frac{\partial \Phi_y}{\partial \zeta}\frac{\partial \Phi_x}{\partial \xi}\right) d\zeta d\xi
\end{aligned}$$

The pullback of other basis functions can be done in the same way, and thus the pullback of the entire 2-form can be constructed. The generalization to differential-forms of other degrees is straightforward.

2.1.6 The Interior Product

The interior product of a k-form, $\alpha^{(k)}$ with a vector-field, $\boldsymbol{v}$, is defined as the operation that takes k-forms to $(k-1)$-forms

$$\mathfrak{i}_{\boldsymbol{v}} : \bigwedge^{k} \rightarrow \bigwedge^{k-1} \tag{2-35}$$

and the operator definition is as follows:

$$\mathfrak{i}_{\boldsymbol{v}} \alpha^{(k)}(\mathbf{b}_1, \mathbf{b}_2, \dots, \mathbf{b}_{k-1}) = \alpha^{(k)}(\mathbf{v}, \mathbf{b}_1, \mathbf{b}_2, \dots, \mathbf{b}_{k-1}) \tag{2-36}$$

Its action on zero-forms is defined to be zero.

$$\mathfrak{i}_{\boldsymbol{v}} \alpha^{(0)} = 0 \tag{2-37}$$

The interior product is simply a way of contracting the differential form with a vector-field. Its most important properties can be outlined as,

1. Linearity: $\mathfrak{i}_{\boldsymbol{v}+\boldsymbol{u}} \alpha^{(p)} = \mathfrak{i}_{\boldsymbol{v}} \alpha^{(p)} + \mathfrak{i}_{\boldsymbol{u}} \alpha^{(p)}$
2. Anti-derivation: $\mathfrak{i}_{\boldsymbol{v}} \left(\alpha^{(p)} \wedge \beta^{(q)}\right) = \mathfrak{i}_{\boldsymbol{v}} \alpha^{(p)} \wedge \beta^{(q)} + (-1)^p \alpha^{(p)} \wedge \mathfrak{i}_{\boldsymbol{v}} \beta^{(q)}$

Physically, the interior product can be defined with the help of a vector-field and the flow generated by it. This is explored here in informal terms. Consider a p-form, $\alpha^{(p)}$, defined on an n-dimensional manifold, $\mathcal{M}^n$. Consider a $(p-1)$-dimensional submanifold of $\mathcal{M}^n$, $\mathcal{N}^{p-1}$. Let this manifold *flow-out* under the influence of the vector-field, $\boldsymbol{v}$, for time t. The flowed out p-dimensional manifold, $\mathcal{K}^p$, is shown in Figure 2-4, where ϕ_t is simply the flow of $\boldsymbol{v}$ [21]. Then, the instantaneous change in time of $\alpha^{(p)}$ evaluated on $\mathcal{K}^p$ is defined as the interior-product of $\alpha^{(p)}$ with $\boldsymbol{v}$.

$$\int_{\mathcal{N}^{p-1}} \mathfrak{i}_{\boldsymbol{v}} \alpha^{(p)} = \left.\frac{d}{dt}\right|_{t=0} \int_{\mathcal{K}^p} \alpha^{(p)} \tag{2-38}$$

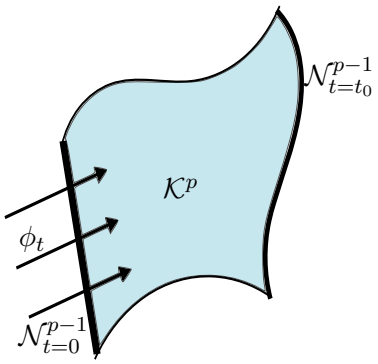

Figure 2-4: Dynamic-definition of the interior-product as outlined in [21, 4, 36, 8]. The $p-1$ dimensional manifold, $\mathcal{N}^{p-1}$, flows out under the influence of a transverse vector-field and forms an *extruded* p-dimensional surface, $\mathcal{K}^p$. The interior-product, or intrusion, is the adjoint of this extrusion.

2.1.7 The Lie Derivative

The Lie-derivative of a p-form, $\alpha^{(p)}$ with a vector-field, $\boldsymbol{v}$, is defined as the operation that takes the p-form to a p-form

$$\mathcal{L}_{\boldsymbol{v}} : \bigwedge^{p} \rightarrow \bigwedge^{p} \tag{2-39}$$

with the operator being defined by Cartan's magic formula as:

$$\mathcal{L}_{\boldsymbol{v}}\alpha^{(p)} = \mathrm{d} \circ \mathfrak{i}_{\boldsymbol{v}} \left(\alpha^{(p)}\right) + \mathfrak{i}_{\boldsymbol{v}} \circ \mathrm{d} \left(\alpha^{(p)}\right) \tag{2-40}$$

Some important properties of this operator can be outlined as,

1. Commutation with the exterior derivative: $\mathcal{L}_{\boldsymbol{v}}\mathrm{d}\alpha^{(p)} = \mathrm{d}\mathcal{L}_{\boldsymbol{v}}\alpha^{(p)}$
2. Derivation: $\mathcal{L}_{\boldsymbol{v}} \left(\alpha^{(p)} \wedge \beta^{(q)}\right) = \mathcal{L}_{\boldsymbol{v}}\alpha^{(p)} \wedge \beta^{(q)} + \alpha^{(p)} \wedge \mathcal{L}_{\boldsymbol{v}}\beta^{(q)}$

Lie-derivatives are an integral element of mechanics. The first property above has an important consequence in that if we have a closed form, $\alpha^{(p)}$, then using Eq. (2-21) we can state that the Lie-derivative of a closed-form yields a closed-form again. This has been utilized, for instance, in the vorticity advection equations written down with the help of Lie-derivatives [21]. More specifically, evolution problems are represented with the help of Lie-derivatives (see Chapter 4 and Chapter 5). Their action on standard volume-forms, σ, can be seen as the effect of the flow generated by $\boldsymbol{v}$ on volumes (see Chapter 5). A volume-form, σ, is simply the standard highest-degree differential-form. For $\mathbb{R}^3$, for instance, this is just $dxdydz$. For a deeper exposition on the Lie-derivative, please see [36, 21].

2.1.8 The Covariant Derivative

Consider a 1-form, $\alpha^{(1)}$, with a_i as its components. Let us take the partial derivative of these components with respect to coordinate direction x^j,

$$A^x_{ij} = \frac{\partial a_j}{\partial x^i} \tag{2-41}$$

If a coordinate transformation from the coordinate system (x) to a coordinate system (x') is made, the above derivative transforms as follows,

$$\begin{aligned} A^{x'}_{ij} &= \frac{\partial a'_j}{\partial x^{i'}} \\ &= \sum_{l,k} \frac{\partial x^l}{\partial x^{i'}} \frac{\partial}{\partial x^l} \left(\frac{\partial x^k}{\partial x^{j'}} a_k \right) \\ &= \sum_{l,k} \frac{\partial x^l}{\partial x^{i'}} \frac{\partial x^k}{\partial x^{j'}} \left(\frac{\partial}{\partial x^l} a_k \right) + \sum_{l,k} a_k \frac{\partial x^l}{\partial x^{i'}} \frac{\partial}{\partial x^l} \frac{\partial x^k}{\partial x^{j'}} \end{aligned} \tag{2-42}$$

The first term on the right-hand side is recognizable as the correct way that a covariant tensor of rank 2 should transform. However, the second term is clearly not a tensor transformation, and what this implies is that the normal partial derivative is not tensorial in nature. The second term on the right hand side can be written down as follows.

$$\sum_{l,k} a_k \frac{\partial x^l}{\partial x^{i'}} \frac{\partial}{\partial x^l} \frac{\partial x^k}{\partial x^{j'}} = \sum_k a_k \frac{\partial^2 x^k}{\partial x^{i'} \partial x^{j'}} \tag{2-43}$$

This is term that is non-tensorial that we must get rid of. We can do this by adopting the following ways to define a new kind of derivative operation:

- Anti-symmetrize the partial derivative of 1-forms to get rid of the non-tensorial term:

$$\left(A^x_{ij} \right)_1 = \frac{\partial a_j}{\partial x^i} - \frac{\partial a_i}{\partial x^j} \tag{2-44}$$

  Since the term in Eq. (2-43) is symmetric in its indices i' and j', anti-symmetrization gets rid of this term.

- Add the negative of the non-tensorial term in Eq. (2-43) to the partial derivative:

$$\left(A^{x'}_{ij} \right)_2 = \sum_{l,k} \frac{\partial x^l}{\partial x^{i'}} \frac{\partial x^k}{\partial x^{j'}} \left(\frac{\partial}{\partial x^l} a_k \right) + \cancel{\sum_k a_k \frac{\partial^2 x^k}{\partial x^{i'} \partial x^{j'}}} - \cancel{\sum_k a_k \frac{\partial^2 x^k}{\partial x^{i'} \partial x^{j'}}} \tag{2-45}$$

The first method of defining the derivative operation, $\left(A^{x'}_{ij} \right)_1$, is exactly how the exterior derivative, d, is defined for 1-forms. For higher-degree forms, a normalization is done with the anti-symmetrization. The second method of defining the derivative is called the covariant derivative, ∇, and the partial derivative defined this way does transform tensorially.

We represent the tensorial version of $\frac{\partial}{\partial\, x^i}$ by ∇_i, and its action is defined as follows on vector- and covector-fields,

$$\begin{aligned} \text{Vector-components, } a^j\text{: } \nabla_i a^j &= \frac{\partial a^j}{\partial x^i} + \Gamma^j_{ik} a^k \\ \text{Covector-components, } a_j\text{: } \nabla_i a_j &= \frac{\partial a^j}{\partial x^i} - \Gamma^k_{ij} a_k \end{aligned} \tag{2-46}$$

where Γ^i_{jk} are the Christoffel symbolds (of the second kind) and transform like the non-tensorial part of normal partial derivatives. This means that they are not tensorial themselves, but help in making another non-tensorial entity, $\frac{\partial}{\partial x^i}$, tensorial.

The covariant derivative is relevant only in a non-flat space since the Christoffel symbols are zero in flat space. In a flat coordinate system, we can compare vector-fields by simply comparing their components since the basis vectors stay essentially the same at every point. The Christoffel symbols can be seen as encoding information about the variation of basis-vectors form one point in space to another.

The Exterior Covariant-differential

The derivative operation defined by Eq. (2-46) has a tensorial nature and it can act on vector- and covector-fields. However, it does not have an anti-symmetric tensorial nature. What we mean by this is that the operation yields tensors, but not the objects of our interest - differential-forms. Moreover, which derivative opeartion do we use for budle-valued differential-forms which, as we will see in Chapter 5, will play a central role in our formulation? Here we introduce the third derivative operator, the exterior covariant-differential [16] and this gets the job done.

The exterior covariant-differential maps a covector-valued p-form to a covector-valued $(p+1)$-form.

$$\mathrm{d}_\nabla : \bigwedge^{1,p} \rightarrow \bigwedge^{1,p+1} \tag{2-47}$$

This is the derivative operation that we need for manipulation of bundle-valued differential forms in a general co-ordinate system. If we have a covector-valued p-form, $\alpha^{(1,p)} = \sum_i \theta^i \otimes \alpha^p_i$, the action of the exterior covariant-differential on it is given by,

$$\mathrm{d}_\nabla \alpha^{(1,p)} = \sum_i \theta^i \otimes \left(\mathrm{d}\alpha^p_i - \sum_r \omega^i_r \wedge \alpha^{(p)}_r \right) \tag{2-48}$$

where ω^i_r are 1-forms related to the Christoffel Symbols. These are zero in a flat-space too.

In this work only flat-space has been considered and the 1-forms ω^i_r have been ignored. The action of the exterior covariant-differential is then treated as just the exterior-derivative applied to the p-form in a covector-valued p-form. This will play a pivotal role in a future work where the extension of this work is done to curvilinear grids.

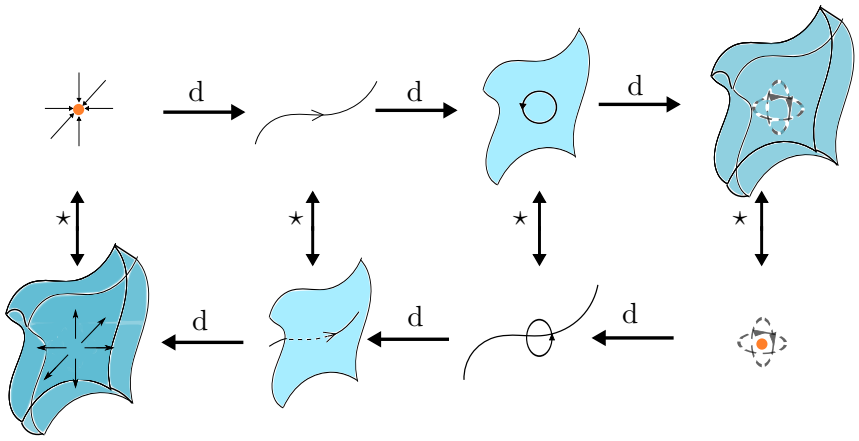

Figure 2-5: The complete double de Rham complex including the connection between objects with different orientations. These connections are achieved with the help of the Hodge-$\star$.

2.1.9 The Hodge-$\star$ operator

The Hodge-$\star$ operator, $\star$, is a generalization of $\alpha^{(1)} \rightarrow \mathbf{i}_{\boldsymbol{A}}\sigma$ by mapping k-forms to $(n-k)$-forms (which are referred to as the Hodge-dual of the respective k-forms),

$$\star : \bigwedge^{k} \rightarrow \bigwedge^{n-k} \tag{2-49}$$

and it does so in the continuous setting. Its action in $\mathbb{R}^3$ can be easily seen as,

$$\star\, dx = dydz, \qquad \star dy = dzdx, \quad \text{and} \quad \star\, dz = dxdy \tag{2-50}$$

$$\star 1 = dxdydz, \quad \text{and} \quad \star\, dxdydz = 1 \tag{2-51}$$

σ is the volume-form

Application of the Hodge-$\star$ twice gives the original k-form back but with a + or - sign in front of it as per the following equation.

$$\star\star\alpha^{(k)} = (-1)^{k(n-k)}\alpha^{(k)} \tag{2-52}$$

It was seen in Figure 2-1 that the exterior derivative forms links between differential forms of the same orientation in the two rows of the double de Rham complex. The Hodge-$\star$ operator is an operator that helps connect the two rows of the de Rham complex. This resembles material laws in a physical problem [3]. It is achieved by associating differential forms from one row of the complex to dual geometric objects, and thus mapping them onto differential forms of different orientation in the other row of the complex. Thus, the complete double de

Rham complex can be constructed as shown in the equation below.

$$\begin{array}{ccccccccc} \mathbb{R} & \longrightarrow & \bigwedge^0 & \xrightarrow{\mathrm{d}} & \bigwedge^1 & \xrightarrow{\mathrm{d}} & \bigwedge^2 & \xrightarrow{\mathrm{d}} & \bigwedge^3 \xrightarrow{\mathrm{d}} 0 \\ & & \uparrow & & \uparrow & & \uparrow & & \uparrow \\ & & \star & & \star & & \star & & \star \\ & & \downarrow & & \downarrow & & \downarrow & & \downarrow \\ 0 & \xleftarrow{\mathrm{d}} & \bigwedge^{\bar{3}} & \xleftarrow{\mathrm{d}} & \bigwedge^{\bar{2}} & \xleftarrow{\mathrm{d}} & \bigwedge^{\bar{1}} & \xleftarrow{\mathrm{d}} & \bigwedge^{\bar{0}} \longleftarrow \mathbb{R} \end{array} \tag{2-53}$$

The tilde in the bottom row represents dual-orientation of the top-row of the complex in Eq. (2-53). The action of the Hodge-$\star$ is also clear from its action in $\mathbb{R}^3$ as demonstrated in Eq. (2-51), where it was seen that the Hodge-$\star$ operator associated, for instance, surface values ($dxdy$) with line values (dz).

A positive-definite inner product between p-forms is introduced here, $\langle ., . \rangle : \bigwedge^p \times \bigwedge^p \to \mathbb{R}$, defined by,

$$\left\langle \alpha_1^{(1)} \wedge \alpha_2^{(1)} \cdots \wedge \alpha_p^{(1)}, \beta_1^{(1)} \wedge \beta_2^{(1)} \cdots \wedge \beta_p^{(1)} \right\rangle := \begin{vmatrix} \left\langle \alpha_1^{(1)}, \beta_1^{(1)} \right\rangle & \cdots & \left\langle \alpha_1^{(1)}, \beta_p^{(1)} \right\rangle \\ \vdots & \vdots & \vdots \\ \left\langle \alpha_p^{(1)}, \beta_1^{(1)} \right\rangle & \cdots & \left\langle \alpha_p^{(1)}, \beta_p^{(1)} \right\rangle \end{vmatrix} \tag{2-54}$$

where $\alpha_i^{(1)}$ and $\beta_j^{(1)}$ are 1-forms, with their point-wise inner product being defined as,

$$\left\langle \alpha_i^{(1)}, \beta_j^{(1)} \right\rangle := \sum_{k,l} (\alpha_i)_k (\beta_j)_l g^{kl} \tag{2-55}$$

where g^{kl} are the coefficients of the inverse of the metric tensor, G. In $\mathbb{R}^3$, for example, G is equal to an identity matrix.

$$G = \begin{bmatrix} 1 & 0 & 0 \\ 0 & 1 & 0 \\ 0 & 0 & 1 \end{bmatrix} \tag{2-56}$$

In the case of a coordinate change, as is evident from the index placement of coefficients of G, the coefficients g_{ij} transform as covariant tensors of rank two. Another useful quantity defined for each metric tensor is g,

$$g := |G| \tag{2-57}$$

The inner product thus defined has a metric built into it, and using it the Hodge-$\star$ can be alternatively defined as,

$$\alpha^{(1)} \wedge \star\beta^{(1)} = \left\langle \alpha^{(1)}, \beta^{(1)} \right\rangle \sigma \tag{2-58}$$

As mentioned above, the Hodge-$\star$ is defined only in the continuous setting, and this is the reason why interpolation functions, introduced in Chapter 3, are needed in the first place. If it weren't for this 'lack of inherent discreteness' in the Hodge, all relations could have

been expressed in purely topological formulations, as will be shown later. This is where the approximations come into the picture, and this is where the use of spectral elements facilitates arbitrary-order approximations and exponential convergence (Chapter 3, Chapter 4 and Chapter 6).

The Codifferential

The codifferential, $d^\star$, is a derivative of a differential form that, unlike the exterior derivative, takes differential forms of rank $(k+1)$ to differential forms of rank k.

$$d^\star : \bigwedge^{k+1} \rightarrow \bigwedge^{k} \tag{2-59}$$

The codifferential is constructed with the combination of the Hodge-$\star$ and the exterior derivative in the following way,

$$d^\star = (-1)^{n(k+1)+1} \star \mathrm{d} \star \tag{2-60}$$

and contains a metric. Using the properties of the exterior derivative and the Hodge,

$$d^\star d^\star = \pm(\star \mathrm{d} \star)(\star \mathrm{d} \star) = \pm \star (\mathrm{dd}) \star = 0$$

The codifferential is in fact adjoint of the exterior derivative on boundary-less manifolds.

$$\left(d^\star \alpha^{(k+1)}, \beta^{(k)}\right)_{\mathcal{M}^n} = \left(\alpha^{(k+1)}, \mathrm{d}\beta^{(k)}\right)_{\mathcal{M}^n} \tag{2-61}$$

If the manifold has a boundary, $\partial\mathcal{M}^n$, the above relation doesn't hold anymore and there is an addional boundary integral that must be considered.

$$\left(d^\star \alpha^{(k+1)}, \beta^{(k)}\right)_{\mathcal{M}^n} = \left(\alpha^{(k+1)}, \mathrm{d}\beta^{(k)}\right)_{\mathcal{M}^n} - \int_{\partial\mathcal{M}^n} \beta^{(k)} \wedge \star\alpha^{(k+1)} \tag{2-62}$$

The above equation states that on manifolds $\mathcal{M}^n$ that are closed, or for differential forms that are zero on the boundaries of $\mathcal{M}^n$, the codifferential operator is the adjoint of the exterior derivative [16]. However, on manifolds with boundaries, one does have a non-zero term on the right hand side which is simply the integral of $\beta^{(k)} \wedge \star\alpha^{(k+1)} \in \bigwedge^{n-1}$ on the boundary of $\mathcal{M}^n$. This is important and should be kept in mind while implementing the codifferential for domains with non-periodic boundaries, or domains with non-zero forms on the boundaries. This is further treated in Chapter 3.

The Laplace Operator

The Laplacian of a function, f, in $\mathbb{R}^3$ can be written down as

$$\nabla^2 f = \nabla.(\nabla f)$$

and that of a vector, $\boldsymbol{f}$, can be written down as

$$\nabla^2 \boldsymbol{f} = \nabla(\nabla.\boldsymbol{f}) - \nabla \times (\nabla \times \boldsymbol{f})$$

In the same spirit, a Laplacian operator for differential forms can be defined that is the negative of the vector-calculus Laplacian and maps k-forms to k-forms.

$$\Delta : \bigwedge^{k} \rightarrow \bigwedge^{k} \tag{2-63}$$

The operator can then be written down in terms of the exterior derivative and the codifferential as,

$$\Delta = \mathrm{d}d^{\star} + d^{\star}\mathrm{d} \tag{2-64}$$

and is a generalization of ∇.

2.2 Algebraic Topology

Topology can most simply be defined as the study of connectivity. It deals with properties that are invariant under continuous deformations of space. Algebraic topology is the discrete counterpart of differential geometry, ans is the perfect tool for translating all purely topological relations - so, the de Rham complex as shown in Figure 2-1 - to a discrete setting. The advantage of this approach is that since topological relations need only the connectivity information of the mesh, it is very easy to set up discrete counterparts of topological relations on all kinds of meshes and, if the connectivity doesn't change, the same relations would hold for moving meshes as well.

2.2.1 Cell Complexes, Chains and Cochains

Cell Complex

In the beginning of Chapter 1, the notion of association of physical variables with points, lines, surfaces and volumes was introduced. This means that the finite dimensional domain where all analysis is done should have all the above mentioned *p-cells*, where p refers to the dimension of the geometric object. This is fortunate because almost all computational meshes built for such analysis do indeed possess all these geometric objects even though they are often not referred to.

Following the above mentioned convention, points, lines, surfaces and volumes can be referred to as 0-, 1-, 2-, and 3- cells as was shown in Figure 1-3. The cells are assumed to be properly joined and that all p-cells 'contain' all the lower dimensional cells that they are directly connected to. This means that a 3-cell contains all of its faces, edges and vertices such that the intersection of two 3-cells is null only if they don't have even a single vertex in common. The boundary of a p-cell is then made up of $(p-1)$-cells and these are referred to as the faces of the p-cell. Similarly, if a p-cell is contained in a $(p+1)$-cell, the latter is referred to as the coface of the former [14, 35].

There was another requirement for the association between physical variables and geometric objects to be meaningful, and this was the requirement of the geometric objects having a

coherent orientation. To facilitate this, we should be able to identify two cell complexes in the computational domain - an inner (outer) oriented primal complex and an outer (inner) oriented dual complex. Once the complexes have been identified as such, global quantities can be placed in the corresponding p-cells with the proper orientation. This is done as shown in Figure 2-5 and it can be seen that the excursion from the primal to the dual complex by the application of the Hodge operator merely changes the geometric objects that physical variables are associated. The scalar field associated to these objects is left unchanged upto a factor of ± 1. Thus, the Hodge-$\star$ operator is often called an identity operation. Compatible orientation of all cells is assumed [3].

Chains and Cochains

A p-chain is defined as a weighted collection of p-cells. If p-cells are denoted with $c_{(p)}$, and chains with C_p,

$$C_p = \sum_{i}^{n_p} w_i c_{((p),i)} \tag{2-65}$$

where n_p is the total number of p-cells in the domain, and w_i are the weights associated with them. Although the weights can be chosen to be anything, it would be easier to work with crisp cells and thus they are restricted to +1/-1 or 0, where the three cases refer to a p-cell having a positive/negative orientation or the p-cell not being a part of the chain, respectively. Thus, a p-chain is a linear combination of all the p-cells that are part of the cell complex. (Positive and negative orientations are going to be introduced shortly.)

Similarly, the concept of cochains can be developed as a set of global quantities, obtained from the integration of p-forms on the relevant p-dimensional geometric entities with the correct orientation and numbering. Denoting a p-cochain by C^p,

$$C^p = \sum_{i}^{n_p} a_i c_i^{(p)} \tag{2-66}$$

The numbers a_i are merely discrete real numbers. As we will see later, with respect to physical problems, these will be global quantities on i^{th} p-cells. In other words, these will be simply results of integration of p-forms on appropriate cells as per the duality pairing shown in Eq. (2-7) and Eq. (2-8). A duality pairing also exists between chains and cochains which can be represented as follows,

$$\langle C^p, C_p \rangle = \sum_{i}^{n_p} \sum_{j}^{n_p} a_i w_j \left\langle c_i^{(p)}, c_{((p),j)} \right\rangle \tag{2-67}$$

Now, $\left\langle c_i^{(p)}, c_{((p),j)} \right\rangle = \delta_{ij}$ since the i^{th} p-cochain is associated with the i^{th} p-cell only. This results in the final expression for the chain-cochain duality pairing as,

$$\langle C^p, C_p \rangle = \sum_{i}^{n_p} a_i w_i \tag{2-68}$$

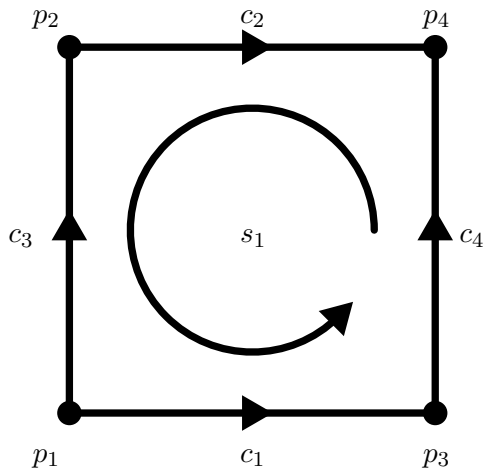

Figure 2-6: The numbering and default orientations chosen for 1- and 2-cells are shown in this figure. The 0-cells are oriented as sinks.

This is similar to the integration of differential forms. We will use the above concept later to replace integration by simple summation of global quantities.

Note that to make notation easier, the symbols $c_i^{(p)}$ and $c_{((p),j)}$ would be dropped henceforth and the duality pairing would be automatically assumed. The subscripts of the cochains will imply which chain they are associated with.

Now that we have the analogy with differential geometry in mind, we can move on to derive an expression for the discrete version of the exterior derivative - the coboundary operator.

2.2.2 The Boundary and Coboundary Operators

Once the orientation of all cells has been determined, the boundary operator can be defined as the operator that, when applied to a p-chain, returns the $(p-1)$-chain that forms its boundary.

$$\partial : C_p \rightarrow C_{p-1} \tag{2-69}$$

Since the boundary of a boundary is empty, application of the boundary operator twice to any chain results in 0,

$$\partial\partial C_p = 0 \tag{2-70}$$

Till this point, we had only talked about inner- and outer-orientations. Let us take a slight detour to talk about positive and negative orientations. The orientation of a chain is said to be positive if it is being considered with its default orientation. On the other hand, it is said to be negative if it is being considered with an orientation that is opposite to its default orientation. For example, consider the inner-oriented and numbered 2-cell shown in Figure 2-6. As is seen in the figure, certain default orientation has been assigned to all the inner-oriented mesh components. This default orientation can be summarized as,

1. Points: All 0-cells are assumed to be oriented as sinks by default (not shown in Figure 2-6).

2. Edges: Default orientation is assumed as going from left to right, or from bottom to top, along the edges.

3. Surfaces: A clockwise sense of rotation inside the surface is assumed to be the assigned default orientation.

Positive and negative orientations can be visualized better with the help of an example. Consider again the oriented 2-cell shown in Figure 2-6. The edges of the 2-cell are shown to be perfectly straight in Figure 2-6, however this is obviously not a requirement and it could be a deformed 2-cell as well, as is shown in Figure 2-7. Consider this oriented 2-cell first, and apply the boundary operator to it. This 2-cell with a sense of clockwise rotation in it induces a matching, or compatible, orientation on its boundary and we are left with the oriented 1-chain as shown in Figure 2-7. Now if we look carefully, it is apparent that some of the edges (c_2 and c_3) shown in Figure 2-7 are being considered in an opposite sense to the default orientation that was provided to them in Figure 2-6. This means that the oriented 2-cell induces a *negative* orientation on these edges. Similarly, we see that some of the edges (c_1 and c_4) are being considered with their default orientation, or, in other words, with a *positive* orientation. If we look back at Eq. (2-65), we see that the weight w_i assigned to the p-cell $c_{((p),i)}$ can then be set as ± 1 to signify positive/negative orientation of this cell.

If the numbering of the cells is as shown in Figure 2-6, we can then write down the boundary operator as,

$$\partial s_1 = \begin{bmatrix} 1 & -1 & -1 & 1 \end{bmatrix} \begin{bmatrix} c_1 \\ c_2 \\ c_3 \\ c_4 \end{bmatrix} \tag{2-71}$$

The oriented 1-chain shown in Figure 2-7 again induces a matching orientation on its boundaries formed by the 0-cells of the mesh. The application of the boundary operator to the 1-cells shown in Figure 2-6 is then equivalent to the following operation.

$$\partial \begin{bmatrix} c_1 \\ c_2 \\ c_3 \\ c_4 \end{bmatrix} = \begin{bmatrix} -1 & 0 & 1 & 0 \\ 0 & -1 & 0 & 1 \\ -1 & 1 & 0 & 0 \\ 0 & 0 & -1 & 1 \end{bmatrix} \begin{bmatrix} p_1 \\ p_2 \\ p_3 \\ p_4 \end{bmatrix} \tag{2-72}$$

The above representations of the boundary operator automatically lead to a discrete repre-

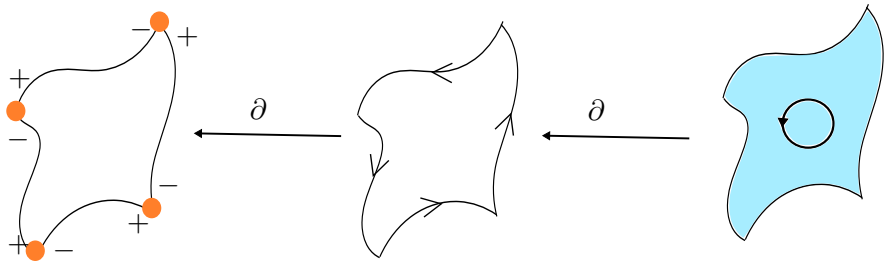

Figure 2-7: The application of the boundary operator is shown for a 2-cell. The numbering of the 2-cell is as shown in Figure 2-7. Since the operator is completely topological, it doesn't matter if the 2-cell edges are highly curved, as shown here, or completely straight, as shown in Figure 2-7.

sentation of Eq. (2-70).

$$\begin{aligned}\partial\partial s_1 &= \partial \begin{bmatrix} 1 & -1 & -1 & 1 \end{bmatrix} \begin{bmatrix} c_1 \\ c_2 \\ c_3 \\ c_4 \end{bmatrix} \\ &= \begin{bmatrix} 1 & -1 & -1 & 1 \end{bmatrix} \begin{bmatrix} -1 & 0 & 1 & 0 \\ 0 & -1 & 0 & 1 \\ -1 & 1 & 0 & 0 \\ 0 & 0 & -1 & 1 \end{bmatrix} \begin{bmatrix} p_1 \\ p_2 \\ p_3 \\ p_4 \end{bmatrix} \\ &= 0 \end{aligned} \tag{2-73}$$

Thus a matrix representation of the boundary operator has been obtained. This can be easily extended to multiple elements.

Let us define the coboundary operator, δ as the formal adjoint of the boundary operator. Then,

$$\langle \delta C^p, C_{p+1} \rangle := \langle C^p, \partial C_{p+1} \rangle \tag{2-74}$$

The analogy with generalized Stokes' theorem, Eq. (2-25), is clear from the above definition. The coboundary operator is thus the discrete analog of the exterior derivative and maps p-cochains to $(p+1)$-cochains. The coboundary operator thus allows a matrix representation which is simply the incidence matrix representing the boundary operator.

Let us represent 0-, 1-, and 2-cochains by p^i, c^i and s^i. This means that if the coboundary is

being applied to 0-cochains, we have,

$$\begin{bmatrix} c^1 \\ c^2 \\ c^3 \\ c^4 \end{bmatrix} = \delta \begin{bmatrix} p^1 \\ p^2 \\ p^3 \\ p^4 \end{bmatrix} = \begin{bmatrix} -1 & 0 & 1 & 0 \\ 0 & -1 & 0 & 1 \\ -1 & 1 & 0 & 0 \\ 0 & 0 & -1 & 1 \end{bmatrix} \begin{bmatrix} p^1 \\ p^2 \\ p^3 \\ p^4 \end{bmatrix} \tag{2-75}$$

Similarly, the application of the coboundary to a 1-chain can be represented by,

$$s^1 = \delta \begin{bmatrix} c^1 \\ c^2 \\ c^3 \\ c^4 \end{bmatrix} = \begin{bmatrix} 1 & -1 & -1 & 1 \end{bmatrix} \begin{bmatrix} c^1 \\ c^2 \\ c^3 \\ c^4 \end{bmatrix} \tag{2-76}$$

It is no surprise then that the discrete representation of the coboundary operator satisfies the property shown in Eq. (2-20).

$$\delta\delta = \partial\partial = 0 \tag{2-77}$$

From the formulation of the incidence matrices, as seen in the above example and listed as a property of the boundary operator as well, we have $\partial \circ \partial = 0$, and this leads to the fact that $\delta \circ \delta = 0$. A discrete de Rham complex can thus be setup in perfect analogy with Eq. (2-24), and this is shown in Eq. (2-78).

$$\mathbb{R} \longrightarrow C^0 \xrightarrow{\delta} C^1 \xrightarrow{\delta} C^2 \xrightarrow{\delta} C^3 \xrightarrow{\delta} 0 \tag{2-78}$$

In the future, we will be representing the coboundary operator acting on p-cochains by $D^{p+1,p}$. This is the notation that is used in Chapter 5 while presenting a discretization of the incompressible Navier-Stokes equations.

A coboundary operator can be defined on the dual grid, and if the orientations of all cells are taken properly, the following important relation between the coboundary operator on the primal and dual grids can be established.

$$D^{(n-p+1,n-p)} = (D^{(\tilde{p+1},\tilde{p})})^T \tag{2-79}$$

where a ~signifies that the operator is defined on the dual complex. This is the discrete representation of the vector calculus identities $\nabla. = -(\nabla)^T$ and $\nabla\times = (\nabla\times)^T$.

The complete de Rham complex thus can be setup as shown in Eq. (2-80). To recapitulate, horizontal links (coboundary operator) signify topological relations and can be represented exactly in a discrete setting, while the vertical links (discrete Hodge) do not appear naturally in a discrete form, and have to be represented as such with the help of approximations made while discretization. A discrete representation of the Hodge-$\star$ is derived in Chapter 3.

$$\begin{array}{ccccccccc} \mathbb{R} & \longrightarrow & C^0 & \xrightarrow{\delta} & C^1 & \xrightarrow{\delta} & C^2 & \xrightarrow{\delta} & C^3 & \xrightarrow{\delta} & 0 \\ & & \uparrow & & \uparrow & & \uparrow & & \uparrow & & \\ & & \star_h & & \star_h & & \star_h & & \star_h & & \\ & & \downarrow & & \downarrow & & \downarrow & & \downarrow & & \\ 0 & \xleftarrow{\delta} & C^{\tilde{3}} & \xleftarrow{\delta} & C^{\tilde{2}} & \xleftarrow{\delta} & C^{\tilde{1}} & \xleftarrow{\delta} & C^{\tilde{0}} & \longleftarrow & \mathbb{R} \end{array} \tag{2-80}$$

2.3 Mimetic Framework

The motivation behind the development of a mimetic framework is that the operations on differential forms of infinite dimensional systems, $\bigwedge^k$, are *mimicked* at the discrete level i.e. in a finite dimensional space, $\bigwedge_h^k$ [7]. Thus, projections, π, that map differential forms in infinite dimensional space to finite dimensional space need to be developed such that given an operation T at the continuous level, the following is satisfied: $\pi \circ T = T \circ \pi$. Thus, the following commutative diagram can be set up.

$$\begin{array}{ccc} \bigwedge^k & \xrightarrow{T} & \bigwedge^l \\ \pi \downarrow & & \pi \downarrow \\ \bigwedge_h^k & \xrightarrow{T} & \bigwedge_h^l \end{array} \tag{2-81}$$

Thus, a projection is defined consisting of two steps - a reduction operation, $\mathcal{R}$, and a reconstruction operation, $\mathcal{I}$. The first helps map the differential forms to cochains, and the second reconstructs finite dimensional expressions for the differential forms using these cochains [5, 7]. The projection, π, can then be simply written down as: $\pi = \mathcal{I} \circ \mathcal{R}$. Now, all that is left is defining the reduction and reconstruction operators with the help of suitable basis functions.

$$\pi : \bigwedge^p \rightarrow \bigwedge_h^p \tag{2-82}$$

2.3.1 Reduction

The reduction operator, $\mathcal{R}$, reduces an infinite-dimensional system to a finite set of numbers (cochains) associated to mesh elements (chains). The action of the reduction operator is defined as,

$$\mathcal{R} : \bigwedge^p(\mathcal{M}) \rightarrow C^p(D) \tag{2-83}$$

where D is the cell-complex (computational mesh). Construction of the above map was mentioned in the section on cochains, and initially while discussing global values. It is simply the conversion of the continuous form to global values, i.e. integration of a p-form, $\alpha^{(p)} \in \bigwedge^p E^*$, on the relevant geometric object, a p-cell, $c_{((p),i)} \in D$

$$\left\langle \mathcal{R}\alpha^{(p)}, c_{((p),i)} \right\rangle := \int_{c_{((p),i)}} \alpha^{(p)} \tag{2-84}$$

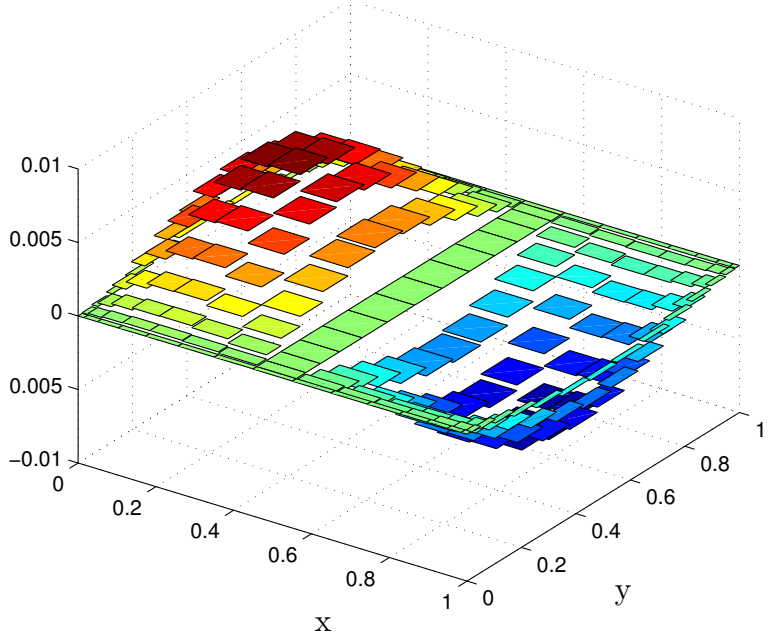

Figure 2-8: A 2-form, $\alpha^{(2)} = \cos(\pi x)\sin(\pi y)\ dxdy$ is reduced on 2-cells of a mesh, and the 2-cochains are plotted.

This operation can be repeated for all p-cells in the cell to form a p-cochain, C^p. Once reduced as such, and using the fact that the discrete counterpart of generalized Stokes' theorem was seen to exist in a framework with chains and cochains, Eq. (2-74), it is easy to see that $\mathcal{R}$ satisfies the following very important property with respect to the exterior derivative's action.

$$\mathcal{R}\mathrm{d} = \delta\mathcal{R} \tag{2-85}$$

The above simply states that we can either first reduce our p-form and then apply the coboundary operator, or first apply the exterior derivative and then reduce the $(p+1)$-form; this is merely a confirmation of the exact nature of the discrete exterior derivative. Another important property that the reduction map satisfies is with respect to the pullback operator. Consider a map $\Phi : \mathcal{M} \to \mathcal{N}$. Then,

$$\mathcal{R}\Phi^* = \Phi^\sharp\mathcal{R} \tag{2-86}$$

where $\Phi^\sharp : C^p(D_\mathcal{N}) \to C^p(D_\mathcal{M})$ is the discrete version of the pullback operator ($D_\mathcal{M}$ and $D_\mathcal{N}$ are the computational meshes on manifolds $\mathcal{M}$ and $\mathcal{N}$). Proofs of these properties can be found in [7]. As an example of $\mathcal{R}$ in 2-dimensions, the reduction of $\alpha^{(2)} = \cos(\pi x)\sin(\pi y)\ dxdy$ defined on $\Omega = [0 \quad 1]^2$ can be seen in Figure 2-8.

2.3.2 Reconstruction

Once differential forms have been reduced to their corresponding 'global quantities' (cochains), we can interpolate them using appropriate basis functions. The choice of basis functions is where some freedom lies and different interpolating forms can be used (B-splines [35];

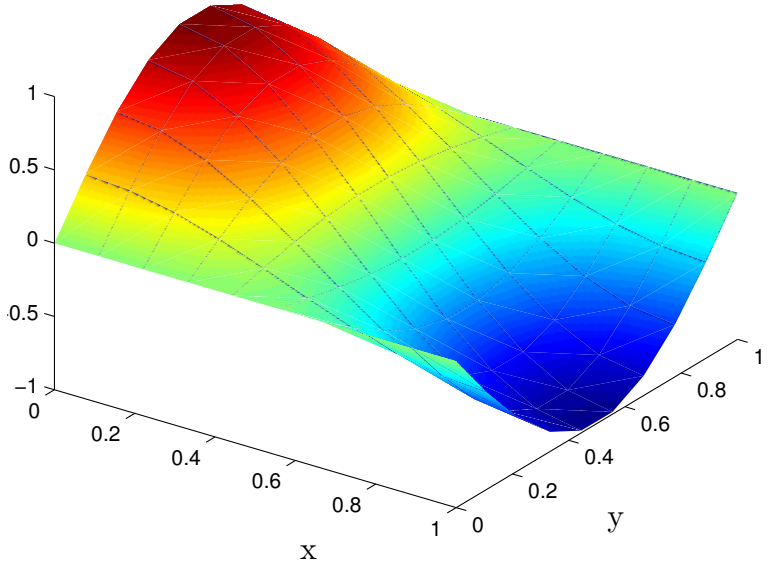

Figure 2-9: The 2-cochains corresponding to $\alpha^{(2)} = \cos(\pi x)\sin(\pi y)\, dxdy$ as shown in Figure 2-8 are interpolated using $\mathcal{I}$. The above is equal to the projection π, see Eq. (2-82), applied to $\alpha^{(2)}$.

Lagrange Polynomials, Edge Functions [29]), subject to some restrictions, as detailed in [7]. Some properties the reconstruction map,

$$\mathcal{I} : C^p(D) \to \bigwedge_h^p(\mathcal{M}) \tag{2-87}$$

should then possess are:

- The reduction operator should be a right-inverse of the interpolation operator.

$$\mathcal{R}\mathcal{I} = \mathbb{I} \tag{2-88}$$

  where $\mathbb{I}$ is the identity matrix.

- The interpolation map should commute with the exterior derivative in the following manner,

$$d\mathcal{I} = \mathcal{I}\delta \tag{2-89}$$

- It should not matter whether the interpolation is performed on cochains pulled back from $D_{\mathcal{N}}$ to $D_{\mathcal{M}}$, or the interpolated forms are pulled back from $\mathcal{N}$ to $\mathcal{M}$

$$\mathcal{I}\Phi^\sharp = \Phi^*\mathcal{I} \tag{2-90}$$

For a list of these properties, see [7]. The choice of interpolating forms was edge functions (1-forms) and Lagrange polynomials (0-forms), with higher dimensional interpolating forms being constructed with the tensor products of these two since quadrilateral elements are used. In the next chapter, implementation of the operators discussed in this chapter is done. An example of interpolated cochains can be seen in Figure 2-9.

Chapter 3

Discretization

One of the most important steps in carrying out numerical analysis is the progression from a continuous setting to its discrete counterpart. This is achieved with the formulation of appropriate reduction and reconstruction operators, $\mathcal{R}$ and $\mathcal{I}$, respectively. In addition to this, a number of other operators were introduced in the continuous setting and their action needs to be translated to the discrete setting with as much structure-preservation as possible. The aim of this chapter is to demonstrate their implementation in a discrete setting, and also to analyse some of their properties. Using the discretizations explained in this chapter, a few test problems will be solved in Chapter 4 and their solutions analysed.

Different ways to reduce the physical variables to relevant cochains will be looked at first in Section 3.1. Then, in Section 3.2, interpolation functions will be introduced in order to achieve a continuous representation of the physical variable from its cochain. However, it should be kept in mind that this continuous representation is not done just to get a better visual representation of the solution; it is the constitutive laws that make this continuous representation necessary for a high-order approximation of material laws. Once the reduction and reconstruction operators have been formulated as such, some of the properties of important parameters will be investigated with the help of convergence plots (i.e. h/p-refinement plots), and their numerical implementation discussed in subsequent sections. To make visualization easier and the text less cluttered, only results for 1D have been provided here. Extension of concepts to 2D is straightforward, thanks to quadrilateral elements. Convergence analysis for all the operators showed optimal convergence, and thus this is not mentioned explicitly with every analysis plot.

3.1 Reduction Operator

As was shown in Eq. (2-84), reduction of differential forms to cochains is simply implemented by integrating the differential forms on their relevant geometric object. In 3D, this means

integration of 0-,1-,2-, and 3- forms on points (in other words, evaluation on points), lines, surfaces and volumes.

Consider a 0-form in 1D, $\phi^{(0)} = \phi(x, y)$, on Ω' which is shown in Figure 3-1. Reduction of $\phi^{(0)}$ on the points defined on the manifold, as can be seen in the lower part of Figure 3-1, can be done by simple evaluation of the differential form on points. A smooth map $\Phi : \Omega \to \Omega'$ is assumed to exist where Ω is the reference element parametrized by ξ where all analysis (with the help of the pullback operator) is performed. If Ω' is embedded in $\mathbb{R}^2$, the manifold can be represented by (x, y) in local coordinates where $(x, y) = (\Phi_x(\xi), \Phi_y(\xi))$. Using these facts and noting that the pullback operator commutes with the reduction operator, $\phi^{(0)}$ can be represented as a 0-cochain in Ω, C^0_Ω, using the notation previously introduced,

$$\begin{aligned} C^0_\Omega &= \Phi^\sharp \mathcal{R}\ \phi^{(0)} \\ &= \mathcal{R}\Phi^\star\ \phi^{(0)} \\ &= \mathcal{R}\ \phi(\Phi_x(\xi), \Phi_y(\xi)) \\ &= \textstyle\sum_i^{n_0} \bar{\phi}_i(\Phi_x(\xi_i), \Phi_y(\xi_i)) \end{aligned} \tag{3-1}$$

where ξ_i is the coordinate of the i^{th} 0-cell on Ω. The 0-cochains is shown in Figure 3-1.

In the same spirit, a one form, $\alpha^{(1)} = \alpha_x(x, y)dx + \alpha_y(x, y)dy$ on Ω' can be discretized by integrating it on line segments.

$$\begin{aligned} C^1_\Omega &= \Phi^\sharp \mathcal{R}\ \alpha^{(1)} \\ &= \mathcal{R}\Phi^\star\ \alpha^{(1)} \\ &= \mathcal{R}\ [\alpha_x\ \alpha_y] \begin{bmatrix} \dfrac{\partial \Phi_x}{\partial \xi} \\ \dfrac{\partial \Phi_y}{\partial \xi} \end{bmatrix} d\xi \\ &= \textstyle\sum_i^{n_1} \bar{\alpha}_i \end{aligned} \tag{3-2}$$

where $\bar{\alpha}_i$ is the global quantity $\int_{C_i} \Phi^* \alpha^{(1)}$ and C_i is the i^{th} line segment on Ω.

This finishes the section on reduction of differential forms in 1D. Similar steps can be followed in 2D for discretizing differential forms, with the exception that, since the mesh will consist of surfaces as well, it will be able to support 2-forms as well, and they will consequently be integrated on surfaces (see Figure 2-8).

3.2 Reconstruction Operator

Now that the differential forms have been reduced to cochains, to project the cochains on a finite dimensional space of differential forms, $\bigwedge_h$, interpolation functions are required. Interpolation through basis functions, $m_i^{(p)}$, is simply the weighted sum of basis function evaluations at points, with the total number of basis functions being equal to the number of degrees

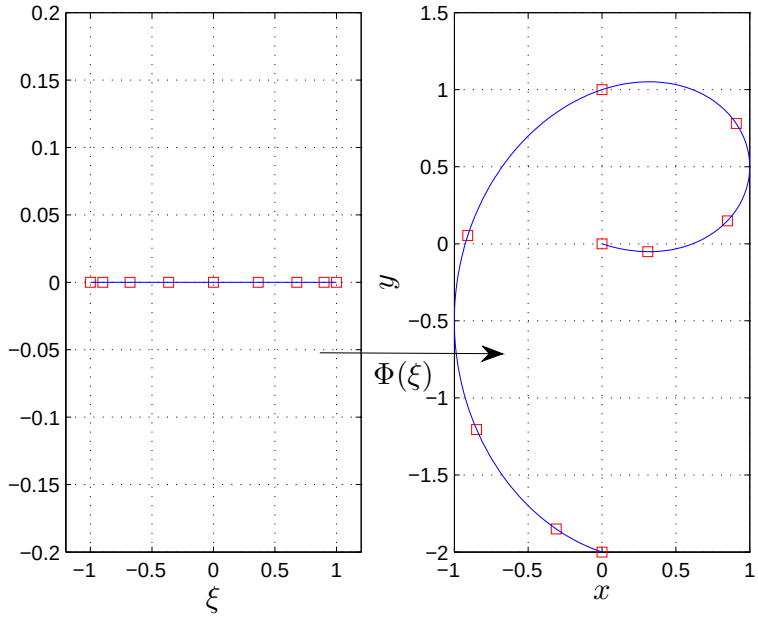

(a) Action of $\Phi : \Omega \to \Omega'$

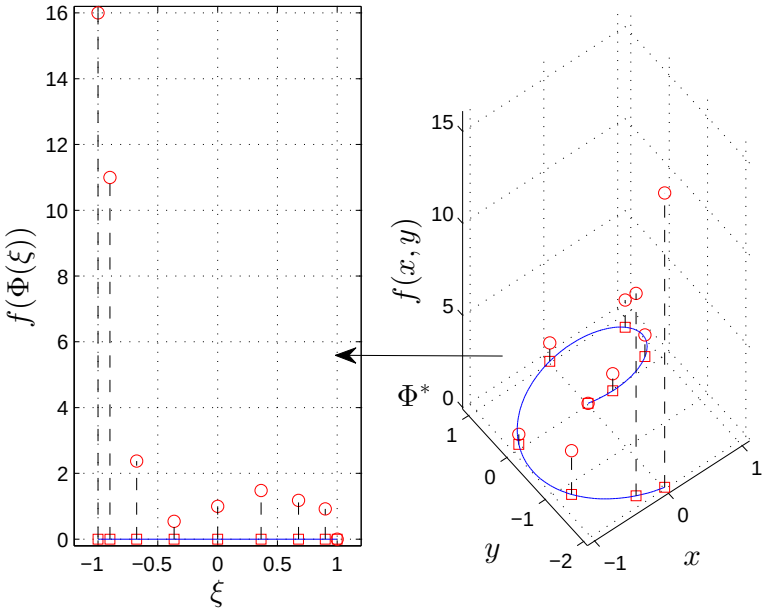

(b) Reduction with the help of $\Phi^* : \bigwedge^p(\Omega') \to \bigwedge^p(\Omega)$

Figure 3-1: Reduction of zero-forms on a 1D domain explained. The 0-form is just pulled back from the physical domain and reduced in the reference domain.

of freedom in the system. In order to formulate such a reconstruction operator, the first and foremost property that should be taken care of is that $\mathcal{I}$ should be the right inverse of $\mathcal{R}$. This means that, as explained before, if $\mathcal{R}$ is applied to $\bigwedge_h$, the appropriate cochains should be reobtained. Specifically, in 1D, the 0-form interpolation basis functions should be such that values in points should be preserved, and 1-form interpolation basis function should be such that the integral values on line-segments are preserved. Ideally, it would be desirable for $\mathcal{I}$ to be the left inverse of $\mathcal{R}$ as well, but this is indeed too much to ask for in a general discrete setting. This means that we have to select the interpolation functions such that $\mathcal{I}\mathcal{R}$ is as close to being an identity as possible. What we usually have is,

$$\mathcal{I}\mathcal{R} = \mathbb{I} + \epsilon$$

In the above equation, ϵ represents the interpolation error and this is the error one would like to reduce as much as possible as this is the error that will influence the solution the most since this is going to be present everytime a non-topological relation is implemented. In other words, this is the error present in discretizing the constitutive equations. Hence, spectral elements make for a tempting choice as they can facilitate arbitrary order formulations and thus make ϵ reduce exponentially according to the order of the element being used. Moreover, spectral element methods have favourable conditioning and element-wise local support [7].

Lagrange Polynomials and Edge Functions [29, 43] have been shown to possess these properties, and these will be used in the work described here.

3.2.1 Lagrange Polynomials $\mathcal{I}C^0_\Omega$

Let $h_i^{(0)}(\xi)$ be the i^{th} Lagrange polynomial defined on Ω as a function on ξ for interpolating 0-cochains to 0-forms (finite dimensional representation). Following earlier convention, let the number of degrees of freedom (number of 0-cells) be n_0; this implies that the highest degree $h^{(0)}$ can have is $(n_0 - 1)$. The nodal positions of the i^{th} 0-cells is denoted as ξ_i. These polynomials are then defined as,

$$h_i^{(0)}(\xi) = \begin{cases} 1, & \xi = \xi_i \\ 0, & \xi = \xi_j \text{ where } i \neq j \end{cases}$$

To reiterate, since the above definition includes n_0 equations, a $h_i^{(0)}$ of order $(n_0 - 1)$ can be uniquely determined. Using these functions, the interpolation is carried out as follows, with ϕ_i^0 being the i^{th} nodal value for a 0-form, $\phi^{(0)}$.

$$\begin{aligned} \phi_h^{(0)} &= (\Phi^{-1})^* \ \phi_h^{(0)}(\xi) \\ &= (\Phi^{-1})^* \ \textstyle\sum_i^{n_0} \phi_i^0 \ h_i^{(0)}(\xi) \\ &= \textstyle\sum_i^{n_0} (\Phi^{-1})^\sharp \ \phi_i^0 h_i^{(0)}(\xi) \\ &= \textstyle\sum_i^{n_0} \phi_i^0 \ h_i^{(0)}(\xi(x,y)) \end{aligned} \tag{3-3}$$

It is quite obvious that $\mathcal{R}\ \phi_h^{(0)}(x)$ will indeed yield nodal values exactly for $\phi^{(0)}$, and thus $\mathcal{I}$ is indeed the right inverse of $\mathcal{R}$.

An example of Lagrange Polynomials can be seen in Figure 3-3. Note that in all h-refinement plots shown, with the theoretical order of convergence shown in **- -**. The convergence analysis results for this operation are shown in Figure 3-4. The complete reduction-reconstruction of a 0-form can be seen in Figure 3-2. A similar example could be constructed for 1-forms, although it is not shown here.

3.2.2 Edge Functions $\mathcal{I}C^1_\Omega$

Consider the reconstruction of 1-forms from 1-cochain, C^1_Ω. The interpolants used for this purpose must, as mentioned earlier, preserve the integral quantities. Thus the definition of the i^{th} Edge Function, $e^{(1)}_i$, associated with i^{th} line segment on Ω, L_i:

$$\int_{L_j} e^{(1)}_i(\xi) = \int_{L_j} \epsilon_i(\xi)\, d\xi = \delta_{ij}$$

The interpolated 1-form, $\alpha^{(1)}_h$, is thus going to be reconstructed as follows from the 1-cochain, C^1_Ω.

$$\begin{aligned}
\alpha^{(1)}_h &= (\Phi^*)^{-1}\ \alpha^{(1)}_h(\xi) \\
&= (\Phi^*)^{-1}\ \textstyle\sum_i^{n_1} \alpha^1_i e^{(1)}_i(\xi) \\
&= (\Phi^*)^{-1}\ \textstyle\sum_i^{n_1} \alpha^1_i \epsilon_i(\xi)\ (d\xi) \\
&= \textstyle\sum_i^{n_1} (\Phi^\sharp)^{-1}\ \alpha^1_i \epsilon_i(\xi)\ (d\xi) \\
&= \textstyle\sum_i^{n_1} \alpha^1_i \epsilon_i(\xi(x,y)) [(\frac{\partial \Phi_x}{\partial \xi})^{-1}\ (\frac{\partial \Phi_y}{\partial \xi})^{-1}] \begin{bmatrix} (dx) \\ (dy) \end{bmatrix}
\end{aligned} \tag{3-4}$$

If a check needs to be done whether the above interpolation preserves integrals (α^1), all that needs to be done is pulling back $\alpha^{(1)}_h$ to Ω and then applying $\mathcal{R}$. This indeeds shows that the integral values are preserved, and, thus, $\mathcal{I}$ is the right inverse of $\mathcal{R}$. A similar interpolation of 1-forms can be done in 2D and 3D while following the exact same steps, with the exception that the expression for Φ^* is going to be more extensive (for instance, Eq. (2-30)).

An example of the edge-basis functions is given in Figure 3-3. The convergence analysis results for this operation can be seen in Figure 3-5. For more information on Edge polynomials, [29, 43] should be perused. An alternative derivation of this integral-preserving basis can be found in [44].

3.3 Discrete Exterior Derivative

The exterior derivative is the easiest to discretize out of all the operators visited so far and this was shown in Chapter 2 in the section on Algebraic Topology, Section 2.2. It was demonstrated how the discrete exterior derivative is adjoint of the boundary operator

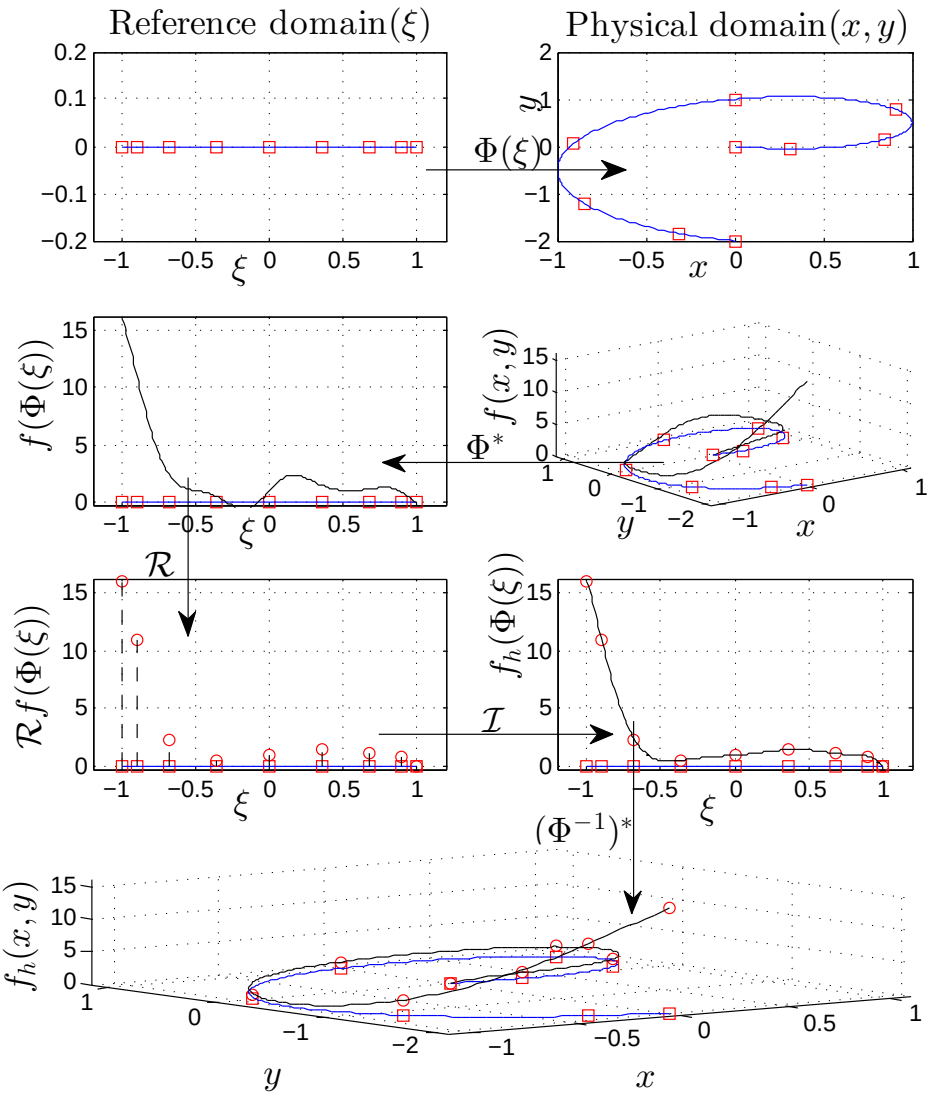

Figure 3-2: A 0-form is pulled back from the physical domain to the reference domain (Φ^*), reduced ($\mathcal{R}$), interpolated ($\mathcal{I}$), and then pulled back to the physical domain ($(\Phi^{-1})^*$). The mesh nodes are shown as □ and mesh edges as ▬ for both domains. The functions are plotted with ▬. Note that the reduction-reconstruction for a 1-form is going to follow the exact same steps with the exception that instead of being reduced in the reference domain on point objects, it would need to be integrated on line objects.

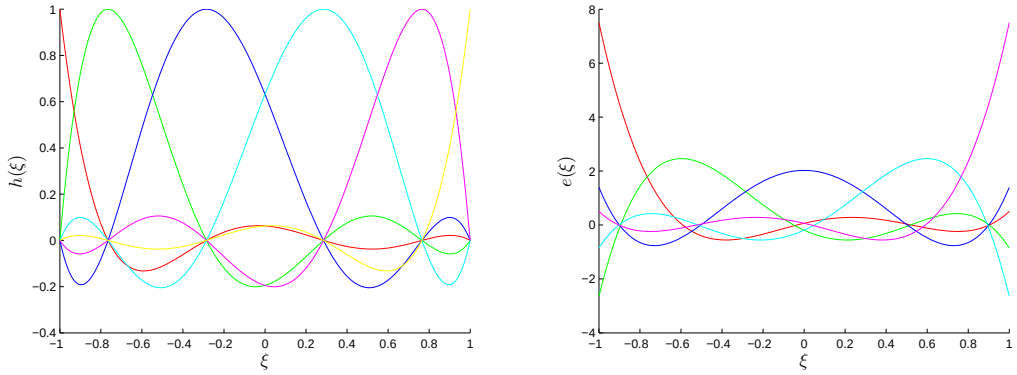

(a) Lagrange basis (b) Edge basis

Figure 3-3: An example of basis functions for 0- and 1-forms. Higher order basis can be constructed by taking the tensor products of these bases.

(hence the name *coboundary* operator). Related to this property is the property that the exterior derivative commutes with the reduction operator, $\mathcal{R}$, making it possible to apply the coboundary operator to the cochains. This property, mentioned before in Chapter 2, is simply stated as,

$$\mathcal{R}\mathrm{d} = \delta\mathcal{R} \tag{3-5}$$

This property is investigated in error convergence plots shown in Figure 3-6 where the RSS error for cochains is investigated. It can be seen that the errors are alwasy practically zero implying that the p-cochains obtained by the application of the coboundary operator to $(p-1)$-cochains are always exact when compared to p-cochains obtained by reduction of the analytical exterior derivative of the $(p-1)$-form. The interpolation errors can be seen in Figure 3-7. This operator is the same as the exterior covariant-derivative introduced in Section 2.1.

3.4 Discrete Hodge Operator

As was seen in Section 2.1, the Hodge operator is a map from primal to dual cochains, and can be used in the discretization of constitutive equations. Now that a method to reconstruct the finite dimensional representations of differential forms from cochains has been defined, the Hodge can be implemented using Eq. (2-58).

Consider the 1D manifold Ω (the reference element) shown in Figure 3-8 and consider a Lobatto quadrature node distribution as the mesh. As is shown in [7], a dual grid with Gauss quadrature nodes can be built, with line segments connecting them, and with Extended Gauss points forming the boundary of the dual mesh. We can define a dual basis, denoted by a $\sim$ in the basis functions - $h^{(\tilde{0})}$ (dual basis Lagrange polynomials), and $e^{(\tilde{1})}$ (dual basis Edge Functions).

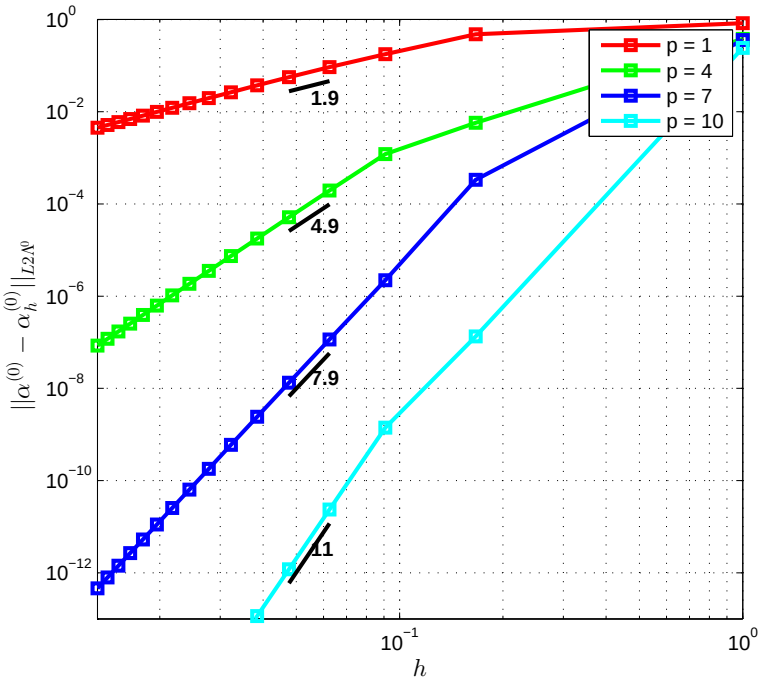

(a) h-refinement

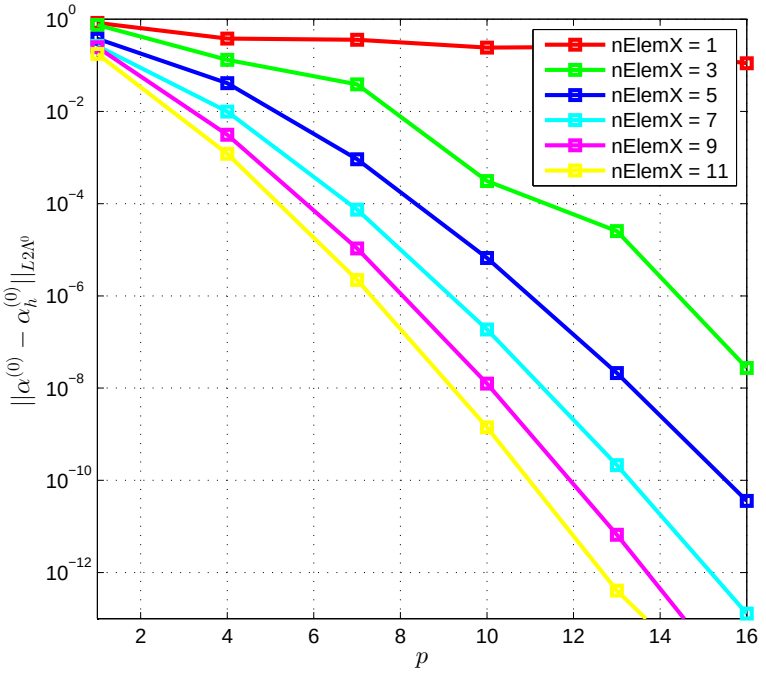

(b) p-refinement

Figure 3-4: Convergence analysis results (L^2 error) for the reduction and reconstruction of $\alpha^{(0)}$ in 1D.

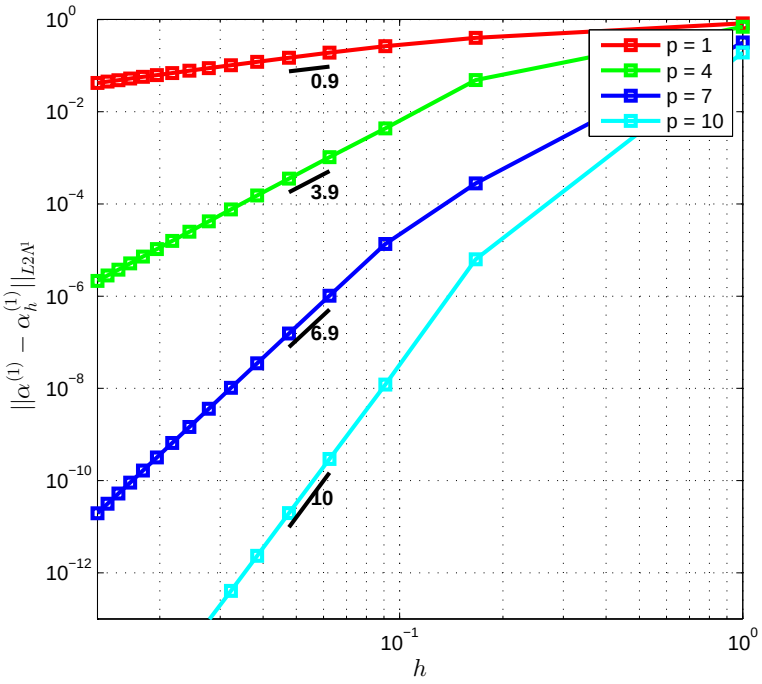

(a) h-refinement

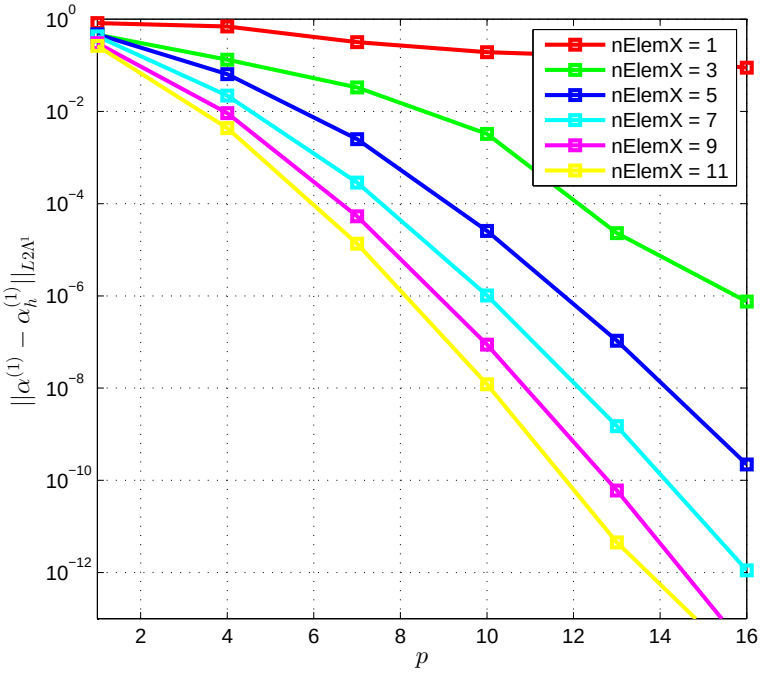

(b) p-refinement

Figure 3-5: Convergence analysis results (L^2 error) for the reduction and reconstruction of $\alpha^{(1)}$ in 1D.

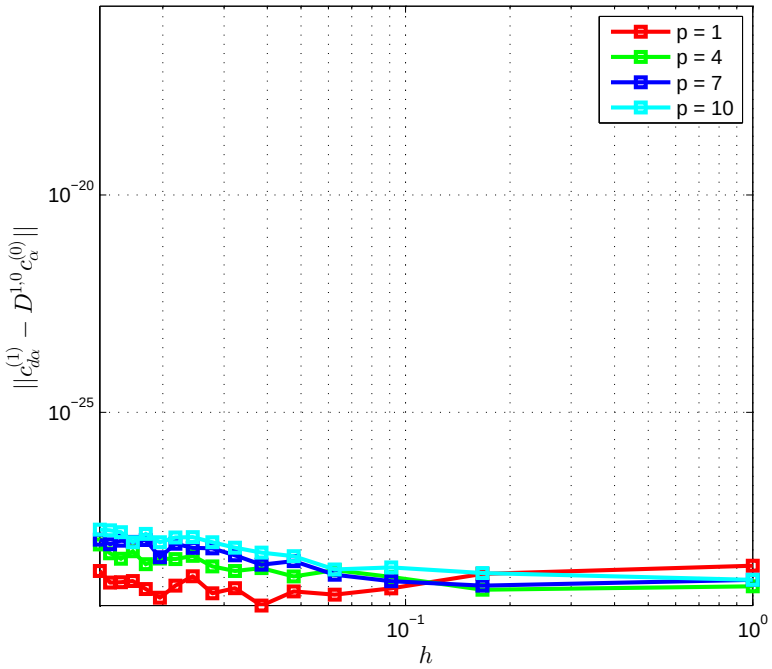

(a) h-refinement

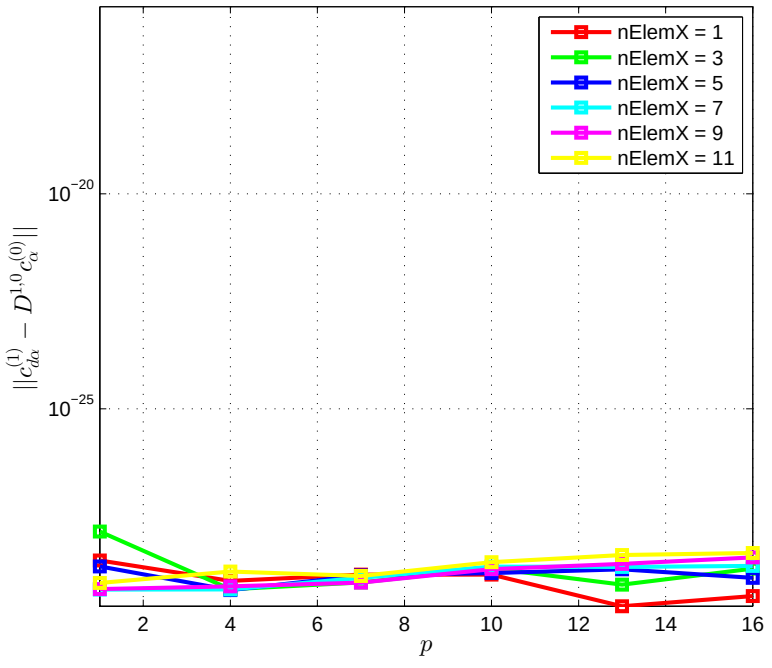

(b) p-refinement

Figure 3-6: Convergence analysis results (RSS error for cochains) for the application of the exterior derivative to 0-forms in 1D. The form is first reduced and then the coboundary operator is applied.

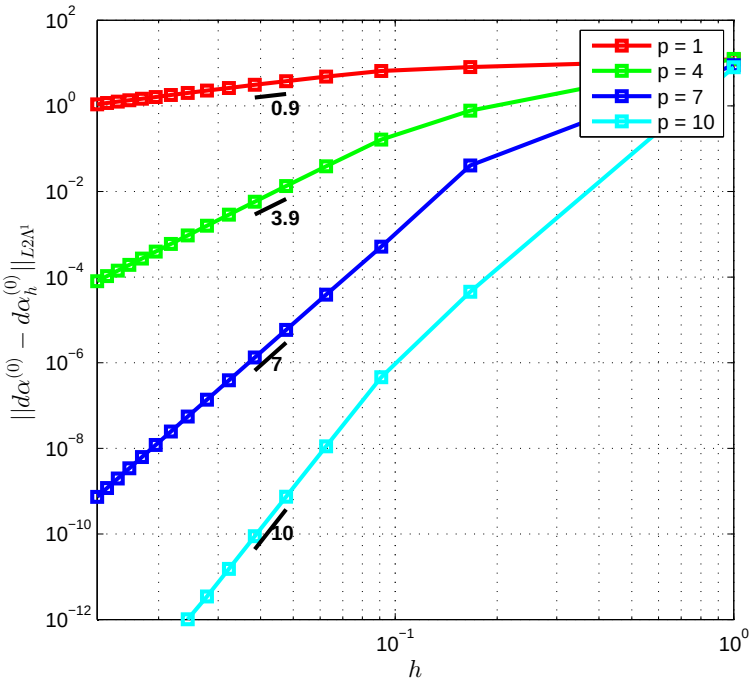

(a) h-refinement

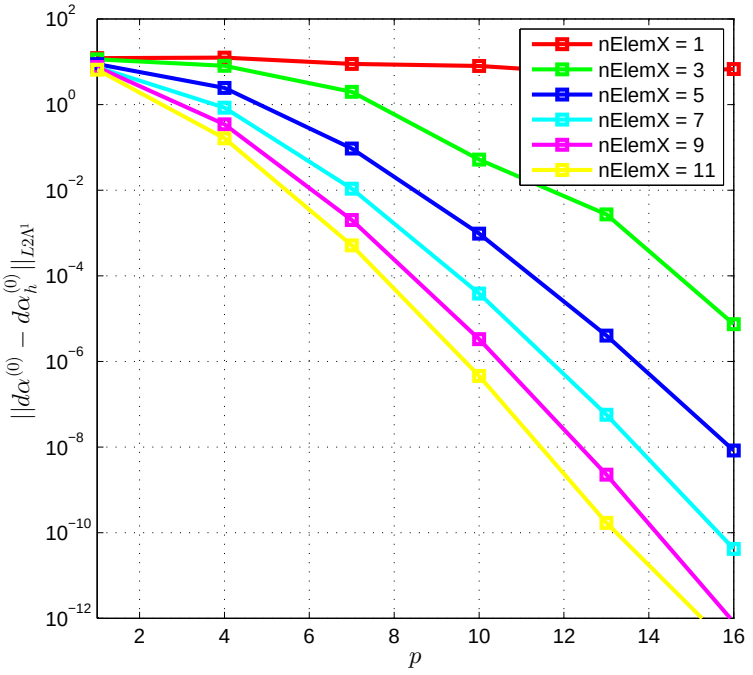

(b) p-refinement

Figure 3-7: Convergence analysis results (L^2 errors in interpolation) for the application of the exterior derivative to 0-forms in 1D.

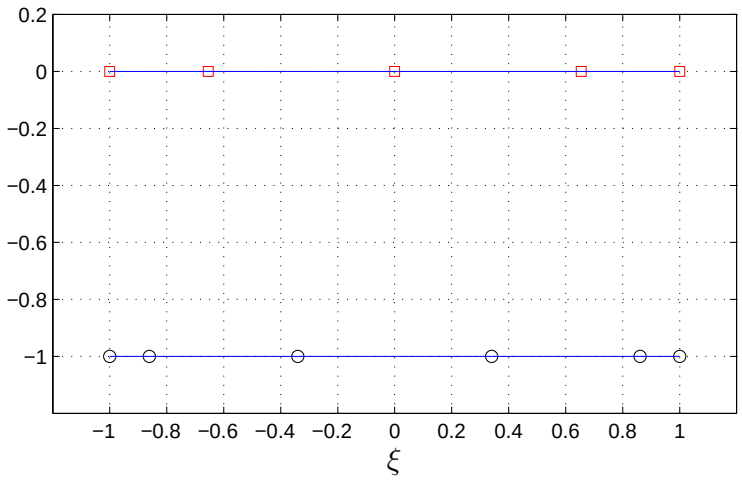

Figure 3-8: Primal (□) and dual (○) meshes shown for a 1D reference elemnt.

Now, consider a 0-form, $\phi^{(0)} \in \bigwedge^0(\Omega)$, and a 1-form, $\alpha^{(\tilde{1})} \in \bigwedge^{\tilde{1}}(\Omega)$. Consider implementation of the Hodge for the zero-forms; the implementation for one-forms can be done in a similar way. Let the following be true.

$$\alpha^{(\tilde{1})} = \star\phi^{(0)} \tag{3-6}$$

So, implementation of the Hodge operator entails that we find $\alpha^{(\tilde{1})} \in \bigwedge^{\tilde{1}}(\Omega)$ given $\phi^{(0)} \in \bigwedge^0(\Omega)$ such that the following is true $\forall \tau^{(\tilde{1})} \in \bigwedge^{\tilde{1}}(\Omega)$.

$$\left(\tau^{(\tilde{1})}, \star\phi^{(0)}\right)_\Omega = \left(\tau^{(\tilde{1})}, \alpha^{(\tilde{1})}\right)_\Omega \tag{3-7}$$

where the global inner product is defined as follows,

$$\left(\alpha^{(p)}, \beta^{(p)}\right)_\Omega := \int_\Omega \alpha^{(p)} \wedge \star\beta^{(p)} = \int_\Omega \left\langle \alpha^{(p)}, \beta^{(p)} \right\rangle \sigma \tag{3-8}$$

This can be further simplified as follows, using the property that $\star\star\,\phi^{(0)} = \phi^{(0)}$,

$$\int_\Omega \left\langle \tau^{(\tilde{1})}, \alpha^{(\tilde{1})} \right\rangle \sigma = \int_\Omega \tau^{(\tilde{1})} \wedge \phi^{(0)} \tag{3-9}$$

Since we only have the finite dimensional representation of $\phi^{(0)}$, what we are working with is, in fact, $\phi_h^{(0)}$, and an expression for this was shown in Eq. (3-3). We are going to obtain $\alpha_h^{(\tilde{1})}$ instead of $\alpha^{(\tilde{1})}$, and hence it can be expressed in the same form as Eq. (3-4). This means that the finite-dimesional representations of the forms can be written down as seen previously in

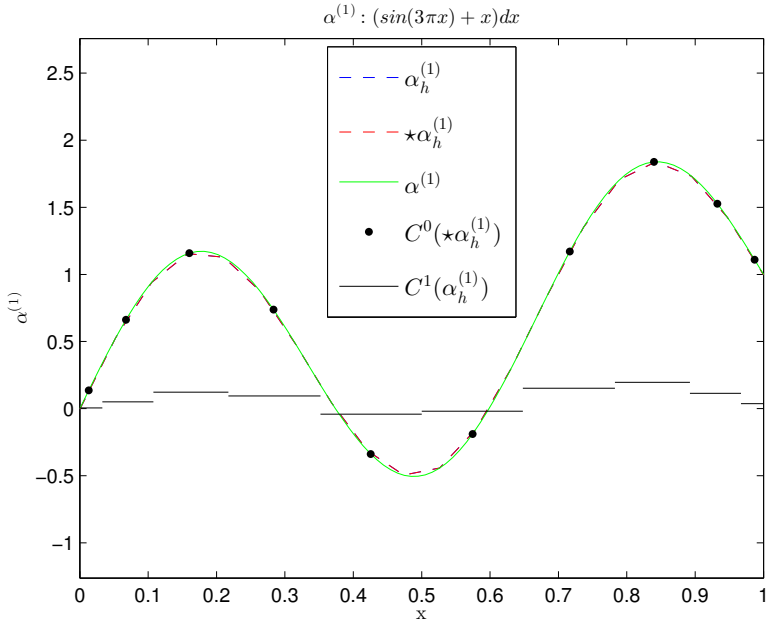

Figure 3-9: Application of the Hodge to 1-forms is shown. Also shown are 1-cochains and 0-cochains and the 0/1-cells on which these are defined.

terms of cochains (denoted by an over-head bar here) and basis functions. Furthermore, $\tau^{(\tilde{1})}$ can be chosen as the basis functions used for interpolations of 1-forms on the dual mesh (the mesh with Extended Gauss points). Using the inner product definitions introduced earlier,

$$(M_{\tilde{1},\tilde{1}}\bar{\alpha})_e = (N_{\tilde{1},0}\bar{\phi})_e \tag{3-10}$$

where $M_{\tilde{1},\tilde{1}}$ is the inner-product matrix formed by the dual edge basis functions, $\left(\tilde{e}^{(1)}, \tilde{e}^{(1)}\right)$, and $N_{\tilde{1},0}$ is the matrix obtained by integrating the wedge products of dual edge basis functions with primal Lagrange polynomials, $\int \tilde{e}^{(1)} \wedge h^{(0)}$. N can be thought of as the matrix that includes the effects of changing the basis from primal 0-forms to dual 1-forms into the system. The subscript e denotes that this is the formulation obtained for one spectral element. For multi-element cases, the matrices can be assembled keeping in mind the cells that are shared between the elements. The final result is as follows.

$$M_{\tilde{1},\tilde{1}}\bar{\alpha} = N_{\tilde{1},0}\bar{\phi} \tag{3-11}$$

The matrix $M^{-1}N$ can be thought of as the discrete Hodge matrix, $\star_{h,e}$, that acts on the 0-cochains contained in $\bar{\phi}_e$ and yields 1-cochains $\bar{\alpha}_e$. Although element-wise discrete Hodge is square and invertible because of M and N being so, it should be noted that, because of the overlap of cells between elements, global discrete Hodge is, in general, not going to be square, but instead is going to be rectangular. However, this doesn't mean that it is not invertible and this is because of the different assembly of the component $\star_{h,e}$ which enables the reverse passage. In practice, M doesn't necessarily need to be inverted and the system matrix can be built up using the mixed-formulation shown above.

An example of this process but instead applied to 1-forms is shown in Figure 3-9, where this was done for going from a primal 1-form to a dual 0-form. It can be seen that the continuous field representation of both $\star\alpha^{(1)}$ and $\alpha^{(1)}$ are the same. It is only the association with geometric objects that changes. Error convergence plots for this process can be seen in Figure 3-10 and Figure 3-11 for 0- and 1-forms, respectively. To see that the Hodge is indeed not an exact relation and involves an approximation, the RSS error (root of sum of squares) of the cochains obtained after the application of the Hodge were plotted and these observations can be seen in Figure 3-12 and Figure 3-13.

It should be noted here that the discrete application of the Hodge-$\star$ involves the numerical evaluation of inner-product integrals, for which a set of quadrature nodes are assigned over space. Then we can assign a material parameter as a kind of multiplying factor to each quadrature node, and this can in principle change from one node to another. This is one way that variable material parameters, such as viscosity, conductivity etc could be taken care of while discretizing constitutive relations using the Hodge-$\star$. This is exploited in the Darcy flow test case shown in Chapter 4.

The above procedure for calculating the discrete representation of the Hodge matrix can be extended and used for calculating the discrete representations of several other operators.

3.5 Discrete Co-differential

The co-differential operator is defined as per Eq. (2-60) and a discrete representation of this operator is going to be investigated in this section. Similar to the procedure followed in the development of $\star_h$, we take a 1-form and apply the co-differential operator to it (co-differential operator applied to 0-forms is always 0).

Consider $\alpha^{(1)} \in \bigwedge^1(\Omega)$ and $\beta^{(0)} \in \bigwedge^0(\Omega)$ such that,

$$d^\star\alpha^{(1)} = \beta^{(0)} \tag{3-12}$$

Similar to the procedure adopted for the Hodge operation, the Galerkin problem translates to finding $\beta^{(0)} \in \bigwedge^0(\Omega)$, given $\alpha^{(1)} \in \bigwedge^1(\Omega)$, such that the following is true $\forall\tau^{(0)} \in \bigwedge^0(\Omega)$,

$$\left(\tau^{(0)}, d^\star\alpha^{(1)}\right)_\Omega = \left(\tau^{(0)}, \beta^{(0)}\right)_\Omega \tag{3-13}$$

Again, on using the definition of the global inner product, Eq. (3-8), we simplify the above equation as,

$$\left(\tau^{(0)}, d^\star\alpha^{(1)}\right)_\Omega = \int_\Omega \left\langle \tau^{(0)}, \beta^{(0)} \right\rangle \sigma \tag{3-14}$$

Using (2-62), we can further simplify our system as follows,

$$\left(\mathrm{d}\tau^{(0)}, \alpha^{(1)}\right)_\Omega - \int_{\partial\Omega} \tau^{(0)} \wedge \star\alpha^{(1)} = \int_\Omega \left\langle \tau^{(0)}, \beta^{(0)} \right\rangle \sigma \tag{3-15}$$

Now, since we only have the discrete representation of $\alpha^{(1)}$, and we can only calculate a discrete representation of $\beta^{(1)}$,

$$\int_\Omega \left\langle \mathrm{d}\tau^{(0)}, \alpha_h^{(1)} \right\rangle \sigma - \int_{\partial\Omega} \tau^{(0)} \wedge \star\alpha_h^{(1)} = \int_\Omega \left\langle \tau^{(0)}, \beta_h^{(0)} \right\rangle \sigma \tag{2-62}$$

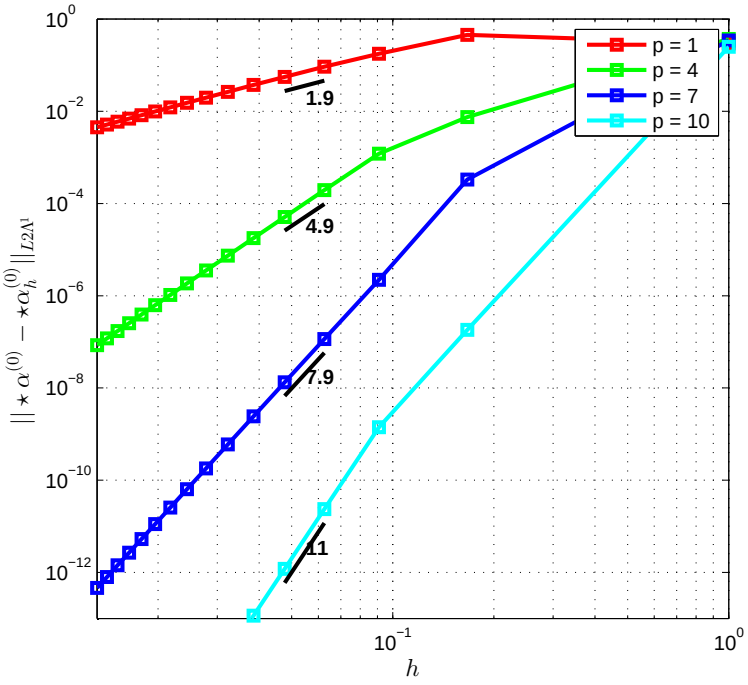

(a) h-refinement

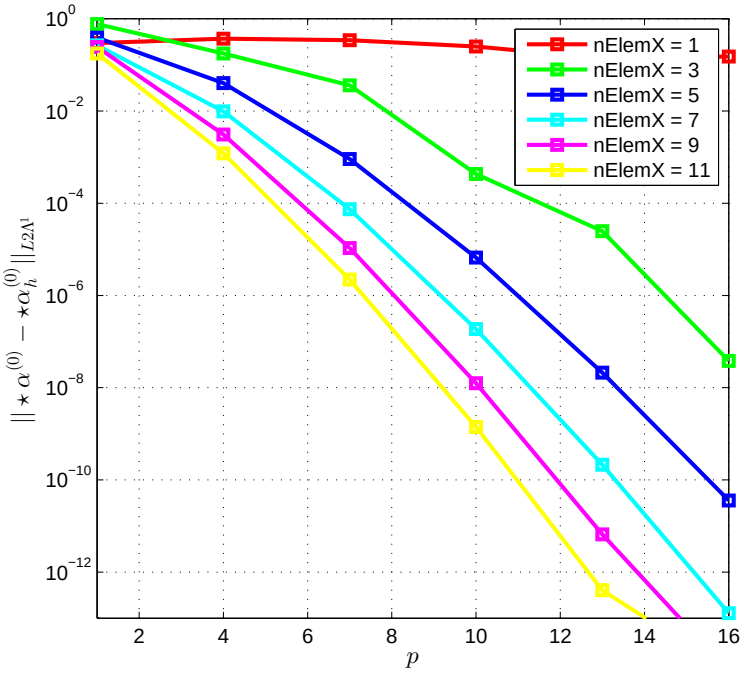

(b) p-refinement

Figure 3-10: Convergence analysis (L^2 error) results for the Hodge-$\star$ applied to a 0-form in 1D.

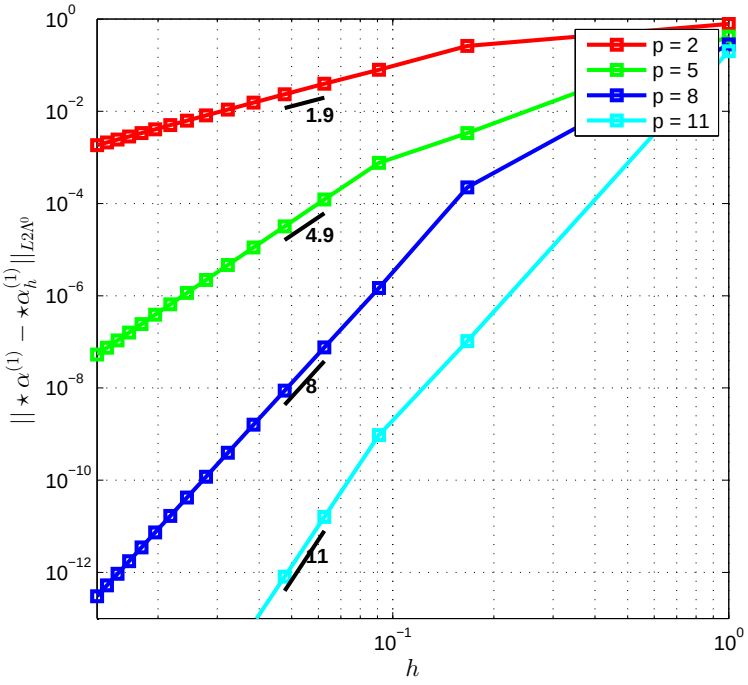

(a) h-refinement

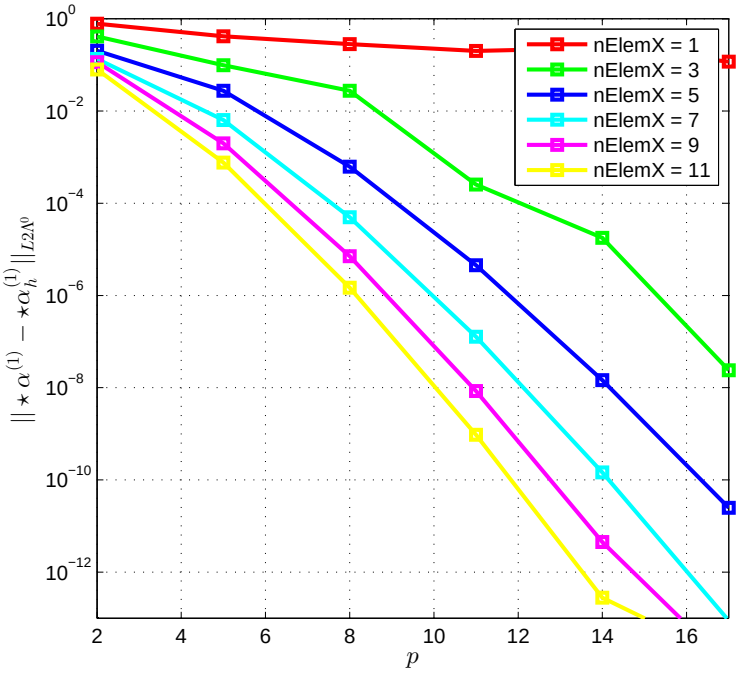

(b) p-refinement

Figure 3-11: Convergence analysis results (L^2 error) for the Hodge-$\star$ applied to a 0-form in 1D.

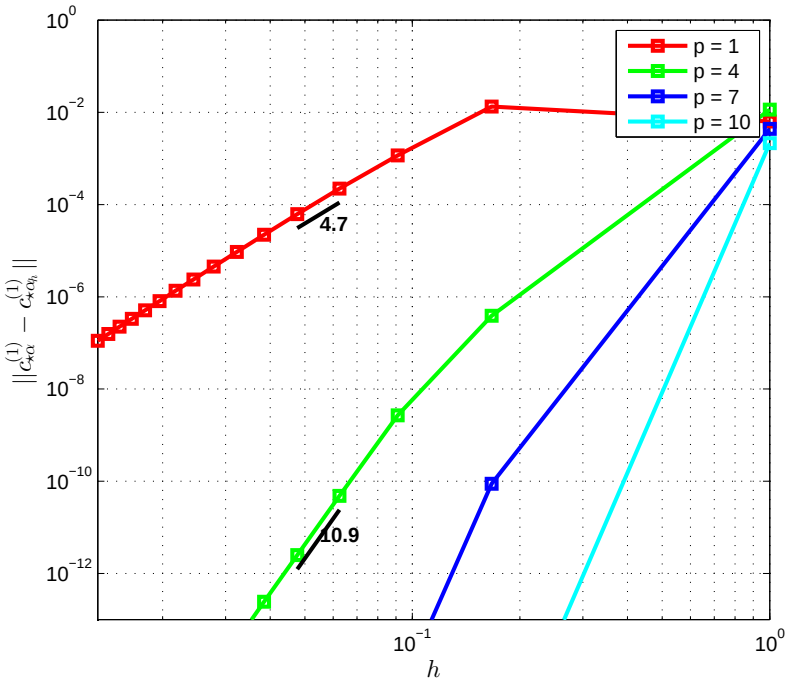

(a) h-refinement

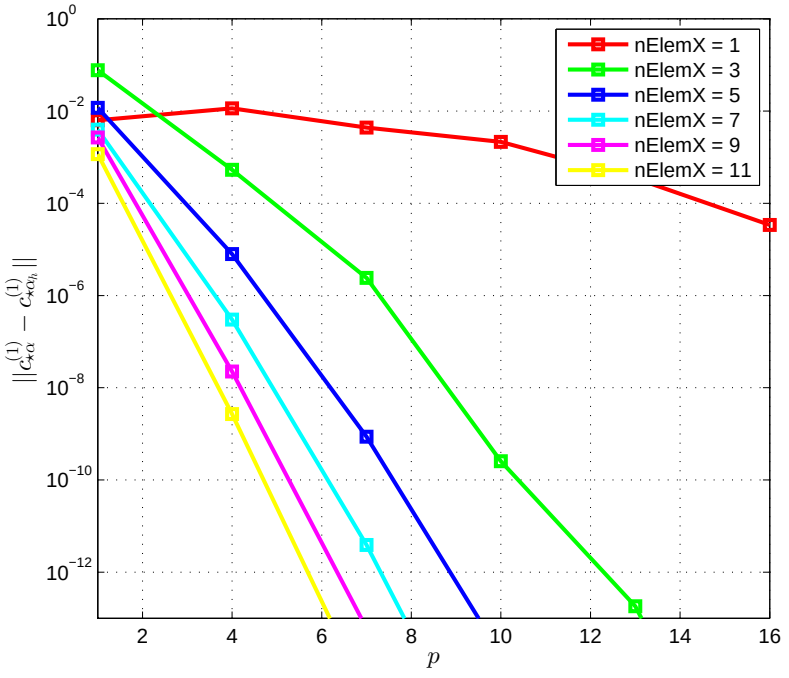

(b) p-refinement

Figure 3-12: Convergence analysis results (RSS error for cochains) for the Hodge-$\star$ applied to a 0-form in 1D.

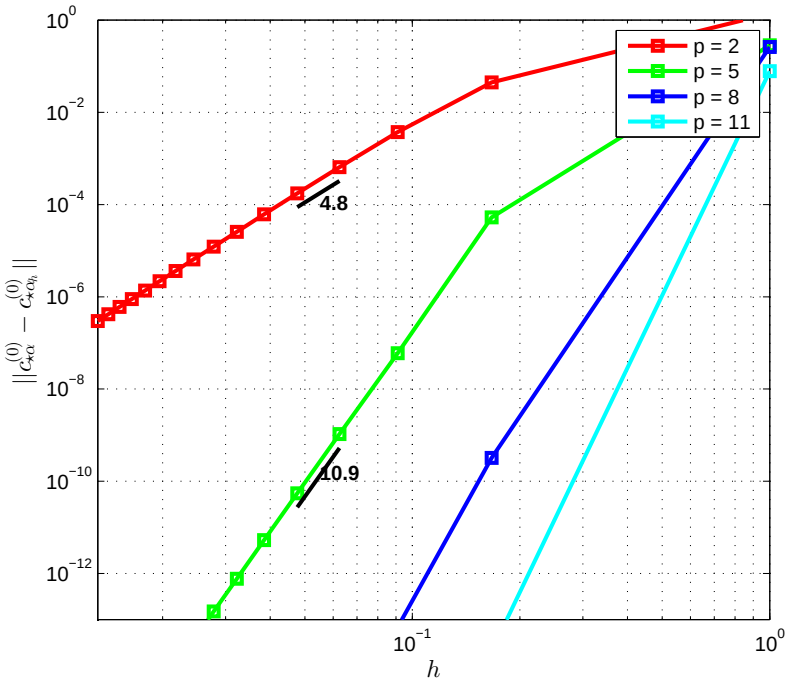

(a) h-refinement

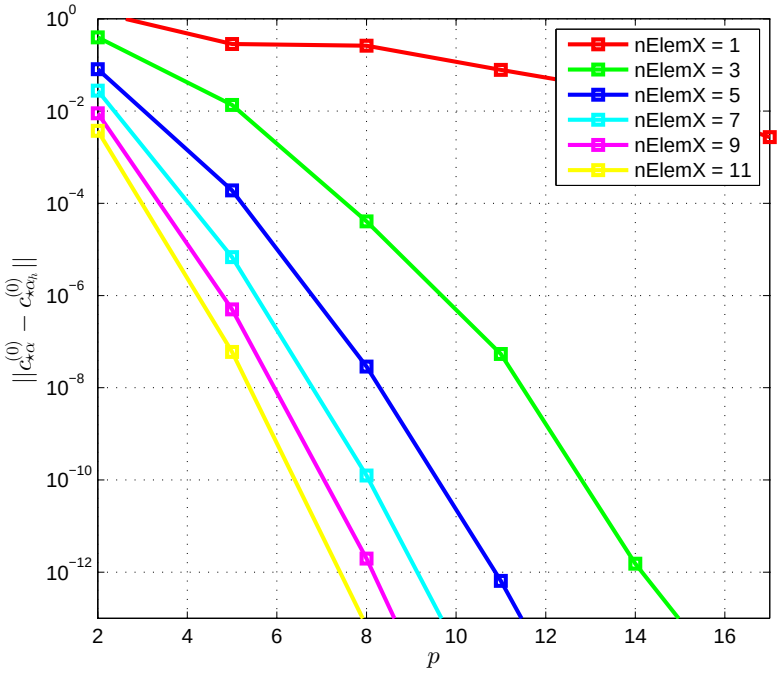

(b) p-refinement

Figure 3-13: Convergence analysis results (RSS error for cochains) for the Hodge-$\star$ applied to a 1-form in 1D.

Depending on the boundary conditions, i.e. if we can calculate $\star\alpha^{(1)}$ at boundaries (in other words $\mathrm{tr} \star \alpha^{(1)}$) or not, the boundary integral in the above equation will be either a known quantity (by imposing $\star\alpha_h^{(1)} = \star\alpha^{(1)}$ at the boundaries), or else it will have to be written in terms of the unknown cochain corresponding to $\alpha^{(1)}$. In case the boundary integral is a known quantity, the type of the boundary conditions is going to be Dirichlet with respect to $\alpha^{(1)}$. The test functions, $\tau^{(0)}$, can be chosen to be the 0-form basis functions and the final equation in matrix representation can be written as,

$$(M_{1,1}\bar{\alpha})_e - B_e = (M_{0,0}\bar{\beta})_e \tag{3-16}$$

Again, note that if Dirichlet boundary conditions are prescribed, the boundary integral matrix, B, can be evaluated, and is simply going to be a column vector. Else, it is going to be a matrix multiplied with the 1-cochain, $\bar{\alpha}$, and can be included in M. The convention, explained in the last section, is reiterated here: $M_{k,k}$ is the global inner-product matrix between the basis functions for k-forms with k-forms; $\bar{\alpha}$ and $\bar{\beta}$ are the 1- and 0-cochains, respectively; and B is the boundary integral matrix.

The errors involved in the cochains (RSS error) are shown in Figure 3-14 and in the interpolation of cochains (L^2 error) in Figure 3-15.

3.6 Discrete Laplace Operator

Laplace-deRham operator, Δ, was defined as shown in (2-64). The construction of the operator is straightforward and it can be done simply by the multiplications of discrete d and $d^\star$ matrices that were derived earlier. A system of equation is easy to setup and solve. This operator is present in the mathematical definitions of a number of physical problems, and some of these will be investigated in the next chapter where solutions of some test cases are presented.

3.7 Discrete Interior Product

The interior product physically represents instantaneous fluxes and, as was explained in Chapter 2, and the discretization is implemented as the formal adjoint of the wedge product [19]. Thus, for $(\alpha^{(1)}, \beta^{(0)}, \tau^{(0)}) \in \bigwedge^1(\Omega) \times \bigwedge^0(\Omega) \times \bigwedge^0(\Omega)$, we have the following,

$$\left\langle \mathfrak{i}_{\boldsymbol{u}}\alpha^{(1)}, \tau^{(0)} \right\rangle = \left\langle \alpha^{(1)}, u^{(1)} \wedge \tau^{(0)} \right\rangle \tag{3-17}$$

Here, $\boldsymbol{u}$ is the velocity field under which the volume form $\alpha^{(1)}$ is changing and $\mathfrak{i}_{\boldsymbol{u}}\alpha^{(1)}$ is like the instantaneous flux of the volume form. Note that $u^{(1)}$ is the 1-form obtained by *lowering the index* of $\boldsymbol{u}$ (i.e. multiplication by the metric tensor which is a second-rank covariant tensor). The implementation of the interior product is thus done through (3-17) with the selection of $\tau^{(0)}$ as the 0-form basis functions. Since we work with integral quantities, the

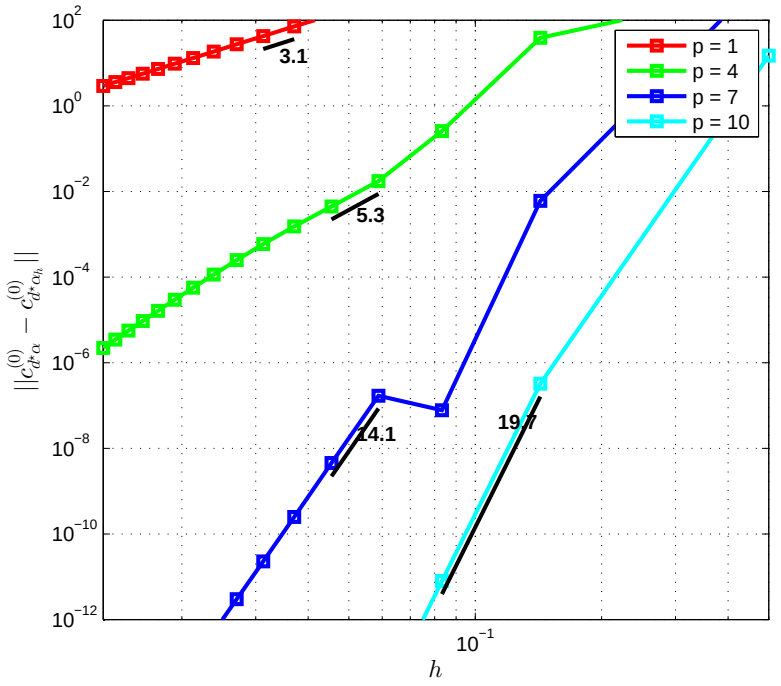

(a) h-refinement

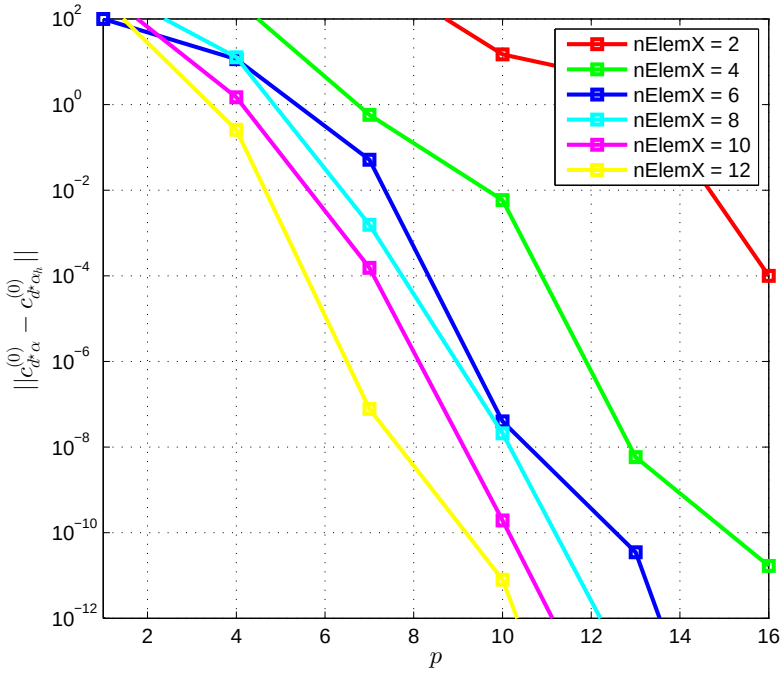

(b) p-refinement

Figure 3-14: Convergence analysis results (RSS error for cochains) for the codifferential applied to a 1-form in 1D.

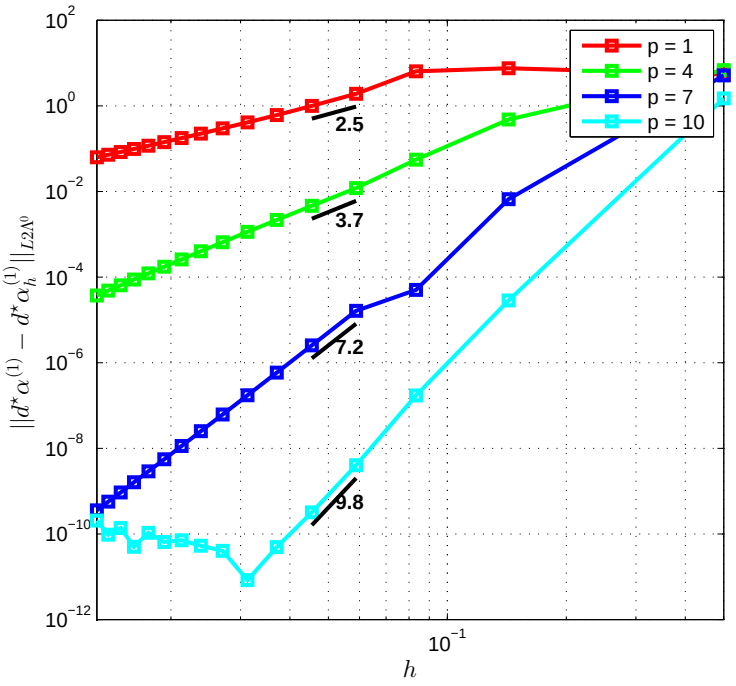

(a) h-refinement

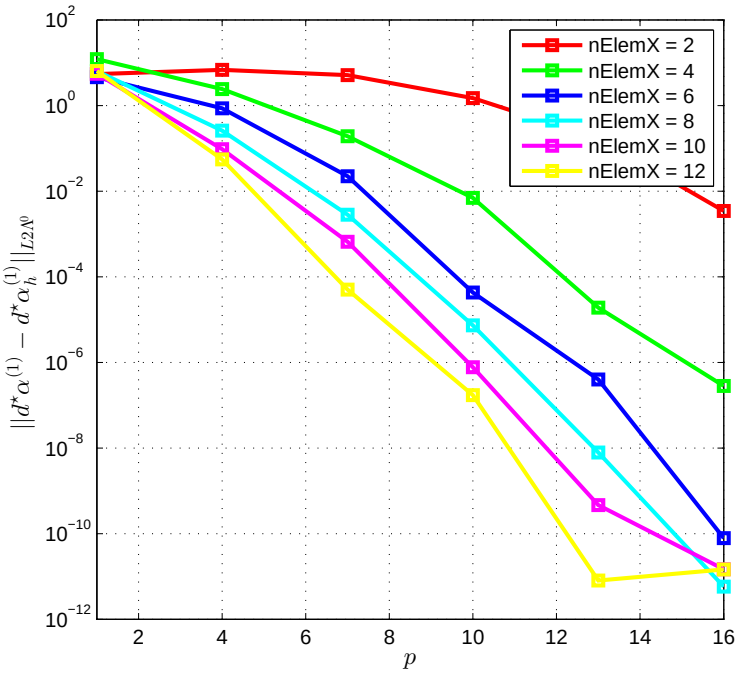

(b) p-refinement

Figure 3-15: Convergence analysis results (L^2 error) for the codifferential applied to a 1-form in 1D.

full statement of interior product's implementation in a discrete setting is obtained as follows after a multiplication with the volume form σ,

$$\int_{\Omega} \left\langle \mathfrak{i}_{\boldsymbol{u}} \alpha^{(1)}, \tau^{(0)} \right\rangle \sigma = \int_{\Omega} \left\langle \alpha^{(1)}, u^{(1)} \wedge \tau^{(0)} \right\rangle \sigma \tag{3-18}$$

This can again be cast in matrix form as, assuming $\beta^{(0)} \in \bigwedge^0(\Omega)$ such that $\mathfrak{i}_{\boldsymbol{u}} \alpha^{(1)} = \beta^{(0)}$,

$$(M_{0,0}\bar{\beta})_e = (A \bar{u}^D C \bar{\alpha})_e \tag{3-19}$$

In the above equation, A is the matrix of the operation $(\tau^0 \wedge \mathcal{I})$, and C is the matrix of the operation $(. \wedge \star\mathcal{I})$, and $\bar{u}^D$ is the diagonalized cochain-vector. This is for one elements and for the multielement case the matrices can be assembled and the interior product implemented.

A convergence plot for the 0-forms obtained after application of the interior product to a volume form in 1D are shown in Figure 3-16, and the errors in interpolation of these 1-forms in Figure 3-17.

3.8 Discrete Lie Derivative

As explained in Section 2.1, the Lie Derivative is simply obtained by applying a combination of the exterior derivative and the interior product to forms. As was seen earlier, the exterior derivative is a topological operator and thus the cochains obtained as such are indeed going to be exact upto the accuracy of the interior product.

3.9 Time-stepping Scheme

Unsteadiness is at the heart of several problems of interest in fluid flow problems. A simple evolution problem in time for $\alpha^{(p)} \in \bigwedge^p(\Omega)$ in the presence of only a velocity field $\boldsymbol{u}$ is simply stated as:

$$\frac{\partial \alpha^{(p)}}{\partial t} + \mathcal{L}_{\boldsymbol{u}} \alpha^{(p)} = 0 \tag{3-20}$$

Now, for the treatment of the above problem in time with a geometric approach, the approach adopted in [8] which is a slight modification of the scheme implemented in [36] is implemented where we treat $\alpha^{(p)}$ as an element of $\bigwedge^p(\Omega) \times \bigwedge^0(T)$ (where T is the domain in time that extends from time-instant t_n to t_{n+1}) - thus, as a p-form in space and as a 0-form in time - $\alpha^{(p)}_{(0)}$. The subscript of (0) signifies the rank of the differential form in time. The above means that $\dfrac{\partial \alpha^{(p)}}{\partial t}$ is treated as a 1-form in time. This implies that $\mathcal{L}_{\boldsymbol{u}} \alpha^{(p)} \in \bigwedge^p(\Omega) \times \bigwedge^1(T)$ and thus it should naturally integrate on time-intervals. However, because of a decouple space and time discretization, $\mathcal{L}_{\boldsymbol{u}} \alpha^{(p)}$ is evaluated at each time-instant, and is thus represented using Lagrange polynomials. In order to get the correct 1-forms in time using this representation, a projection on edge-basis functions in temporal direction should be done. Thus, without such a projection, $\mathcal{L}_{\boldsymbol{u}} \alpha^{(p)}$ is going to be represented as $\mathcal{L}_{\boldsymbol{u}} \alpha^{(p)}_{(0)}$

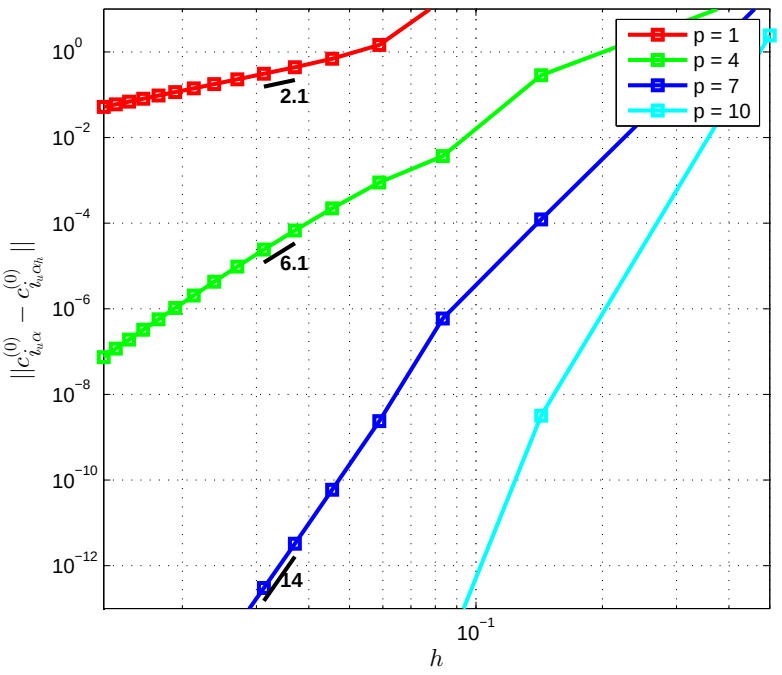

(a) h-refinement

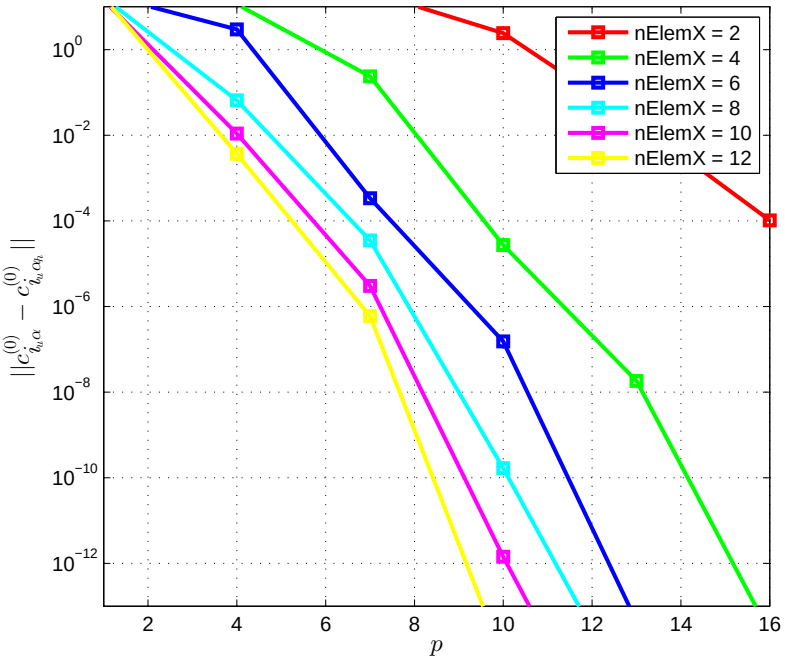

(b) p-refinement

Figure 3-16: Convergence analysis results (L^2 error) for the interior-product of 1-forms in 1D.

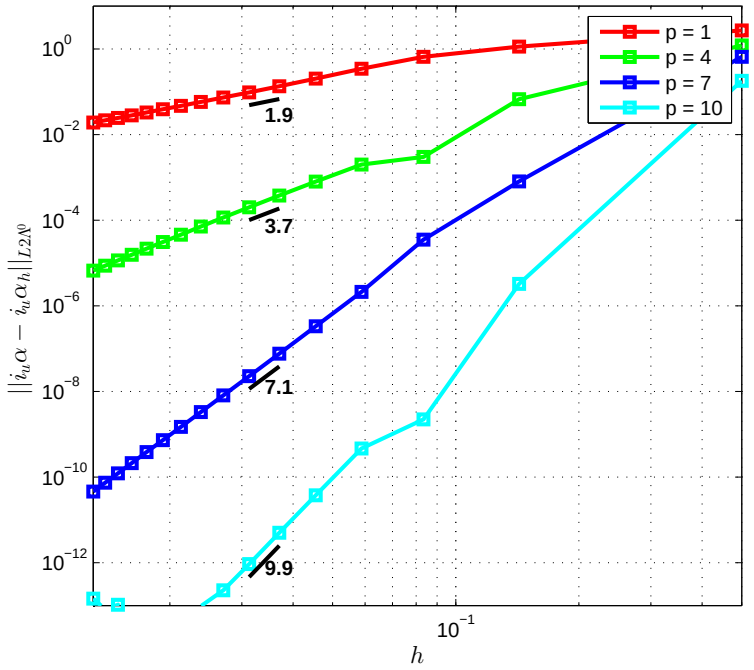

(a) h-refinement

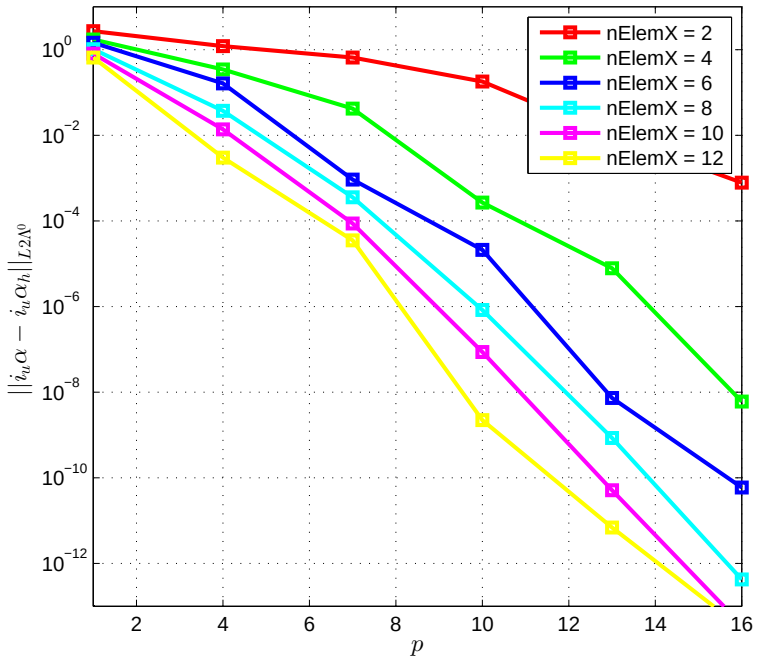

(b) p-refinement

Figure 3-17: Convergence analysis results (RSS error in cochains) for the interior-product of 1-forms in 1D.

Now, (3-20) can be posed in the following integral form,

$$\alpha^{(p)}_{(0)}\Big|_{t_{n+1}} - \alpha^{(p)}_{(0)}\Big|_{t_n} + \int_T \mathcal{L}_{\boldsymbol{u}} \alpha^{(p)}_{(0)} = 0 \tag{3-21}$$

It is easy to see that the first two terms in the above equation represent simply the coboundary operator applied to $\alpha^{(p)}_{(0)}$ in time. The discretization of the above in time can thus be performed in a similar manner as explained in earlier sections. For the 1- and 0-forms in time, we again use the Edge and Lagrange basis functions for interpolation.

Let $-\mathcal{L}_{\boldsymbol{u}}\alpha^{(p)}$ be represented by $\beta^{(p)}_{(0)} \in \bigwedge^p(\Omega) \times \bigwedge^0(T)$, then the problem reduces to finding $\beta^{(p)}_{(1)}$ such that the following holds $\forall \tau^{(p)}_{(1)} \in \bigwedge^p(\Omega) \times \bigwedge^1(T)$:

$$\left(\tau^{(p)}_{(1)}, \frac{\partial \alpha^{(p)}_{(0)}}{\partial t}\right)_T = \left(\tau^{(p)}_{(1)}, \beta^{(p)}_{(0)}\right)_T$$

To simplify the above expression, it is assumed that the Lie-derivative's action can be represented by the matrix L acting on the spatial p-cochains, $\bar{\alpha}$ that are 0-forms in time. Then, for the above equation, we can get the following matrix system in terms of 0- and 1-cochains in time,

$$(M_{1,1} D_t^{1,0} \bar{\alpha})_e = (N_{1,0} L \bar{\alpha})_e$$

where the subscript e indicates that this equation is for one temporal element or, in other words, for one time-step. The matrix $D_t^{1,0}$ is the coboundary matrix in time which, when applied to 0-forms in time, yields 1-forms in time; M represents the inner-product of temporal Edge basis functions; and the matrix N represents the wedge product of temporal Edge basis functions with temporal Lagrange polynomials.

Using this system, the evolution of $\alpha^{(p)}_{(0)}$ can be solved for. If the Lie-derivative matrix depends on the values of $\alpha^{(p)}_{(0)}$ as well (non-linear evolution), solution can be obtained for the above system by linearizing it with an initial guess and then iterating till convergence is obtained.

Now that we have outlined the implementation of the operators that come handy in the solution of steady as well as unsteady problems, we look at some test problems that we can solve by simple application of these operators in Chapter 4.

Chapter 4

Test Cases

In this chapter, a step forward is taken by presenting the discretization of a set of standard physical problems. We start by reviewing steady cases (1D and 2D) in Section 4.1, and then a few unsteady cases are presented in Section 4.2.

4.1 Steady Test Cases

The first problems that are tried out are steady in nature thereby eliminating the use of the time-stepping scheme and simplifying the analysis.

4.1.1 One-dimensional Problems

Helmholtz Eigenvalue Problem This problem describes the solution of different modes of vibration for a acoustic pressure wave in a pipe. It has a similar structure to the equation used for describing the modes of vibrations of a string. We investigate everything from the acoustic-wave perspective.

The problem definition in vector calculus for pressures, (p), can be simply stated as:

$$\nabla^2 p + k^2 p = 0, \qquad \text{in } \Omega \tag{4-1}$$

- A general boundary condition:

$$a\frac{dp}{dx} + bp = c, \qquad \text{on } \partial\Omega \tag{4-2}$$

where $\Omega = [0 \quad 1]$.

This problem has analytical solutions for pressures with which we can compare our solution. The general form of the boundary condition above can be used to impose Dirichlet or Neumann boundary conditions depending on the values of a, b and c.For homogeneous Dirichlet/Neumann boundary conditions on the pressures,

$$\text{Homogeneous Dirichlet: } (a, b, c) = (0, 1, 0)$$
$$\text{Homogeneous Neumann: } (a, b, c) = (1, 0, 0)$$

the eigenfunctions for this problem are sinusoidal (see Figure 4-1).

An attempt is now made to translate the above problem in differential geometry terms. Selection of an inner-oriented mesh is made, and on this mesh, pressures are treated as 0-forms (or the duals of pressures, see Section 5.2). Remembering the relation between the vector-calculus Laplace-operator and the Laplace operator used in differential geometry (see Chapter 2), we can reformulate the problem as:

$$-\Delta p^{(0)} + k^2 p^{(0)} = 0, \qquad \text{in } \Omega \tag{4-3}$$

In order to translate the boundary conditions, we note that since pressure is being treated as a 0-form, its exterior derivative must be a 1-form. In order to prescribe the value of this 1-form on the boundary of our 1-dimensional manifold (which would be a 0-dimensional manifold), we make use of the trace-operator which is defined for this particular case as follows.

$$\text{tr} : \bigwedge^k \mathcal{M} \to \bigwedge^k \partial\mathcal{M} \tag{4-4}$$

For more properties of the operator, please see [45]. It can be seen as the evaluation of the k-form, that is usually evaluated on $\mathcal{M}$, on a part of $\mathcal{M}$ (the boundary, in this case). Using this operator, the boundary conditions can be written down as,

- Homogeneous boundary conditions:

$$tr(\star dp^{(0)}) = 0, \qquad \text{on } \partial\Omega_1 \qquad \text{(Neumann; prescribed flux)} \tag{4-5a}$$
$$p^{(0)} = 0, \qquad \text{on } \partial\Omega_2 \qquad \text{(Dirichlet; prescribed pressure)} \tag{4-5b}$$

where Ω_1 and Ω_2 compose $\partial\Omega$. The results for eigenfunctions can be seen in Figure 4-1.

4.1.2 Two-dimensional Problems

Maxwell Eigenvalue Problem

The Maxwell Eigenvalue problem can be seen as the problem describing the modes of vibration of electric-field intensity confined to a cavity. It is a vector-laplacian problem, and can be formulated in vector calculus notation for electric field intensity ($\boldsymbol{u}$) as follows:

$$\nabla \times (\nabla \times \boldsymbol{u}) = \lambda \boldsymbol{u} \qquad \text{in } \Omega \tag{4-6a}$$
$$\nabla . \boldsymbol{u} = 0 \qquad \text{in } \Omega \tag{4-6b}$$

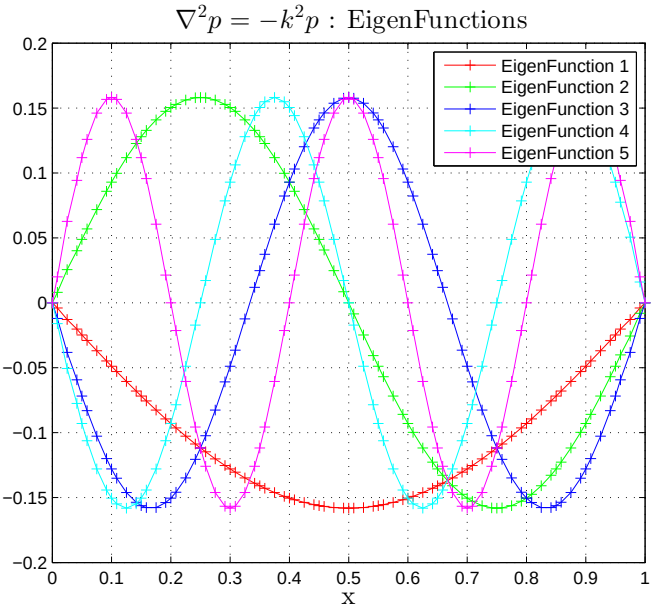

(a) Dirichlet-Dirichlet

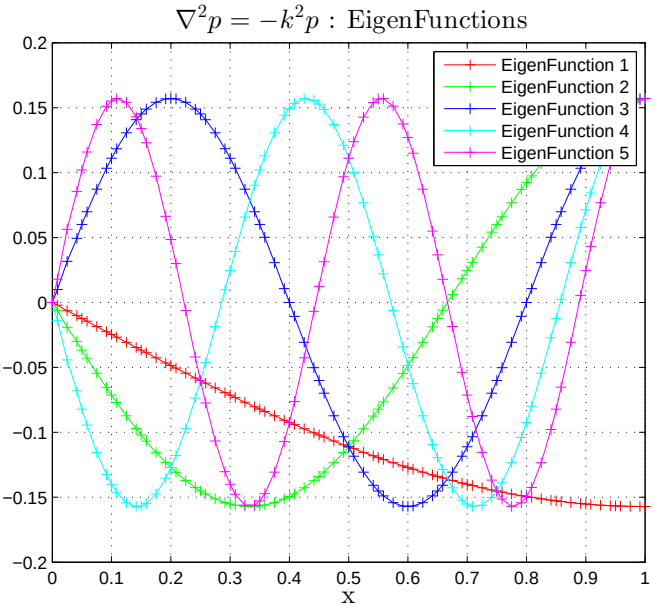

(b) Dirichlet-Neumann

Figure 4-1: Helmholtz Equation: Eigenfunctions for the Helmholtz eigenvalue problem are shown above for different sets of boundary conditions. A homogeneous Dirichlet condition on pressure implies zero perturbation pressure (i.e. the open end of a pipe that is in touch with outside air), and a homogeneous Neumann condition on pressure implies zero flux (i.e. the closed end of a pipe which does not allow perpendicular velocities). Number of elements = 20; Order of elements = 4

- Boundary conditions:

$$\boldsymbol{u} \times \boldsymbol{n} = 0 \qquad \text{on } \partial\Omega \tag{4-7}$$

where $\Omega = [0 \quad \pi]^2$. This problem, for the mentioned domain, admits solutions of the type (see Figure 4-2):

$$\lambda = a^2 + b^2, \qquad a, b = 0, 1, 2, ... \tag{4-8}$$

The integer-solutions that λ should admit are not seen in conventional nodal finite-element method discretization; a continuous spectrum of eigenvalues is obtained. This is precisely the kind of spurious modes that need to be avoided.

In order to formulate the problem in differential geometry terms, we note that electric-field intensity is defined on lines, and has a sense of being *along* these lines. Thus, choosing the mesh as inner-oriented and treating electric-field intensity as a 1-form, the problem is rewritten in the following form:

$$d^\star du^{(1)} = \lambda u^{(1)} \qquad \text{in } \Omega \tag{4-9a}$$

$$d^\star u^{(1)} = 0 \qquad \text{in } \Omega \tag{4-9b}$$

- Homogeneous boundary conditions:

$$tr(u^{(1)}) = 0 \qquad \text{on } \partial\Omega \tag{4-10}$$

The boundary condition is synonymous to saying that the tangential component of electric-field intensity at the boundaries should be zero. The obtained eigenvalues in this way are shown in Figure 4-2.

Potential Flow Problem

In this part a potential flow problem for flow around a circular cylinder is solved. This kind of problem describes what the flow would be if it were inviscid, incompressible, and irrotational. The problem can be formulated in vector calculus as follows for the velocity potential (ϕ):

$$\nabla^2 \phi = 0, \qquad \text{in } \Omega \tag{4-11a}$$

$$\nabla \phi = \boldsymbol{v}_0, \qquad \text{on } \partial\Omega \tag{4-11b}$$

where $\boldsymbol{v}_0$ is the known velocity on $\partial\Omega$. The computational domain here is, $\Omega(r, \theta) = [1 \quad 10] \times [-\pi \quad 0]$, and the radius of the cylinder is 1 units. The θ domain only extends from $[-\pi \quad 0]$ because the problem is symmetric about the diameter parallel to the freestream velocity of the flow - so, only one half of the physical domain needs to be treated.

In order to reformulate the problem in differential geometry terms, the nature of ϕ needs to be established first. It is known that ϕ is a scalar function, and thus should be a 0- or a 2-form

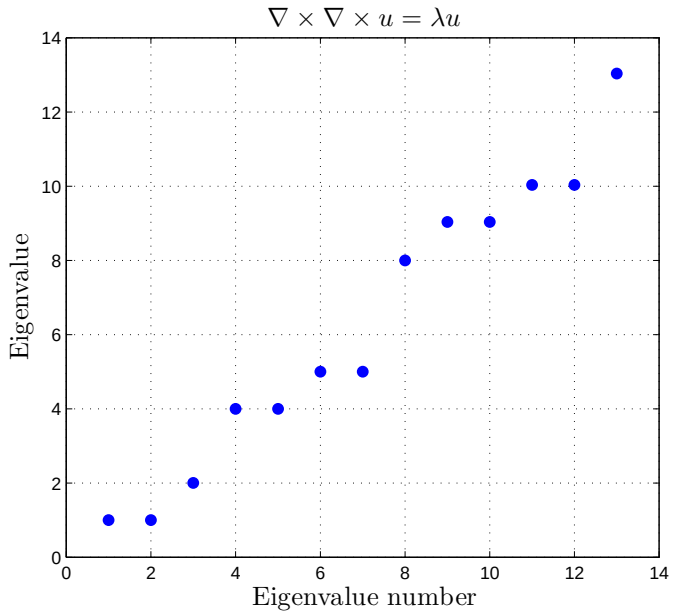

Figure 4-2: Maxwell eigvenvalue problem: Eigenvalues for the Maxwell eigenvalue problem for an electromagnetic resonant cavity. Only the non-zero eigenvalues are shown. A number of numerical methods fail to capture the discrete eigenvalue spectrum [46]. Number of elements (X, Y) = (1,1); Order of elements = 7

in 2D. In addition, it is known that on taking the gradient of ϕ, velocities are obtained. To be more specific, since

$$\begin{aligned} d\phi &= \frac{\partial \phi}{\partial x}\, dx + \frac{\partial \phi}{\partial y}\, dy \\ &= u\, dx + v\, dy \end{aligned} \tag{4-12}$$

it seems that the differential of ϕ yields inner-oriented quantities (u along dx and so on). Then, it seems obvious to associate ϕ with inner-oriented 0-forms. Then, choosing an inner-oriented mesh, rewriting the problem in differential geometry terms becomes straightforward:

$$-\Delta \phi^{(0)} = 0 \tag{4-13}$$

- Boundary Conditions:

$$tr(d\phi^{(0)}) = v_0^{(1)}, \qquad \text{on } \partial\Omega \qquad \text{(Neumann; prescribed velocity/fluxes)} \tag{4-14}$$

The boundary conditions are synonymous in the sense that the velocities are prescribed everywhere on the boundary. Note that this yields a purely Neumann problem for ϕ implying that it can be solved upto a constant only. The results for the velocity- and pressure-fields can be seen in Figure 4-3.

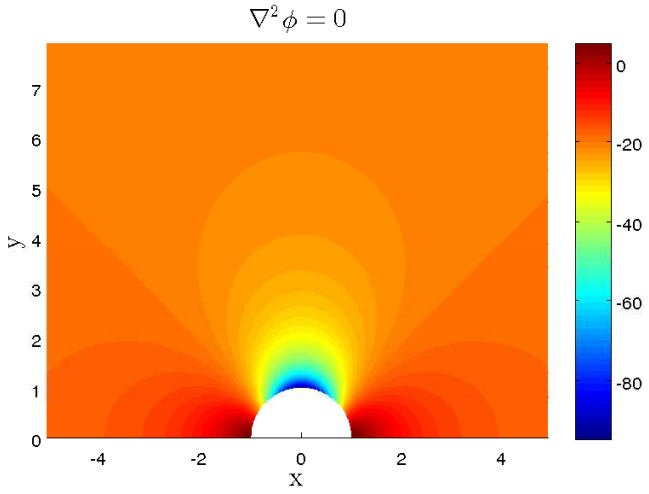

(a) Pressure-field

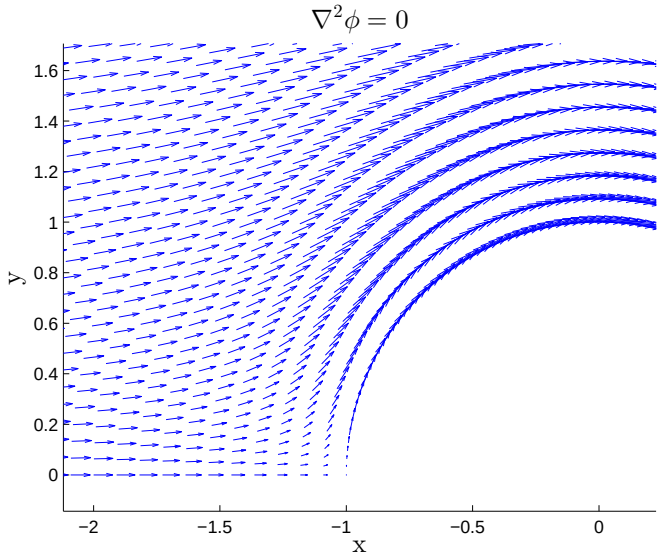

(b) Velocity close to the cylinder

Figure 4-3: Potential flow: Solutions for the pressure-field ($p = \frac{1}{2}(V^2 - U_\infty^2)$), and the velocity close to the cylinder($\boldsymbol{v} = \nabla\phi$). It can be seen visually that they display the expected traits (high-pressure stagnation regions and low-pressure high-velocity regions at the correct positions, as well as no flux through the cylinder walls). The results were compared to analytical solutions and displayed exponential convergence (graphs not shown) with increasing order of the method. Number of elements(R, θ) = (1,1); Order of elements = 15.

Darcy Flow Problem

Darcy flow is a steady, pressure-driven flow through a porous media where the fluxes and pressures are linearly related. The problem definition in vector calculus in terms of pressures (p) and fluxes ($\boldsymbol{q}$) can be given as:

$$\boldsymbol{q} + \frac{K}{\mu}\nabla p = 0 \qquad \text{in } \Omega \tag{4-15a}$$

$$\nabla \cdot \boldsymbol{v} = \phi \qquad \text{in } \Omega \tag{4-15b}$$

- Boundary conditions:

$$\boldsymbol{q} = \boldsymbol{q}_0 \qquad \text{on } \partial\Omega \tag{4-16}$$

where $\Omega = [0 \quad 1]^2$; K, μ are material properties (permeability and viscosity); and ϕ is the divergence of the velocity, $\boldsymbol{v}$ (so basically mass generation). Note that fluxes, $\boldsymbol{q}$, and velocities, $\boldsymbol{v}$, are obviously dependent variables.

The Darcy law establishes a relation between the pressures and the fluxes, and fluxes are known to be associated with crossing directions through geometric objects (outer-oriented forms). Thus, an outer-oriented mesh is chosen for solving the problem with the pressures (outer-oriented volume-forms; see Section 5.2) and velocities being treated as main unknowns.

$$p^{(\tilde{2})} = \star p^{(0)}, \qquad q^{(\tilde{1})} = \star(u\ dx + v\ dy) \tag{4-17}$$

Using the above unknowns and dropping the $\tilde{}$ notation since the primal mesh is now outer-oriented, we can rewrite the Darcy problem as follows:

$$q^{(1)} + \star_{K/\mu} d \star p^{(2)} = 0 \qquad \text{in } \Omega \tag{4-18a}$$

$$dq^{(1)} = \phi^{(2)} \qquad \text{in } \Omega \tag{4-18b}$$

- Boundary conditions:

$$q^{(1)} = q_0^{(1)} \qquad \text{on } \partial\Omega \tag{4-19}$$

The above problem states the same things as the original problem: fluxes are linearly related to pressure gradients; volumetric-strain rate is dictated by the source of mass generation (depletion) in the domain; and the fluxes through boundaries are known.

Two test cases were run for this problem corresponding to [27, 47]. The [27] test case is a manufactured-solution test-case with the following exact-solution:

$$\begin{aligned} p^{(2)} &= \cos(\pi x)\cos(\pi y) \\ \phi^{(2)} &= 2\pi^2 \cos(\pi x)\cos(\pi y) \end{aligned} \tag{4-20}$$

The [47] test case is a patch-test with a discontinuous velocity-profile prompted by discontinuous material parameters through the domain. This discontinuous velocity profile is given by,

$$\begin{aligned} u(x,y) &= \begin{cases} 0.3, & (x,y) \in [0 \quad \frac{1}{3}) \times [0 \quad 1] \\ 0.7, & (x,y) \in [\frac{1}{3} \quad \frac{2}{3}) \times [0 \quad 1] \\ 0.5, & (x,y) \in [\frac{2}{3} \quad 1] \times [0 \quad 1] \end{cases} \\ v(x,y) &= 0, \quad \forall\ (x,y) \in \Omega \end{aligned} \tag{4-21}$$

The results for this problem can be seen in Figures 4-4 and 4-5.

4.2 Unsteady Test Cases

The time-stepping scheme as explained in Chapter 3 was implemented for a simple test cases which are also outlined in [48] and a brief overview of the results is given here.

4.2.1 One-dimensional Problems

Active Field Advection

A velocity-field represented by 0-forms in 1D on an outer-oriented mesh, $q^{(0)}$, evolves under its own influence. The evolution equation is defined by 1D Burgers' equation as follows:

$$\frac{\partial q^{(0)}}{\partial t} + \mathcal{L}_{\boldsymbol{u}} q^{(0)} = -\nu \Delta q^{(0)} \tag{4-22}$$

, where $q^{(0)} = \star u^{(1)}$, ν is the viscosity, and $u^{(1)}$ is the 1-form associated with the velocity.

A small amount of diffusion is added to the equation in the form of ν in order to prevent the solution from becoming too oscillatory after a point. This happens because of the shock formation which causes a discontinuity in the solution. This kind of solution can not be represented by Lagrange basis functions that were used because they assume that 0-form solutions can be represented in a continuous way across elements. A few time-frames from the simulation are shown in Figure 4-6. The movie can be seen here:

http://www.youtube.com/watch?v=Ze3dd9q0btE

4.2.2 Two-dimensional Problems

Passive Field Advection

A passive scalar-field represented by the 2-form , $\rho^{(2)}$ ($= \sin(\pi x)\sin(\pi y)\ dx \wedge dy$), is carried by a velocity field. The evolution equation is then represented as follows:

$$\frac{\partial \rho^{(2)}}{\partial t} + \mathcal{L}_{\boldsymbol{u}} \rho^{(2)} = 0 \tag{4-23}$$

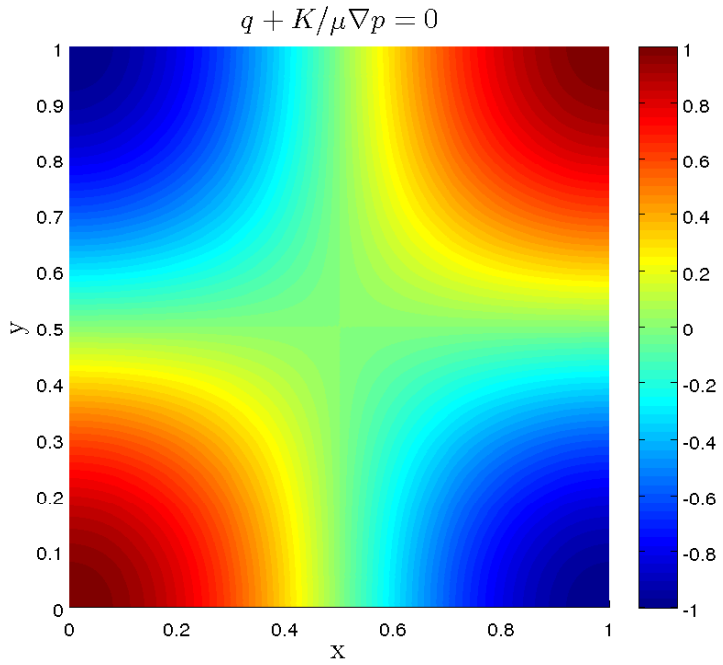

(a) Pressures

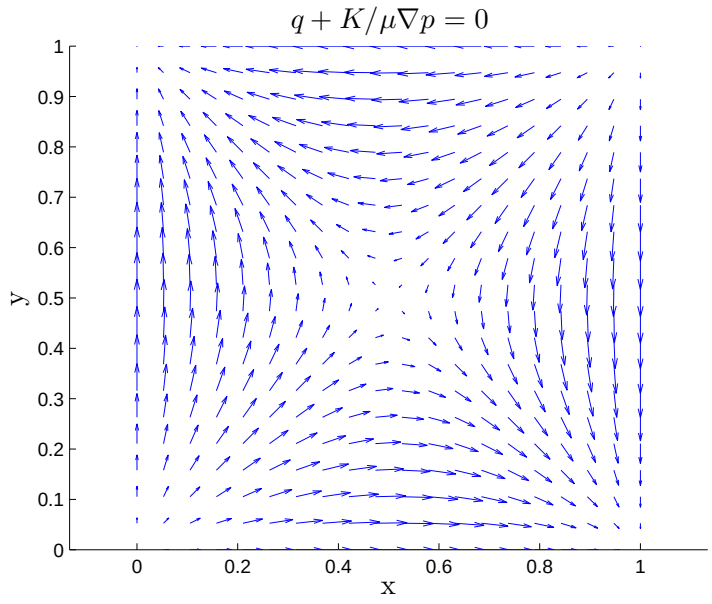

(b) Velocity vectors

Figure 4-4: Darcy Flow: Solutions for the manufactured solution. The results compare well with the analytical values, and show exponential convergence with the order of method (not shown). Number of elements (X, Y) = (1,1); Order of elements = 10.

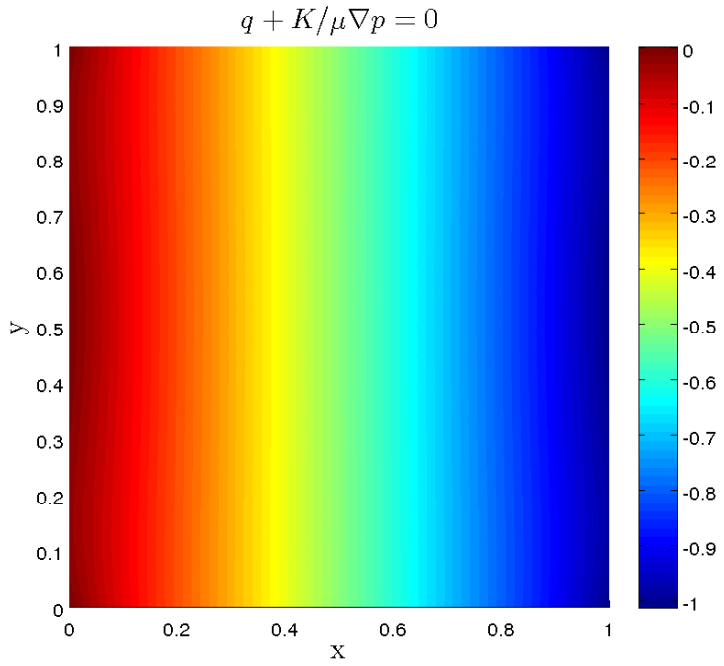

(a) Pressures

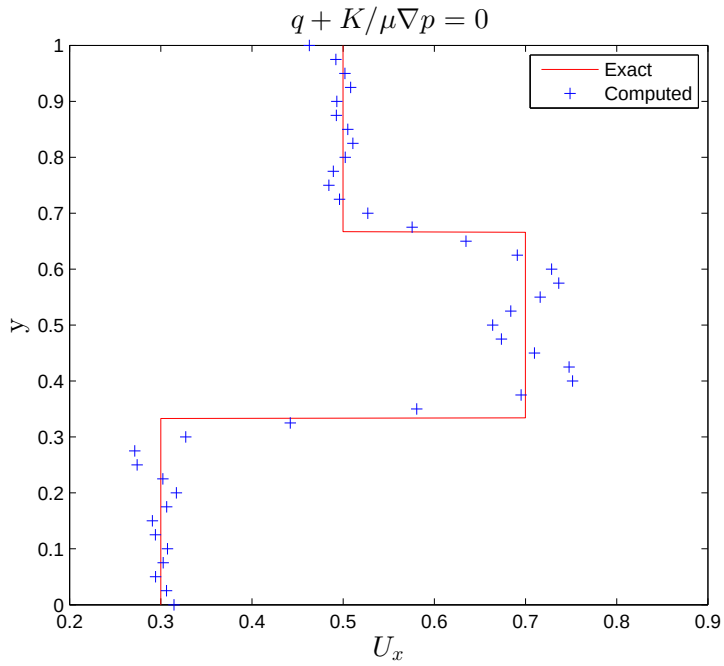

(b) Velocities computed at a fixed X

Figure 4-5: Darcy Flow: Solutions for a patch test with discontinuous velocity profile. If the discontinuity coincides with the element boundaries, the solution is always exact, but when the discontinuities lie inside elements, as shown above, the solution is oscillatory, and these don't disappear (Gibb's phenomenon). Although, as can be seen from the pressure profile, the pressures in this case are still perfectly linear. Number of elements(X, Y) = (1,1); Order of elements = 20.

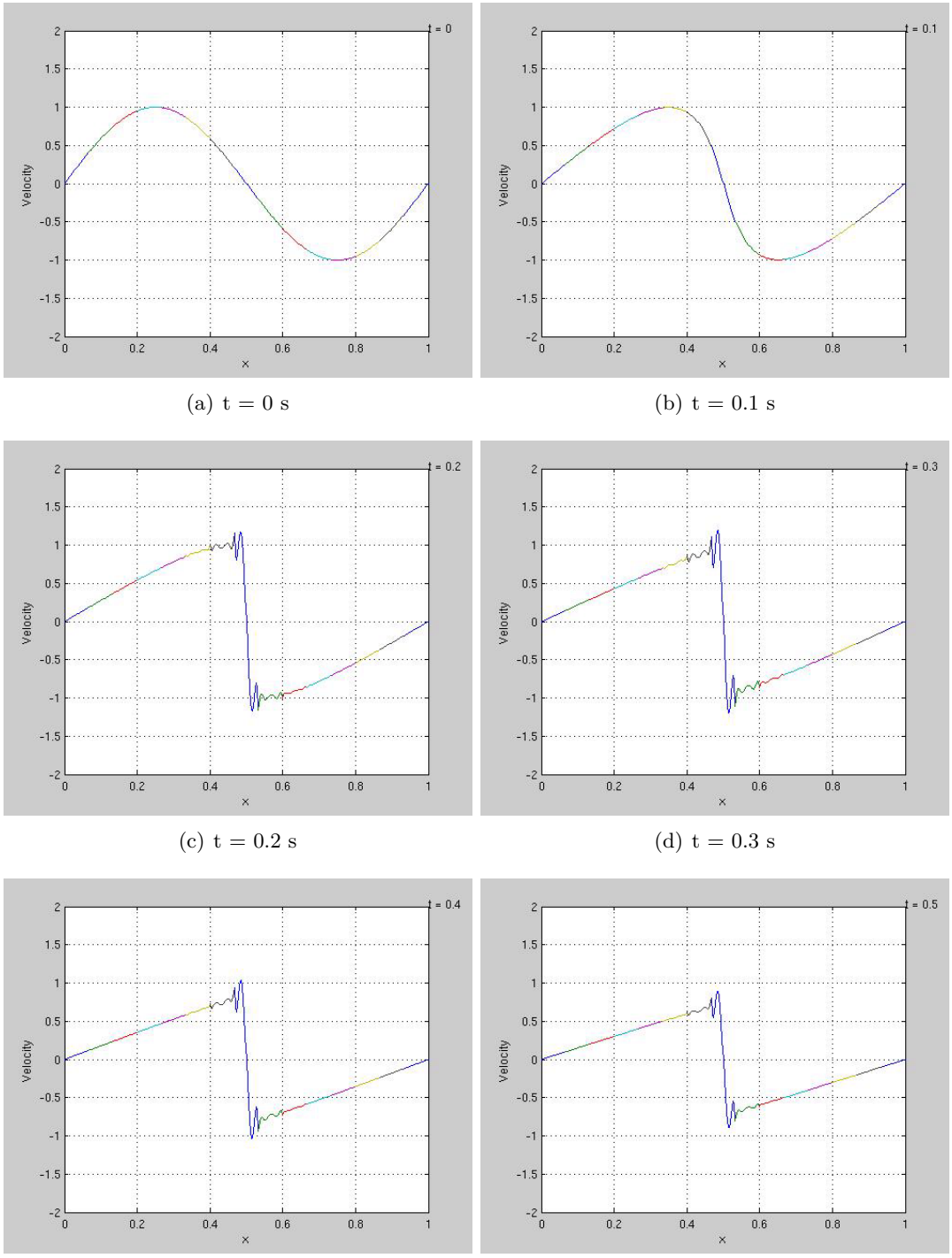

(a) t = 0 s (b) t = 0.1 s

(c) t = 0.2 s (d) t = 0.3 s

(e) t = 0.4 s (f) t = 0.5 s

Figure 4-6: Shock development (t = 0.2 s) for an initial sinusoidal velocity distribution (t = 0 s) is shown. The shock causes a discontinuity in the solution which is not supported by Lagrange basis-functions, and this causes the oscillatory solution (t = 0.2 + sec). A small amount of diffusion is added to stop the oscillations from becoming too big. Number of elements = 15; Order of elements = 4

where $u^{(1)}$ ($= \sin(\pi x)\cos(\pi y)\ dx - \cos(\pi x)\sin(\pi y)\ dy$) is the 1-form associated with the velocity-field. A few time-frames from the movie are shown in Figure 4-7. Mid-way through the movie, the velocity-field is changed to its additive inverse, and exact reversibility of the procedure is demonstrated. Mass is conserved to machine precision during the entire simulation. The movie can be seen here:

http://www.youtube.com/watch?v=Ze3dd9q0btE

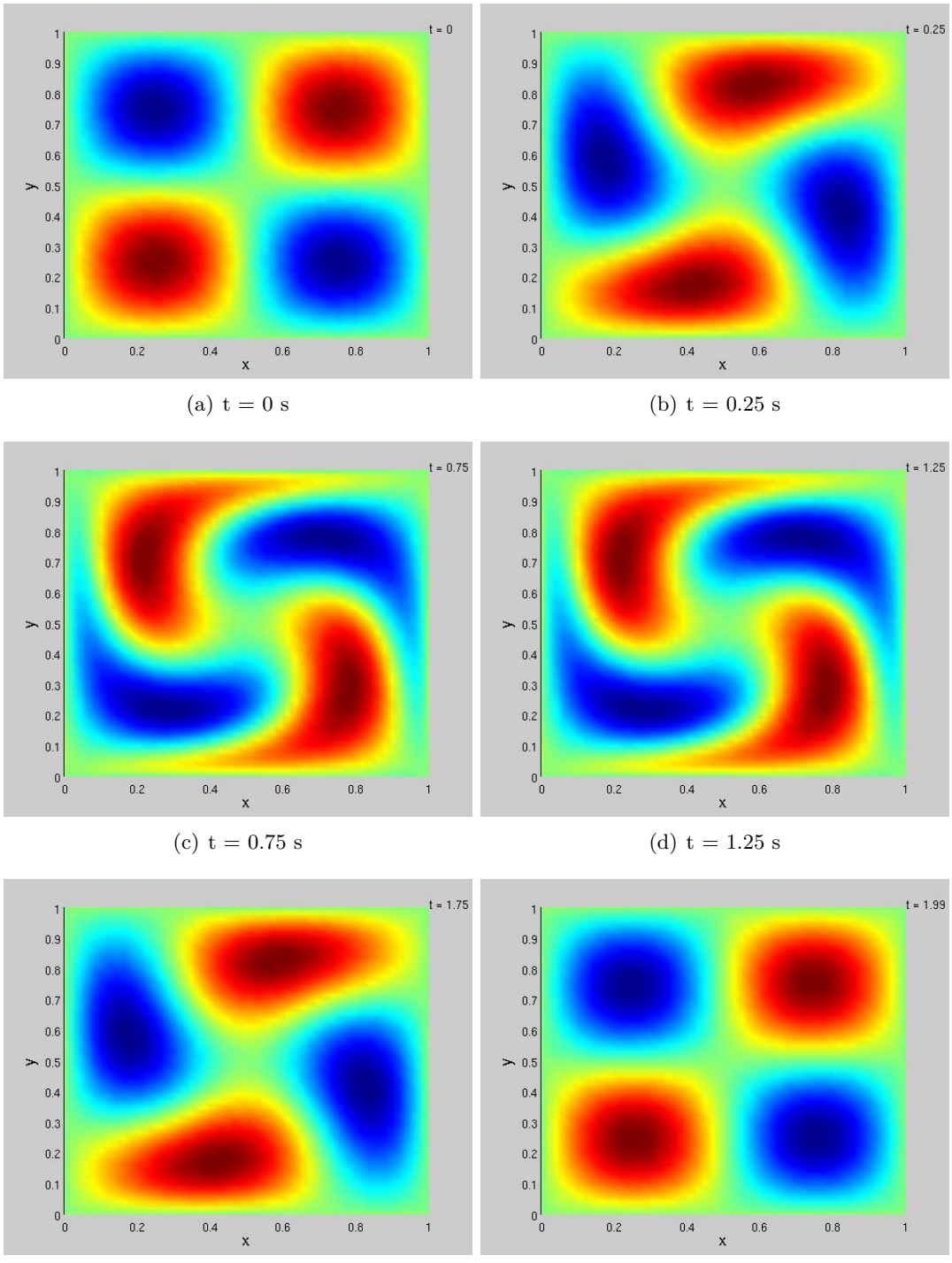

(a) t = 0 s (b) t = 0.25 s

(c) t = 0.75 s (d) t = 1.25 s

(e) t = 1.75 s (f) t = 1.99 s

Figure 4-7: A passive scalar field whose initial distribution is the one given in t = 0 s frame is advected with a constant velocity-field. At t = 1, the velocity field is reversed and the initial redistribution is reobtained. Number of elements (X, Y) = (4,4); Order of elements = 8

Chapter 5

Incompressible Navier-Stokes

The equations governing fluid-flow are the Navier-Stokes equations, and they are shown for a 2D space in Eq. (5-1a) and Eq. (5-1b).

$$\frac{\partial \rho}{\partial t} + \frac{\partial \rho u}{\partial x} + \frac{\partial \rho v}{\partial y} = 0 \tag{5-1a}$$

$$\begin{aligned} \frac{\partial \rho u}{\partial t} + \frac{\partial \rho u^2}{\partial x} + \frac{\partial \rho uv}{\partial y} &= -\frac{\partial p}{\partial x} + \mu \left(\frac{\partial^2 u}{\partial x^2} + \frac{\partial^2 u}{\partial y^2} \right) \\ \frac{\partial \rho v}{\partial t} + \frac{\partial \rho uv}{\partial x} + \frac{\partial \rho v^2}{\partial y} &= -\frac{\partial p}{\partial y} + \mu \left(\frac{\partial^2 v}{\partial x^2} + \frac{\partial^2 v}{\partial y^2} \right) \end{aligned} \tag{5-1b}$$

These equations simply represent the conservation laws pertaining to mass Eq. (5-1a) and momentum Eq. (5-1b), and are the fundamental building blocks for fluid-flow analysis in an Eulerian framework. Mass conservation can alternatively be represented as in Eq. (5-2) where it is assumed that the ρ is constant, and hence only the divergence of velocity needs to be enforced as zero for mass conservation. This is the incompressibility constraint.

$$\nabla . \boldsymbol{v} = 0 \tag{5-2}$$

In this chapter, the above two basic conservation laws are talked about. We take a look at the variables in the equations one by one in Section 5.2 and Section 5.3, and then by figuring out the necessary operators needed to represent the laws as shown above. A control-volume approach, shown in Section 5.1 that can be found in any Aerodynamics textbook ([49], for instance) is adopted for this task as it is, in spirit, a measurement-based derivation that implicitly stays strongly rooted in the principles of mimetic discretization. Next, in Section 5.4, we look at how we can discretize the above two equations while sticking to the principles of mimetic discretizations introduced earlier. Final formulations are shown in Section 5.5.

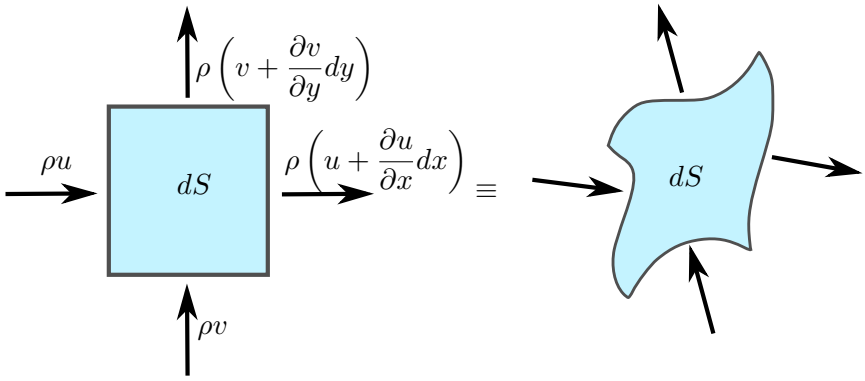

Figure 5-1: Mass-conservation is a scalar-conservation law and remains the same even if the volume is deformed. This is because the fluxes are scalar in nature as well.

5.1 A Control-Volume Formulation

A quick recap is done of the basic structure of control-volume approach towards derivation of mass and momentum conservation laws for the Navier-Stokes equations. For this purpose, consider a cartesian infinitesimal 2D-volume element, dS, shown on the left-side of Figure 5-1 and Figure 5-2, which is one of the many parts of a larger volume, S (not shown).

5.1.1 Mass conservation

Let the velocity in 2D be represented by,

$$\boldsymbol{v} = u\ \boldsymbol{\partial_x} + v\ \boldsymbol{\partial_y} \tag{5-3}$$

Then mass contained inside the 2D-volume, S, can be written down as,

$$\int_S \rho\ dS$$

and the change in this amount of mass should depend solely on the mass-fluxes through the walls of the control volume (in the absence of a mass source/sink inside the volume). This is written in form of the following familiar equation,

$$0 = \frac{\partial}{\partial t}\int_S \rho\ dS + \int_C \rho(\boldsymbol{v}.\boldsymbol{n})\ dC \tag{5-4}$$

where C is the curve bounding the 2D-volume ($= \partial S$), and $\boldsymbol{n}$ is the outward normal direction to this 2D-volume. In case there is a mass source/sink inside the volume, it would appear on the left-hand side of the equation. As shown in Figure 5-1, since this is a scalar conservation law, even if the volume is not a cartesian volume as shown but rather a deformed one, the conservation law takes on an equivalent form.

Note that here we are talking only about static volumes. If the volume was itself moving, then the velocity, $\boldsymbol{v}$, used for calculating the mass-flux through the bounding surface, $\int_C \rho(\boldsymbol{v}.\boldsymbol{n})\ dC$, would be the velocity of the fluid relative to the bounding surface.

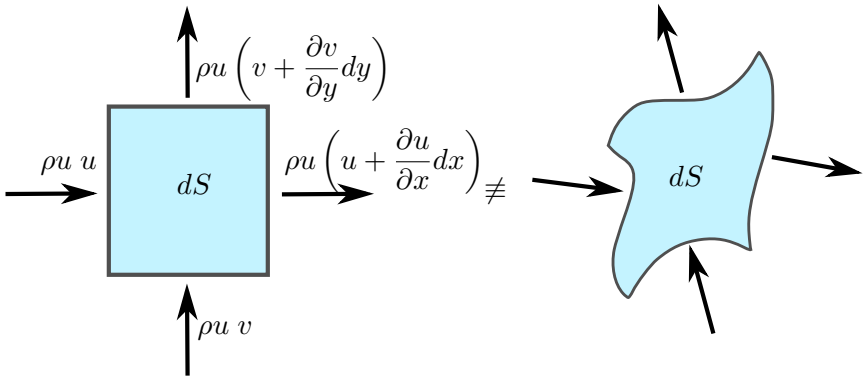

Figure 5-2: Momentum-conservation is a vector-conservation law and the fluxes involved are vector in nature as well. This means that fluxes at two different positions can not be simply added/subtracted unless it is known how the coordinate system changes.

5.1.2 Momentum Conservation

Momentum conservation has essentially the same formulation as mass conservation. Consider, for instance, only the momentum in x-direction. This quantity of momentum contained in S can be represented as,

$$\int_S \rho u \, dS$$

The change in this amount of momentum then should be equal to the total force being applied on the control-volume (Newton's second law) augmented by the net outflow/inflow of momentum because of the velocity field. This is represented as follows,

$$\sum F_S + \sum F_C = \frac{\partial}{\partial t}\int_S \rho u \, dS + \int_C \rho u(\boldsymbol{v}.\boldsymbol{n}) \, dC \tag{5-5}$$

where, again, C is the curve bounding the 2D-volume ($= \partial S$), and $\boldsymbol{n}$ is the outward normal direction to this 2D-volume. The derivation of this conservation law in other directions follows suit.

It can be seen that there are two kinds of forces that are being applied to the control-volume and these are categorized as follows:

- Surface-forces (applied on C): *pressure-force, stresses etc*
- Body-forces (applied on S): *buoyancy, electric-force etc*

What is clear from the above formulations of mass and momentum is the presence of hints of association of variables with only certain kinds of geometric objects. For instance, *surface*-forces and convective momentum-fluxes are integrated on C, and *body*-forces and momenta are integrated on S. Preserving this association is precisely the point of this exposition. Next, it is explored how the above procedure can be carried out using the framework developed in Chapter 2 and Chapter 3.

As shown in Figure 5-2, the outflow/inflow of momentum can be calculated by just adding/-subtracting the components in any direction. This is however not possible for a deformed control volume as the coordinate system may change from one point to another, and there would be no way to add/subtract flux-components unless the way the vector/covector-basis changes is known. This is exactly the information encoded in the Christoffel symbols, Γ^i_{jk}, that were used in Eq. (2-46) and the 1-forms, ω^i_r used in Eq. (2-48).

Note that in the following, only 2D space is considered. As a result, all body-forces are forces acting on 2D geometric objects which are referred to as *volumes*, S, and all surface-forces are forces acting on 1D geometric objects which are referred to as *surfaces*, C. In addition to this, point geometric objects are referred to as P.

5.2 Primary Variables' Formulation

The primary variables involved in fluid-flow are velocity and pressure. Before talking about the discretization of these variables, we should first try to associate these variables with appropriate geometric objects. The discretization then should follow directly from these associations. Therefore, it is fruitful to invest some time in understanding where these variables *live*. This section only deals with continuous formulations of these variables, and discretization is looked at in the next section.

5.2.1 Velocity

The PIV example that was presented in Section 1.1 showed that velocity naturally integrates with respect to time to yield the displacement of a particle. In a space-time coupled framework, velocity would be most appropriately associated with temporal curves if an Eulerian view is adopted (and with a space-time curve, or a particle's pathline, for a Lagrangian view). However, as was explained in Section 3.9, we work with discretizations that are decoupled in space and time. Hence, we must find a way to associate velocities appropriate geometric objects in space.

Velocity, in space, is most appropriately visualized as a contravariant vector-field. This is represented using the contravariant coordinate basis vectors in $\mathbb{R}^2$ as:

$$\mathbf{v} = \boldsymbol{\partial_x} \otimes u + \boldsymbol{\partial_y} \otimes v \tag{5-6}$$

The above can be seen as a variable that is a *vector-valued zero-form*.

5.2.2 Pressure

Pressure is a scalar-field variable. This makes it obvious that its treatment must be as a 0-form or a volume-form - but which one? The choice becomes clearer if we include orientation in our consideration. Consider the treatment of pressure as a 0-form.

$$p^{(0)} = p \tag{5-7}$$

Then, if we take the exterior derivative of the pressure, we get,

$$\mathrm{d}p^{(0)} = \frac{\partial p}{\partial x}\, dx + \frac{\partial p}{\partial y}\, dy \tag{5-8}$$

It is already known that, for instance, a term such as $\frac{\partial p}{\partial x}$ gives a sense of de-acceleration to the flow in x-direction. Visualizing this de-acceleration as a forcing term in x-direction, we see that this gives a sense of a force *along* the x-direction. This implies that the application of the exterior derivative, d, to 0-form pressures yields inner-oriented 1-forms. This means that treatment of pressure as a 0-form should correspond to inner-oriented 0-forms.

Once the above has been established, it is trivial to state that the treatment of pressure as a 2-form (the dual of 0-form pressure) should be associated to outer-oriented volumes (the duals of inner-oriented 0-forms). From here onwards, even if orientation is not specified, the particular treatment of pressures (as a 0- or a 2-form) should make it clear what the orientation is. We select the outer-oriented volume-form as our primary view, and then the inner-oriented 0-form pressures are simply the duals of our primary variable, which are outer-oriented 2-form pressures.

5.2.3 Density

Treatment of density is one for which everyone has a very good physical intuition - it is known that density integrates naturally on volumes to give mass (see Section 1.1).

$$\rho^{(2)} = \rho\, dxdy \tag{5-9}$$

This, however, doesn't complete the formulation because, just like pressures, we still have to assign an orientation to the volume $dxdy$. This can be done if we think about the form of mass conservation that was introduced in Eq. (5-1a).

$$\frac{\partial \rho}{\partial t} + \frac{\partial \rho u}{\partial x} + \frac{\partial \rho v}{\partial y} = 0 \tag{5-1a}$$

We can choose to write down Eq. (5-1a) in the an integral formulation which is most suitable for our mimetic methods.

$$\int_S \frac{\partial \rho}{\partial t}\, dS + \int_{\partial S} \rho \boldsymbol{v}.\boldsymbol{dC} = 0 \tag{5-10}$$

The above equation states that the net change in ρ can be related to the boundary integral of its *fluxes*. Noting that fluxes are outer-oriented forms (in other words, variables associated with a *crossing* direction through geometric objects), we see that the above equation makes perfect sense for tracking the changes in an outer-oriented volume-form - thus, $dxdy$ should be endowed with an outer-orientation. This reasoning can in fact be applied to all kinds of densities (mass/momentum/energy).

Mass Conservation

The constraint for mass-conservation, Eq. (5-1a), can now be formulated using the above ingredients. In differential geometry terms, the mass inside an outer-oriented volume, S, can be written down with the help of the 2-form, $\rho^{(2)} = \rho\ dxdy$, as

$$\int_S \rho\ dxdy$$

In essence, Eq. (5-1a) is a conservation law for the 2-form, $\rho\ dxdy$. Let us represent this 2-form by the symbol, σ_ρ. The evolution equation for this density-weighted standard volume-form can be written down in integral form as,

$$\int_S \frac{\partial \sigma_\rho}{\partial t} + \int_S \mathcal{L}_{\boldsymbol{v}}\ \sigma_\rho = 0 \tag{5-11}$$

The first term in Eq. (5-11) doesn't need to be explained. The second term can be explained with the help of a flux-oriented interpretation of the interior-product. We know that the Lie-derivative of σ_ρ can be written down as follows.

$$\mathcal{L}_{\boldsymbol{v}}\ \sigma_\rho = \mathrm{di}_{\boldsymbol{v}}\ \sigma_\rho \tag{5-12}$$

The interior-product of σ_ρ evaluated on a 1D-surface, C, can be interpreted as the transverse-flux of σ_ρ through this surface. In other words, it just the mass-flux through the surface. We also know that the application of the exterior derivative to these fluxes is analogous to the evaluation of their boundary integral through the boundary of S (see Section 2.1). Then the Lie-derivative of σ_ρ is simply the net-outflow of this volume-form (mass-outflow) through the boundaries of the volume, S, and Eq. (5-11) is seen to make sense as the conservation law for mass.

Note that since we work only with fluids with constant densities, it is easy to see that after some manipulation, Eq. (5-11) can be reduced to Eq. (5-13). This is simply the differential geometry formulation for Eq. (5-2)! It is known that this formulation simply equates the volumetric-strain rate to zero.

$$\mathcal{L}_{\boldsymbol{v}}\ dxdy = 0 \tag{5-13}$$

Even though the above equation should suffice for constant density flows, in this work we choose to work with Eq. (5-11) simply because it conveys more information physically. Thus, a final form of mass-conservation for the test cases considered here is the following.

$$\mathcal{L}_{\boldsymbol{v}}\ \sigma_\rho = 0 \tag{5-14}$$

5.3 Derived Variables' Formulation

Now that the formulations of primary variables have been established, we look at the variables that are derived from these variables and are present in the momentum Eq. (5-1b): namely momentum, momentum flux, pressure-forces, and stresses.

5.3.1 Momentum

If we look at Eq. (5-1b), it would seem like the discretization of conservation of momentum could be done simply by conserving a 1-form associated to the vector-velocity, $\boldsymbol{v}$. This was done in [50] where a formulation for Stokes' equation was done using At this point, if we recall the definition for momentum, or "quantity of motion" that is given in [11],

> The quantity of motion is the measure of the same, arising from the velocity and quantity of matter conjointly.

, we see that the conservation of momentum should be geometrically related to quantity of matter as well. A 1-form is then not the correct way to go as an association with quantity of matter, or mass, clearly implies the association with volumes! Turning to control-volume based derivations of momentum conservation, we know that momentum (density) is something that

- integrates on a volume, and
- has a vectorial nature i.e. has components.

In addition to the above, we know that the work done, W, is the path integral of forces, F,

$$W = \int \boldsymbol{F}.\boldsymbol{dx} \tag{5-15}$$

and that forces are related to momenta, m, by,

$$\Delta \boldsymbol{m} = \int \boldsymbol{F}\ dt \tag{5-16}$$

The above suggests that, since work should be coordinate independent and metric free, force should be covector-valued forms in space (and time, but we don't consider that here). Therefore, the momenta are then treated as *covector-valued volume-forms* here, $m^{(1,2)}$. This idea was also mentioned in [51]. In other words, momentum densities are things that integrate on volumes to give components, and these components are covectors. Note that, as has already been explained, the volume-form with which momentum densities are associated, $dxdy$, are outer-oriented.

Before formulating an expression for the momenta, we first take a look at the Euclidean metric tensor in 2D. The metric tensor, as defined in Chapter 2, for $\mathbb{R}^2$ is simply,

$$G = \begin{bmatrix} 1 & 0 \\ 0 & 1 \end{bmatrix} \tag{5-17}$$

but this is a purely mathematical version of the metric. It should be mentioned here that there is no canonical way to connect vectors and covectors and this must be done by introducing extra-structure on the manifold (the Lagrangian, see [16] p.55). We thus attempt to introduce

a more physical version of the metric tensor by looking at the kinetic energy and how it depends on velocities. Kinetic energy, T, is frequently represented as a positive definite symmetric form in the velocities, and can be written down in the following *local* form.

$$T_L = \frac{1}{2}\sum_{i,j} g_{ij} v^i v^j \tag{5-18}$$

This is called a *local* form of kinetic energy here because this assumes point-particles, and their masses are contained in the metric, g_{ij}, as is shown in [16]. For our fluid continuum, kinetic energy should really be associated with volumes. From a physical perspective, kinetic energy associated with a *point* in a continuum doesn't make sense. Being a scalar, its association with volume-forms is then obvious. We thus work with the *global* form of kinetic energy, and this is represented in the following form.

$$T_G = \frac{1}{2}\sum_{i,j} g_{ij} v^i v^j \; dxdy \tag{5-19}$$

At the same time, kinetic energy can also be represented with a duality pairing between the *global* form of momentum (covector-valued volume-forms) and velocities (vector-valued 0-forms). Then, if we represent the global form of momenta by $m^{(1,2)}$, we can write down the above duality pairing as,

$$T_G = \frac{1}{2}\left\langle m^{(1,2)}, \boldsymbol{v} \right\rangle \tag{5-20}$$

Comparing the above equation with the global form of kinetic energy, we see that the global form of momenta should be represented as,

$$m^{(1,2)} = \sum_{i,j} dx^j \otimes g_{ij} v^j \; dxdy \tag{5-21}$$

Moreover, we know that the usual expression for momentum contains a mass/density term in it. Therefore we choose to include the mass/density term in the metric, g_{ij}. We modify the metric, G, to include the density, ρ, in it and write it in the following form.

$$\begin{aligned} G_\rho &= \begin{bmatrix} \rho & 0 \\ 0 & \rho \end{bmatrix} \\ &= \rho \; dx \otimes dx + \rho \; dy \otimes dy \end{aligned} \tag{5-22}$$

Using the above, the global form of momenta would be given by,

$$\begin{aligned} m^{(1,2)} &= dx \otimes \rho u \; dxdy + dy \otimes \rho v \; dxdy \\ &= dx \otimes m_x^{(2)} + dy \otimes m_y^{(2)} \end{aligned} \tag{5-23}$$

If one so wishes, one can also define a local form of momenta as follows.

$$\begin{aligned} m^{(1,0)} &= G_\rho(\boldsymbol{v}) \\ &= dx \otimes \rho u + dy \otimes \rho v \end{aligned} \tag{5-24}$$

Then the global form of kinetic energy can also be represented as,

$$T_G = \frac{1}{2}\left\langle m^{(1,2)}, \boldsymbol{v}\right\rangle \tag{5-25}$$

Before progressing to the treatment of other variables, the duality pairings being done here are explained more thoroughly in order to make the entire formulation as unambiguous as possible.

Duality Pairings Explained

Consider a 2D manifold, $\mathcal{S}$. The duality pairing that exists between a general vector basis, $\boldsymbol{e}_j$, and a covector basis, θ^i, on $\mathcal{M}$ is recounted from Section 2.1 as,

$$\theta^i(\boldsymbol{e}_j) = \delta^i_j \tag{2-3}$$

It should be noted that the above pairing for the vector- and covector-basis is only defined *at a particular point*. In other words, θ^i and $\boldsymbol{e}_j$ belong to the cotangent- and tangent-spaces defined at a point, $p \in \mathcal{S}$, $\mathcal{S}^k_{p^*}$ and $\mathcal{S}^k_p$. This should mean that when the duality pairing between momentum and for instance, a vector-basis located at point p, $\boldsymbol{\partial_i}|_p$ is done, it should yield only the momentum volume-form associcated to the particular p. If p be represented by (x_0, y_0) in the local coordinates, (x, y), this should mean that the duality pairing yields the i^{th} component of momentum evaluated at (x_0, y_0) following.

$$\begin{aligned}\left\langle m^{(1,2)}, \boldsymbol{\partial_i}|_p\right\rangle &= m^{(2)}_i\Big|_p \\ &= m^{(2)}_i\Big|_{(x_0,y_0)}\end{aligned} \tag{5-26}$$

Then, to get a global description of this particular component of momentum, the duality pairing should be done with all i^{th} vector-basis situated at all points on the manifold, that is with a *vector-field* spanning the entire manifold with the i^{th} vector-basis. This vector-field is going to be represented by $\boldsymbol{\partial_i}$, i.e. without the subscript of p to denote that this is not a vector at a point but a vector-field spanning the entire manifold. In all the work that follows, we will be working with vector-fields only.

Then, using the above, the global description of momentum components can be given as follows, which also serves as a relation between momentum and velocity components.

$$\begin{aligned}m^{(2)}_i &= \left\langle m^{(1,2)}, \boldsymbol{\partial_i}\right\rangle \\ &= \star\left\langle m^{(1,0)}, \boldsymbol{\partial_i}\right\rangle \\ &= \star\left(g_{ij}v^j\right)\end{aligned} \tag{5-27}$$

where $i, j = 1, 2$ refer to x- and y-directions, respectively. Note that these components are themselves volume-forms. We can extend the above equation to account for a general vector-fields, $\sum_i b^i\boldsymbol{\partial_i}$, rather than just the constant vector-fields, $\boldsymbol{\partial_x}$ or $\boldsymbol{\partial_y}$. Thus, the coefficients b^i are allowed to vary everywhere in space (and, in some cases, even in time as we'll see later).

$$\begin{aligned}\left\langle m^{(1,2)}, b^i\boldsymbol{\partial_i}\right\rangle &= \star\left\langle m^{(1,0)}, b^i\boldsymbol{\partial_i}\right\rangle \\ &= \sum_i m^{(2)}_i b^i\end{aligned} \tag{5-28}$$

The above is a simple extension from Eq. (5-27), and, if we think about the rules that a vector-space must follow, the above seems almost trivial. We'll be using the above extension a lot over the coming parts.

An expression for momentum-densities has, thus, been formulated associated with outer-oriented volumes. Assuming for a while that these covector-valued volume-forms can be reduced (integrated, in other words), we note that these outer-oriented volumes are going to be surrounded by outer-oriented surfaces (edges in 2D), and with these surfaces we can associate different kinds of momentum fluxes. We take a look at how we can formulate these fluxes now.

5.3.2 Convective Momentum Flux

In 2D, fluxes are associated with 1D geometric objects, and the first kind of momentum-flux that we look at is the convective flux. Convective fluxes in our formulation are covector-valued $(n-1)$-forms, which in 2D means covector-valued 1-forms. Let us represent these by the symbol $\mathcal{F}^{(1,1)}$. The calculation of these fluxes for the i^{th} component of the momentum-conservation equation is defined as,

$$\begin{aligned}\mathcal{F}_i^{(1)} &= \left\langle \mathcal{F}^{(1,1)}, \boldsymbol{\partial_i} \right\rangle \\ &= \mathfrak{i}_{\boldsymbol{v}} \left\langle m^{(1,2)}, \boldsymbol{\partial_i} \right\rangle \\ &= \mathfrak{i}_{\boldsymbol{v}} m_i^{(2)}\end{aligned} \tag{5-29}$$

Thus, we expect the fluxes in i^{th} direction to depend only on the momentum in that direction. This is used here in the context of $\mathbb{R}^2$, but in fact the above is expected to be true for all orthogonal coordinate systems. Of course, the covector-valued fluxes, $\mathcal{F}^{(1,1)}$, don't necessarily need to be weighted by a constant vector-field, and for general vector-fields the flux calculation can be extended just like it was extended for the momenta.

$$\begin{aligned}\left\langle \mathcal{F}^{(1,1)}, \sum_i b^i \boldsymbol{\partial_i} \right\rangle &= \mathfrak{i}_{\boldsymbol{v}} \left\langle m^{(1,2)}, \sum_i b^i \boldsymbol{\partial_i} \right\rangle \\ &= \sum_i \mathfrak{i}_{\boldsymbol{v}} b^i m_i^{(2)}\end{aligned} \tag{5-30}$$

As an example, using the above, we can easily derive an expression for momentum-flux components in $\mathbb{R}^2$ as shown below.

$$\begin{aligned}\mathcal{F}_i^{(1)} &= \mathfrak{i}_{\boldsymbol{v}} m_i^{(2)} \\ &= \mathfrak{i}_{\boldsymbol{v}} m_i \; dxdy \\ &= m_i \; dxdy(u \; \boldsymbol{\partial_x} + v \; \boldsymbol{\partial_y}) \\ &= m_i u \; dxdy(\boldsymbol{\partial_x}) + m_i v \; dxdy(\boldsymbol{\partial_y}) \\ &= m_i(u \; dy - v \; dx)\end{aligned} \tag{5-31}$$

5.3.3 Pressure Force

As is known from control-volume derivations of momentum conservation, pressure-forces act on surfaces bounding control-volumes (*surface* forces). This means, that in our 2D setting, we will have pressure-forces as covector-valued 1-forms, $\mathcal{H}^{(1,1)}$, just like convective momentum fluxes.

To define the components of our pressure-force, $\mathcal{H}^{(1,1)}$, the scalar-field pressures, $p^{(2)}$, defined in Section 5.2 are made use of along with the interior product.

$$\begin{aligned} \mathcal{H}_i^{(1)} &= \left\langle \mathcal{H}^{(1,1)}, \boldsymbol{\partial_i} \right\rangle \\ &= \mathfrak{i}_{\boldsymbol{\partial_i}} p^{(2)} \end{aligned} \tag{5-32}$$

The above can be understood with the help of the dynamic definition of $\mathfrak{i}_{\boldsymbol{v}}$, as was explained in Chapter 2. Consider the 2D space, and analyse the above formulation of pressure-force as follows. Pressure is a 2-form given by the following expression.

$$p^{(2)} = p\ dxdy \tag{5-33}$$

The interior product of the above 2-form with, for instance, a constant vector-field in x-direction, $\boldsymbol{\partial_x}$, yields,

$$\begin{aligned} \mathcal{H}_x^{(1)} &= \mathfrak{i}_{\boldsymbol{\partial_x}} p^{(2)} \\ &= p\ dxdy(\boldsymbol{\partial_x}) \\ &= p\ dy \end{aligned} \tag{5-34}$$

The interior product of the volume $dxdy$ above is the *opposite* of the extrusion of the surface dy under the transverse vector-field given by $\boldsymbol{\partial_x}$. In fact, these operations are adjoints of each other, as was also hinted at in Section 2.1 while defining the interior product (see Eq. (2-38), Figure 2-4). The above formulation then calculates the transverse *flux* of pressure through surfaces. Moreover, this formulation also suggests a symmetry between mass-conservation, Eq. (5-14), and pressures.

As a result of the above operation in $\mathbb{R}^2$, the scalar pressure-field is seen to integrate on edges dy and dx to yield forces in directions $\boldsymbol{\partial_x}$ and $\boldsymbol{\partial_y}$ (or $\mathcal{H}_x^{(1)}$ and $\mathcal{H}_y^{(1)}$), respectively. These can also be extended for a general vector-field in the same way as was done for convective fluxes and momenta.

5.3.4 Stress

Stresses are surface forces as well, just like the last two momentum-fluxes that we looked at. These are then covector valued 1-forms, $\mathcal{T}^{(1,2)}$, that represent the diffusion of momentum through surfaces that bound the control-volume. These also involve a material parameter, μ, in their formulation and this is, in fact, the first constitutive equation that we are going to model. The formulation for viscous stresses in i^{th} direction in vector-calculus notation is given by:

$$\boldsymbol{\tau}^i = \mu \nabla u^i \tag{5-35}$$

In a similar vein, the stresses in i^{th} direction in $\mathbb{R}^2$ can be modeled in our formulation as,

$$\begin{aligned}\mathcal{T}_i^{(1)} &= \left\langle \mathcal{T}^{(1,1)}, \boldsymbol{\partial_i} \right\rangle \\ &= d^\star_{\mu/\rho} \left\langle m^{(1,2)}, \boldsymbol{\partial_i} \right\rangle \\ &= d^\star_{\mu/\rho} m_i^{(2)}\end{aligned} \tag{5-36}$$

The above is our final formulation for diffusion of momentum fluxes. Of course, the stresses at all points pointing in a general direction can be obtained by a linear-combination of stresses weighted by vector-fields $\boldsymbol{\partial_x}$ and $\boldsymbol{\partial_y}$, as was shown for convective momentum-fluxes.

Note that all previous variables before stresses are expected to be true for a general coordinate system even though they have been presented only for $\mathbb{R}^2$. The formulation for stresses as represented above, however, holds only in coordinates where the basis vectors, $\boldsymbol{\partial_i}$, are constant in space. In other words, these are coordinate systems where two vectors located at different points in space can be compared based only on their components. In case of a general coordinates, the formulation should contain terms that take into account the variation of basis-vectors in space. In other words, it should contain the application of the exterior covariant-differential as was introduced in Section 2.1 and its adjoint instead of the exterior-derivative and the codifferential. In this work the treatment of these coordinate systems has been left out, and this should be taken up in a future work.

In Eq. (5-36), the subscript of μ/ρ on $d^\star$ is merely a reminder of the fact that the material parameter used for modeling diffusion of momentum is the kinematic viscosity. The application of material parameters, variable and constant, was discussed in Section 3.4.

Momentum Conservation

We have identified three different kinds of momentum fluxes so far - $\mathcal{F}_i^{(1)}, \mathcal{H}_i^{(1)}$ and $\mathcal{T}_i^{(1)}$. Now, we only need to relate the net outflow/inflow of momentum due to these fluxes to its total change. The total outflow of momentum because of these fluxes can be written down as,

$$\text{Net Outflow} : \mathrm{d}(\mathcal{F}_i^{(1)} + \mathcal{H}_i^{(1)} - \mathcal{T}_i^{(1)})$$

Note that the above fluxes are situated at different points in the control-volumes. In order to compare these fluxes located at different points in space, only the use of the exterior derivative with the flux-components is found to be sufficient. This is because, as was explained for stresses, the coordinate basis vectors that we use for $\mathbb{R}^2$ don't change in space. If this had not been the case, we would have had to incorporate Christoffel symbols and the exterior covariant-differential, which has been left for future work.

The conservation law for momentum is then formulated as,

$$\frac{\partial m_i^{(2)}}{\partial t} + \mathrm{d}(\mathcal{F}_i^{(1)} + \mathcal{H}_i^{(1)} - \mathcal{T}_i^{(1)}) = 0 \tag{5-37}$$

The translation of the complete Navier-Stokes equation from vector-calculus to differential-geometry is complete, and is shown below.

$$\mathcal{L}_{\boldsymbol{v}}\ \sigma_\rho = 0 \tag{5-14}$$

$$\frac{\partial m_i^{(2)}}{\partial t} + \mathrm{d}(\mathcal{F}_i^{(1)} + \mathcal{H}_i^{(1)} - \mathcal{T}_i^{(1)}) = 0 \tag{5-37}$$

Secondary Conservation Laws

A more general form of the momentum equation can be written as follows,

$$\sum_i b^i \frac{\partial \left\langle m^{(1,2)}, \boldsymbol{\partial_i} \right\rangle}{\partial t} + \sum_i b^i \mathrm{d}\left(\left\langle \mathcal{F}^{(1,1)}, \boldsymbol{\partial_i} \right\rangle + \left\langle \mathcal{H}^{(1,1)}, \boldsymbol{\partial_i} \right\rangle - \left\langle \mathcal{T}^{(1,1)}, \boldsymbol{\partial_i} \right\rangle \right) = 0 \tag{5-39}$$

It should be noted that Eq. (5-39) is the same as Eq. (5-37) with the exception that

- it is the momentum equation weighted with a general vector-field instead of a constant one, and
- the fact that it makes clear the origin of the components of momentum by writing them in terms of the duality pairing that exists between covector-fields and vector-fields.

Now, if we allow this equation to hold $\forall\ \boldsymbol{b} = \sum_i b^i \boldsymbol{\partial_i} \in T\mathcal{M}^2$, then the coefficients b^i can, in general, be functions of space and time. In such a case, we can rewrite the above equation as,

$$\begin{aligned} &\frac{\partial \left\langle m^{(1,2)}, \boldsymbol{b} \right\rangle}{\partial t} + \mathrm{d}\left(\left\langle \mathcal{F}^{(1,1)}, \boldsymbol{b} \right\rangle + \left\langle \mathcal{H}^{(1,1)}, \boldsymbol{b} \right\rangle - \left\langle \mathcal{T}^{(1,1)}, \boldsymbol{b} \right\rangle \right) = \cdots \\ \cdots &\sum_i \left\langle m^{(1,2)}, \boldsymbol{\partial_i} \right\rangle \frac{\partial b^i}{\partial t} + \sum_i \left(\left\langle \mathcal{F}^{(1,1)}, \boldsymbol{\partial_i} \right\rangle + \left\langle \mathcal{H}^{(1,1)}, \boldsymbol{\partial_i} \right\rangle - \left\langle \mathcal{T}^{(1,1)}, \boldsymbol{\partial_i} \right\rangle \right) \wedge \mathrm{d}b^i \end{aligned} \tag{5-40}$$

The above is a generalized equation for momentum conservation. Since it should hold $\forall\ \boldsymbol{b} \in T\mathcal{M}^2$, it should also hold for $\boldsymbol{b} = \boldsymbol{v} = u\ \boldsymbol{\partial_x} + v\ \boldsymbol{\partial_y}$. For this specific vector-field, Eq. (5-40) will transform to the evolution equation for Kinetic Energy. Similarly, for different vector-fields such as position and vorticity, conservation laws for angular-momentum and helicity may be obtained! Thus, we make use of this equation in the discretization of incompressible Navier-Stokes equations that is described in the next section. Note that the variables $\left\langle \mathcal{F}^{(1,1)}, \boldsymbol{b} \right\rangle$ and $\left\langle \mathcal{T}^{(1,1)}, \boldsymbol{b} \right\rangle$ can also be written down as,

$$\begin{aligned} \left\langle \mathcal{F}^{(1,1)}, \boldsymbol{b} \right\rangle &= \mathfrak{i}_{\boldsymbol{v}} \left\langle m^{(1,2)}, \boldsymbol{b} \right\rangle \\ \left\langle \mathcal{T}^{(1,1)}, \boldsymbol{b} \right\rangle &= \sum_i b^i d^\star_{\mu/\rho} \left\langle m^{(1,2)}, \boldsymbol{\partial_i} \right\rangle \end{aligned} \tag{5-41}$$

5.4 Discretisation and Implementation

So far, we have encountered vector-fields, differential-forms, and covector-valued differential forms. Discretization of some of these terms is straightforward applying the principles discussed so far, and for some of these we need to take extra care in making the jump from the infinite-dimensional world to the finite-dimensional one. This section takes a look at how this can be done for all of our variables. Note that all discretizations are done assuming an inner-oriented primal mesh.

5.4.1 Velocity and Momentum Variables

Velocity and Mass-conservation

Our final formulation for velocity is given in Eq. (5-6), and for mass-conservation in Eq. (5-13). It would seem that there is only one way of discretizing the velocity thus introduced, but we take a look at two equivalent forms of Eq. (5-13) that lead to two possible ways of discretizing the velocity.

Let $\alpha^{(1)}$ be the 1-form associated with the vector, $\boldsymbol{A}$, using the metric tensor, G.

$$\alpha^{(1)} = G(\boldsymbol{v}) \tag{5-42}$$

Then the Hodge-$\star$ can also be seen as a generalization of the following identity (see [16], Ch.14),

$$\star\, \alpha^{(1)} = \mathfrak{i}_{\boldsymbol{A}} \sigma \tag{5-43}$$

where σ is the standard volume-form (which in $\mathbb{R}^2$ is $dxdy$).

In our formualtion, the above means that we can write Eq. (5-14) in the following two equivalent forms using the metric-tensor, G_ρ.

$$\mathcal{L}_{\boldsymbol{v}}\ \sigma_\rho = \mathrm{d} \star G_\rho(\boldsymbol{v}) = 0 \tag{5-44}$$

It was pointed out that discretization is the most obvious for differential forms because of the fact that they integrate naturally on elements of the mesh to give discrete sets of numbers. Then, the two possible discretizations of velocity that can be done in accordance with Eq. (5-44) are:

1. One could discretize the one-forms associated to velocities, $\boldsymbol{v}$. This, in $\mathbb{R}^2$ using G_ρ, would be given by,
$$v^{(1)} = \rho u\ dx + \rho v\ dy \tag{5-45}$$
Let us represent this inner-oriented, density-weighted velocity by $v^{(1)}$. Its reduction is simply integration on 1-chains of the mesh, C^x_{ij} and C^y_{ij}, which are 1-chains along x- and y-axis.
$$\int_{C^x_{ij}} v^{(1)}\ dC = \bar{v}^x_{ij} \tag{5-46}$$

$$\int_{C^y_{ij}} v^{(1)}\, dC = \bar{v}^y_{ij} \tag{5-47}$$

The finite-dimensional approximation of this outer-oriented, density-weighted velocity is then,

$$v^{(1)}_h = \sum_{i,j} \bar{v}^x_{ij} e_i(x) h_j(y) + \sum_{i,j} \bar{v}^y_{ij} h_i(x) e_j(y) \tag{5-48}$$

Conservation of mass, Eq. (5-14), would then be represented in a discrete sense as follows.

$$D^{2,1} \star_h \bar{v} = 0 \tag{5-49}$$

which is simply the right-hand side of Eq. (5-44). The implementation of the exterior derivative and the Hodge-$\star$ in a discrete setting, $D^{2,1}$ and $\star_h$, has already been discussed in Chapter 2 and Chapter 3.

2. Alternatively, velocity, $\mathbf{v}$, can be treated component-wise. In this way, velocity components, u and v, are simply 0-forms evaluated at the inner-oriented 0-cells of the mesh, and since the variable is vector-valued, there are two 0-forms that need to be discretized at each 0-cell, namely u and v. Then, the appropriate velocity 0-cochains, $\bar{u}_{ij}$ and $\bar{v}_{ij}$, on 0-chains, F_{ij}, are

$$u(F_{ij}) = \bar{u}_{ij} \tag{5-50}$$

$$v(F_{ij}) = \bar{v}_{ij} \tag{5-51}$$

The finite-dimensional approximation of velocity vector discretized as such is,

$$\begin{aligned} \boldsymbol{v}_h &= u_h\, \boldsymbol{\partial_x} + v_h\, \boldsymbol{\partial_y} \\ &= \sum_{i,j} \bar{u}_{ij} h_i(x) h_j(y)\, \boldsymbol{\partial_x} + \sum_{i,j} \bar{v}_{ij} h_i(x) h_j(y)\, \boldsymbol{\partial_y} \end{aligned} \tag{5-52}$$

In such a discretization, the incompressibility constraint is given by the left-hand side of Eq. (5-44),

$$\mathcal{L}_{\boldsymbol{v}} \rho\, dxdy = 0 \tag{5-53}$$

As was shown earlier, the complete operation of the Lie-derivative on $\rho\, dxdy$ can be seen as the derivation of fluxes from the volume-form σ_ρ by an interior product with the velocity-field. These are obtained on outer-oriented 1-chains.

$$\begin{aligned} \mathfrak{i}_{\boldsymbol{v_h}} \rho\, dxdy &= \rho u_h\, dx(\boldsymbol{\partial_x}) dy - \rho v_h\, dy(\boldsymbol{\partial_y}) dx \\ &= -\rho v_h\, dx + \rho u_h\, dy \end{aligned} \tag{5-54}$$

If the above fluxes are represnted by $f^{(\tilde{1})}$, they can be reduced on the dual 1-chains of the mesh, $\tilde{C}^x_{ij}$ and $\tilde{C}^y_{ij}$, which are 1-chains along x- and y-axis. To reiterate, in our convention the $\tilde{}$ represents things associated to the dual-mesh. These need to be reduced on the dual mesh because fluxes are outer-oriented, and our primal mesh, as was mentioned at the beginning of this section, is inner-oriented.

$$\int_{\tilde{C}^x_{ij}} f^{(\tilde{1})}\, dC = \bar{f}^x_{ij} \tag{5-55}$$

$$\int_{\tilde{C}^y_{ij}} f^{(\tilde{1})}\, dC = \bar{f}^y_{ij} \tag{5-56}$$

Once we have the above outer-oriented 1-cochains, incompressibility can be enfored by taking their discrete exterior derivative.

$$D^{\tilde{2},1}\bar{f} = 0 \tag{5-57}$$

Note that in the above, the finite-dimensional density, ρ_h, is missing. Instead, ρ is being treated as though we have its infinite-dimensional representation, and this is true because we only consider cases with constant ρ.

We have managed to pose the constraint of mass-conservation in terms of velocity-unknowns (or, velocity-cochains), and now we look at the unknowns in the momentum equation and try to connect all the unknowns in a suitable way.

Momentum

If we take a look at the momentum equation as given in Eq. (5-40), we can see that the form of unknowns that we have for the momenta are simply,

$$\left\langle m^{(1,2)}, \boldsymbol{b} \right\rangle \text{ and } \left\langle m^{(1,2)}, \boldsymbol{\partial_i} \right\rangle$$

Moreover, for the vector-field, $\boldsymbol{b}$, that is being used in Eq. (5-40), we have b^i as the unknowns $\forall\, \boldsymbol{b}$. To make sense of all of this, one of the ways of treating these unknowns arises out of the following observations.

1. In our discrete setting, we have only a handful of different vector-fields that we can represent. Their general expansion can be written down in the equation below, following the convention introduced in the section on velocity's discretization.

$$\begin{aligned} \boldsymbol{b}_h &= \sum_{i,j} \bar{b}^x_{ij} h_i(x) h_j(y)\, \boldsymbol{\partial_x} + \sum_{i,j} \bar{b}^y_{ij} h_i(x) h_j(y)\, \boldsymbol{\partial_y} \\ &= \sum_{i,j} b^x_h\, \boldsymbol{\partial_x} + b^y_h\, \boldsymbol{\partial_y} \end{aligned} \tag{5-58}$$

2. Therefore, if we have $(N+1)$ points in the i and j directions, the maximum number of different $\bar{b}^x_{ij}$ and $\bar{b}^y_{ij}$ that we can have are $(N+1)^2$ independently of each other. With regards to the general form of momentum conservation shown in Eq. (5-40), we can consider the following components of the $(N+1)^2$ vector-fields in each direction, x and y.

$$\begin{aligned} x : (\bar{b}^x_{ij}, \bar{b}^y_{ij}) &= \begin{cases} (1,0) & \text{if } (i,j) = (i_0, j_0) \\ (0,0) & \text{if } (i,j) \neq (i_0, j_0) \end{cases} \\ y : (\bar{b}^x_{ij}, \bar{b}^y_{ij}) &= \begin{cases} (0,1) & \text{if } (i,j) = (i_0, j_0) \\ (0,0) & \text{if } (i,j) \neq (i_0, j_0) \end{cases} \end{aligned} \tag{5-59}$$

3. Note that the above vector fields $\forall\ (i_0, j_0)$ form a partition of unity in each directions, x and y. So, if we denote the (i_0, j_0) vector-field corresponding to direction x or y by $\boldsymbol{b}^x_{i_0j_0}$ or $\boldsymbol{b}^y_{i_0j_0}$, we can write down the following:

$$\begin{aligned}(\boldsymbol{b}^x_{i_0j_0})_h &= \sum_{i,j}(\bar{b}^x_{ij})_{i_0j_0}h_i(x)h_j(y)\ \boldsymbol{\partial_x}\\ (\boldsymbol{b}^y_{i_0j_0})_h &= \sum_{i,j}(\bar{b}^y_{ij})_{i_0j_0}h_i(x)h_j(y)\ \boldsymbol{\partial_y}\end{aligned} \tag{5-60}$$

such that for a particular k equal to x or y, we have

$$\begin{aligned}\sum_{i_0,j_0}(\boldsymbol{b}^k_{i_0j_0})_h &= \sum_{i_0,j_0}\sum_{i,j}(\bar{b}^k_{ij})_{i_0j_0}h_i(x)h_j(y)\boldsymbol{\partial_k}\\ &= \sum_{i_0,j_0}\sum_{i,j}(\bar{b}^k_{ij})_{i_0j_0}h_i(x)h_j(y)\boldsymbol{\partial_k}\\ &= \boldsymbol{\partial_k}\end{aligned} \tag{5-61}$$

because the Lagrange polynomials form a partition of unity.

Thus, using the above, we can consider momentum-components weighted by vector-fields,

$$\left\langle m^{(1,2)}, (\boldsymbol{b}^k_{i_0j_0})_h \right\rangle$$

as our primary unknowns. Let us call these *partial-momenta*. If the 2-cochains for these partial-momenta in the k^{th} direction, weighted by the (i_0, j_0) vector-field, and associated with 2-chains specified by $\tilde{S}_{ij}$, are denoted by $(\bar{m_k})^{i_0j_0}_{ij}$, we have the following expansion for the k^{th} component of these partial-momenta.

$$\begin{aligned}\left\langle m^{(1,2)}, (\boldsymbol{b}^k_{i_0j_0})_h \right\rangle &= (m^{(2)}_k)^{i_0j_0}_h\\ &= \sum_{i,j}(\bar{m_k})^{i_0j_0}_{ij}\tilde{e}_i(x)\tilde{e}_j(y)\end{aligned} \tag{5-62}$$

for k equal to x or y. Keeping in mind that the vector-fields $(\boldsymbol{b}^k_{i_0j_0})_h$ form a partition of unity in the k^{th} direction, we can establish the following relation.

$$\sum_{i_0,j_0}\left\langle m^{(1,2)}, (\boldsymbol{b}^k_{i_0j_0})_h \right\rangle = \left\langle m^{(1,2)}, \boldsymbol{\partial_k} \right\rangle \tag{5-63}$$

In the specific case that the vector-fields being used to weight the momentum components are only $\boldsymbol{\partial_x}$ and $\boldsymbol{\partial_y}$, we will, of course, we dropping the superscript of i_0j_0 from momentum components.

Thus, all three unknowns related to momentum that were identified at the beginning of this section have been taken care of.

Velocity And Momentum: Relation

We know that we can, and should be able to, establish a one-to-one relation between the cochains of velocity and the cochains of momentum. Such a relation has already been established in a continuous setting, Eq. (5-27), and can be done in the discrete setting in the following ways.

Note the following two things about this analysis:

- We consider only momentum components weighted by a constant vector-field, $\boldsymbol{\partial_k}$, or else the notation would become even more confusing!
- We show how to extract momentum-cochains if velocity cochains are being treated as the main unknowns. In case the momentum cochains are being treated as main unknowns, the velocity cochains can be obtained from the following by starting from a finite-dimensional representation of momentum, and progressing in the same spirit as below. We address this at the end of this analysis as well.

The analysis can be done for the two ways of velocity discretization that were explored earlier.

1. If the velocities are discretized as outer-oriented 1-forms, $v^{(1)}$, we have their finite-dimensional representation given by,

$$\begin{aligned} v_h^{(1)} &= \sum_{i,j} \bar{v}_{ij}^x e_i(x) h_j(y) + \sum_{i,j} \bar{v}_{ij}^y h_i(x) e_j(y) \\ &= \sum_{i,j} \bar{v}_{ij}^x \epsilon_i(x) h_j(y)\ dx + \sum_{i,j} \bar{v}_{ij}^y h_i(x) \epsilon_j(y)\ dy \\ &= (-\rho v_h)\ dx + (\rho u_h)\ dy \end{aligned} \tag{5-64}$$

2. Alternatively, if the velocities are discretized as vector-valued 0-forms, $\boldsymbol{v}$, we have their finite-dimensional representation given below.

$$\begin{aligned} \boldsymbol{v}_h &= \sum_{i,j} \bar{u}_{ij} h_i(x) h_j(y)\ \boldsymbol{\partial_x} + \sum_{i,j} \bar{v}_{ij} h_i(x) h_j(y)\ \boldsymbol{\partial_y} \\ &= u_h\ \boldsymbol{\partial_x} + v_h\ \boldsymbol{\partial_y} \end{aligned} \tag{5-65}$$

   We can then find out the finite-dimensional representation of the 1-form associated with this vector-field, $G_\rho(\boldsymbol{v})$, as

$$\begin{aligned} G_\rho(\boldsymbol{v}_h) &= (\rho\ dx \otimes dx + \rho\ dy \otimes dy)(u_h\ \boldsymbol{\partial_x} + v_h\ \boldsymbol{\partial_y}) \\ &= \rho u_h\ dx + \rho v_h\ dy \end{aligned} \tag{5-66}$$

Once we have the above expressions for ρu_h and ρv_h, we can look back at the equation for momentum components that was derived earlier, Eq. (5-27), and write down momentum component (fields) as,

$$\begin{aligned} (m_x^{(2)})_h &= \rho u_h\ dxdy \\ (m_y^{(2)})_h &= \rho v_h\ dxdy \end{aligned} \tag{5-67}$$

and the corresponding cochains can then be obtained by the reduction of these 2-form fields on appropriate outer-oriented 2-chains, $\tilde{S}_{ij}$. Momentum weighted by a general vector-field can be obtained by a linear combination of the above 2-form fields, as was shown in Eq. (5-28). The cochains for the constant vector-fields, ∂_i, are given below

$$\begin{aligned} \mathcal{R}(m_x^{(2)})_h &= \int_{\tilde{S}_{ij}} \rho u_h \, dxdy = (\bar{m}_x)_{ij} \\ \text{and, } \mathcal{R}(m_y^{(2)})_h &= \int_{\tilde{S}_{ij}} \rho v_h \, dxdy = (\bar{m}_y)_{ij} \end{aligned} \tag{5-68}$$

The finite-dimensional continuous representation of momentum would then be given by,

$$m_h^{(1,2)} = dx \otimes \sum_{i,j} (\bar{m}_x)_{ij} e_i^{(\tilde{1})}(x) e_j^{(\tilde{1})}(y) + dy \otimes \sum_{i,j} (\bar{m}_y)_{ij} e_i^{(\tilde{1})}(x) e_j^{(\tilde{1})}(y) \tag{5-69}$$

The above analysis can be concisely represented as,

$$\begin{aligned} \bar{u}_{ij} &\xrightarrow{\mathcal{I}} u_h \overset{Eq.\ (5-27)}{\longrightarrow} (m_x^{(2)})_h \xrightarrow{\mathcal{R}} (\bar{m}_x)_{ij} \\ \bar{v}_{ij} &\xrightarrow{\mathcal{I}} v_h \overset{Eq.\ (5-27)}{\longrightarrow} (m_y^{(2)})_h \xrightarrow{\mathcal{R}} (\bar{m}_y)_{ij} \end{aligned} \tag{5-70}$$

In the above analysis, if we were to start with momentum-cochains, the extraction of velocities would be the exact same analysis, but now progressing in the opposite direction.

$$\begin{aligned} (\bar{m}_x)_{ij} &\xrightarrow{\mathcal{I}} (m_x^{(2)})_h \overset{Eq.\ (5-27)}{\longrightarrow} u_h \xrightarrow{\mathcal{R}} \bar{u}_{ij} \\ (\bar{m}_y)_{ij} &\xrightarrow{\mathcal{I}} (m_y^{(2)})_h \overset{Eq.\ (5-27)}{\longrightarrow} v_h \xrightarrow{\mathcal{R}} \bar{v}_{ij} \end{aligned} \tag{5-71}$$

Similarly, if we have partial-momentum cochains as our unknowns, we can write down the *partial-velocity* cochains in their terms as follows,

$$\begin{aligned} (\bar{m}_x)_{ij}^{i_0 j_0} &\xrightarrow{\mathcal{I}} (m_x^{(2)})_h^{i_0 j_0} \overset{Eq.\ (5-27)}{\longrightarrow} u_h^{i_0 j_0} \xrightarrow{\mathcal{R}} \bar{u}_{ij}^{i_0 j_0} \\ (\bar{m}_y)_{ij}^{i_0 j_0} &\xrightarrow{\mathcal{I}} (m_y^{(2)})_h^{i_0 j_0} \overset{Eq.\ (5-27)}{\longrightarrow} v_h^{i_0 j_0} \xrightarrow{\mathcal{R}} \bar{v}_{ij}^{i_0 j_0} \end{aligned} \tag{5-72}$$

These partial-velocity cochains will form a partition of unity of the total velocities, and this can be written down as:

$$\begin{aligned} \bar{u}_{ij} &= \sum_{i_0, j_0} \bar{u}_{ij}^{i_0 j_0} \\ \bar{v}_{ij} &= \sum_{i_0, j_0} \bar{v}_{ij}^{i_0 j_0} \end{aligned} \tag{5-73}$$

It is important to note that these one-to-one relation between velocities and momentum are maintained throughout because these are indeed dependent variables (this results in a staggered-mesh formulation in our work; Chapter 6).

Once the discretization of momentum is complete, we can write down the flux-cochains and stress-cochains used in momentum equations using the discrete operators (Chapter 3) on our momentum-cochains in the discrete-setting. This is trivial to perform once we have

the momentum cochains and discrete-operators if we use Eq. (5-41). Let us represent the respective cochains as follow for fluxes,

$$\begin{aligned} \mathcal{R}\left\langle \mathcal{F}^{(1,1)}, (\boldsymbol{b}^k_{i_0 j_0})_h \right\rangle &\longrightarrow (\bar{\zeta_k})^{i_0 j_0}_{ij} \\ \mathcal{R}\left\langle \mathcal{F}^{(1,1)}, \boldsymbol{\partial_k} \right\rangle &\longrightarrow (\bar{\zeta_k})_{ij} \\ &= \sum_{i_0, j_0} (\bar{\zeta_k})^{i_0 j_0}_{ij} \end{aligned} \tag{5-74}$$

and for stresses as,

$$\begin{aligned} \mathcal{R}\left\langle \mathcal{T}^{(1,1)}, (\boldsymbol{b}^k_{i_0 j_0})_h \right\rangle &\longrightarrow (\bar{\tau_k})^{i_0 j_0}_{ij} \\ \mathcal{R}\left\langle \mathcal{T}^{(1,1)}, \boldsymbol{\partial_k} \right\rangle &\longrightarrow (\bar{\tau_k})_{ij} \\ &= \sum_{i_0, j_0} (\bar{\tau_k})^{i_0 j_0}_{ij} \end{aligned} \tag{5-75}$$

5.4.2 Scalar-pressures and Pressure-forces

Scalar-pressure Field

The discretization of pressure is simply the reduction of pressures on dual 2-chains for an inner-oriented mesh, or on primal 2-chains for an outer-oriented mesh. Therefore, for our inner-oriented mesh where we have dual 2-chains given by, $\tilde{S}_{ij}$, the pressure cochains will be given by,

$$\int_{\tilde{S}_{ij}} p^{(2)} = \bar{p}_{ij} \tag{5-76}$$

with a finite-dimensional approximation as follows.

$$\begin{aligned} p^{(2)}_h &= \sum_{i,j} \bar{p}_{ij} e_i(x) e_j(y) \\ &= \sum_{i,j} \bar{p}_{ij} \epsilon_i(x) \epsilon_j(y)\, dxdy \end{aligned} \tag{5-77}$$

Pressure-forces and Scalar-pressures

From the generalized-momentum conservation equation as given in Eq. (5-40), we see that our main pressure-variables are:

$$\left\langle \mathcal{H}^{(1,1)}, \boldsymbol{\partial_i} \right\rangle \text{ and } \left\langle \mathcal{H}^{(1,1)}, \boldsymbol{b} \right\rangle$$

From momentum discretization, we already know that if we treat

$$\left\langle \mathcal{H}^{(1,1)}, \boldsymbol{b} \right\rangle$$

Weighting vector-field	$\boldsymbol{b}^x_{i_0j_0}$ and $\boldsymbol{b}^y_{i_0j_0}$	$\boldsymbol{\partial_x}$ and $\boldsymbol{\partial_y}$
Velocity	$\bar{u}^{i_0j_0}_{ij}$, $\bar{v}^{i_0j_0}_{ij}$	$\bar{u}_{ij}$, $\bar{v}_{ij}$
Momentum	$(\bar{m_x})^{i_0j_0}_{ij}$, $(\bar{m_y})^{i_0j_0}_{ij}$	$(\bar{m_x})_{ij}$, $(\bar{m_y})_{ij}$
Convective-flux	$(\bar{\zeta_x})^{i_0j_0}_{ij}$, $(\bar{\zeta_y})^{i_0j_0}_{ij}$	$(\bar{\zeta_x})_{ij}$, $(\bar{\zeta_y})_{ij}$
Stresses	$(\bar{\tau_x})^{i_0j_0}_{ij}$, $(\bar{\tau_y})^{i_0j_0}_{ij}$	$(\bar{\tau_x})_{ij}$, $(\bar{\tau_y})_{ij}$
Pressure-force	$(\bar{\lambda_x})^{i_0j_0}_{ij}$, $(\bar{\lambda_y})^{i_0j_0}_{ij}$	$(\bar{\lambda_x})_{ij}$, $(\bar{\lambda_y})_{ij}$

Table 5-1: Cochain notation to be used for the discrete Navier-Stokes setup

as our primary unknowns, and use the partition-of-unity vector-fields introduced earlier,

$$\boldsymbol{b} = \boldsymbol{b}^k_{i_0j_0} \qquad \forall\ (i_0, j_0, k)$$

we can establish the following relation between $\left\langle \mathcal{H}^{(1,1)}, \boldsymbol{\partial_i} \right\rangle$ and $\left\langle \mathcal{H}^{(1,1)}, \boldsymbol{b} \right\rangle$.

$$\begin{aligned} \mathcal{H}^{(1)}_k &= \left\langle \mathcal{H}^{(1,1)}, \boldsymbol{\partial_k} \right\rangle \\ &= \sum_{i_0, j_0} \left\langle \mathcal{H}^{(1,1)}, \boldsymbol{b}^k_{i_0j_0} \right\rangle \end{aligned} \tag{5-78}$$

We will call the variable corresponding to $\left\langle \mathcal{H}^{(1,1)}, \boldsymbol{b}^k_{i_0j_0} \right\rangle$ *partial-pressure force*, and the cochains corresponding to this variable can be determined with the help of Eq. (5-32) and a discrete application of the interior-product, as was shown in Chapter 3. If the cochains corresponding to this variable are represented by $(\bar{\lambda_k})^{i_0j_0}_{ij}$, and the discrete vector-field $(\boldsymbol{b}^k_{i_0j_0})_h$ by simply $\boldsymbol{a}$, we have the following representation of the above.

$$\bar{p}_{ij} \xrightarrow{\mathcal{I}} p^{(2)}_h \xrightarrow{\mathtt{i}_{\boldsymbol{a}}} (\lambda^{i_0j_0}_k)_h \xrightarrow{\mathcal{R}} (\bar{\lambda_k})^{i_0j_0}_{ij}, \qquad k = x, y$$

5.5 Final Discrete Formulation

We have managed to obtain discrete representations of all our variables, and the notation that has been introduced for our cochains far is as shown in Table 5-1. Using this notation, the discrete-counterpart of Navier-Stokes equations, as shown in Eq. (5-14) and Eq. (5-40), can be written down.

- Mass Conservation:
  - If velocity is discretized as the 1-form associated to velocity vectors:

$$D^{2,1} \star_h [\bar{v}_{ij}] \tag{5-79}$$

– If velocity unknowns are vector-valued 0-forms:

$$D^{2,1}\mathbf{i}_{\boldsymbol{v_h}}\left[\mathcal{R}\sigma_\rho\right] \tag{5-80}$$

- Partial-Momenta Conservation:

$$\begin{aligned}\sum_k \frac{\partial(\bar{m_k})_h^{i_0j_0}}{\partial t} + \sum_k D^{2,1}\left([(\bar{\zeta_k})_{ij}^{i_0j_0}] + [(\bar{\lambda_k})_{ij}^{i_0j_0}] - [(\bar{\tau_k})_{ij}^{i_0j_0}]\right) = \cdots \\ \cdots \sum_k [(\bar{m_k})_{ij}] \cancel{\frac{\partial(b^k_{i_0j_0})_h}{\partial t}} + \sum_k \left([(\bar{\zeta_k})_{ij}] + [(\bar{\lambda_k})_{ij}] - [(\bar{\tau_k})_{ij}]\right) \wedge D^{1,0}[(\bar{b}^k_{ij})_{i_0j_0}]\end{aligned} \tag{5-81}$$

where square-brackets, $[\cdot]$, around a cochain means the matrix of those cochain values. The above equations need to be solved for all possible vector-fields, i.e. for all possible variations of the indices i_0 and j_0. Notice that the vector-fields, $\boldsymbol{b}^x_{i_0j_0}$ and $\boldsymbol{b}^y_{i_0j_0}$, were chosen just as functions of space and partitions of unity, and this is the reason why the time-derivative of their components is set to zero in Eq. (5-81). Secondary-conservation properties are treated in the next sub-section.

5.5.1 Discrete Secondary-variable Conservation

In Eq. (5-40), it was stated that by weighting the momentum equation with a general vector-field we can conserve a lot of secondary variables (kinetic energy, enstrophy *etc*). This is a straightforward extension from the partial-momenta conservation law that is given in Eq. (5-81). As was noted for Eq. (5-81), the coefficients of the weighting vector-fields $\boldsymbol{b}^x_{i_0j_0}$ and $\boldsymbol{b}^y_{i_0j_0}$ were constant in time, and thus the only thing that we were conserving in Eq. (5-81) was partial-momenta. We can get expressions for a general vector-field by allowing the coefficients to vary in time. This is expressed below as:

$$\begin{aligned}(\boldsymbol{b}^x_{i_0j_0})_h &= \sum_{i,j} (\bar{b}^x_{ij})_{i_0j_0}(t) h_i(x) h_j(y)\ \boldsymbol{\partial_x} \\ (\boldsymbol{b}^y_{i_0j_0})_h &= \sum_{i,j} (\bar{b}^y_{ij})_{i_0j_0}(t) h_i(x) h_j(y)\ \boldsymbol{\partial_y}\end{aligned}$$

where $(\bar{b}^x_{ij})_{i_0j_0}(t)$ and $(\bar{b}^y_{ij})_{i_0j_0}(t)$ are the time-variable coefficients. Now, we expand these time-variable coefficients as 0-forms in the direction of time with our Lagrange polynomials.

$$\begin{aligned}(\bar{b}^x_{ij})_{i_0j_0}(t) &= \sum_r (\bar{b}^x_{ij})^r_{i_0j_0} h_r(t) \\ (\bar{b}^y_{ij})_{i_0j_0}(t) &= \sum_r (\bar{b}^y_{ij})^r_{i_0j_0} h_r(t)\end{aligned}$$

In the above, the index r denotes the time-level (for example, time-integration with order 4 will have 5 time-levels for each time-step).

If we consider the above as components of the vector-field and look at Eq. (5-81), we see that the time-variability of the coefficients will simply be a multiplying-factor for the spatial

derivative terms (divergence of fluxes), and the only terms that will be significantly changed are the time-derivative terms. Thus, we consider only the time-derivative terms in detail.

$$\sum_k \frac{\partial (\bar{m_k})_h^{i_0 j_0}}{\partial t}$$

$$\sum_k [(\bar{m_k})_{ij}] \frac{\partial (b_{i_0 j_0}^k)_h}{\partial t}$$

The above time-derivatives will transform to the following,

$$\sum_r \sum_k (\bar{b}_{ij}^k)_{i_0 j_0}^r \frac{\partial (\bar{m_k})_h^{i_0 j_0} h_r(t)}{\partial t}$$

$$\sum_r \sum_k (\bar{b}_{ij}^k)_{i_0 j_0}^r [(\bar{m_k})_{ij}] \frac{\partial (h_r(t)}{\partial t}$$

As a result of the above modifications, the quantities we will be preserving are,

$$(\bar{m_k})_h^{i_0 j_0} h_r(t)$$

that is, all the partial-momenta, $(\bar{m_k})_h^{i_0 j_0}$, weighted by $h_r(t)$. It is easy to see that since the time-varying coefficients will just be multiplying-factors for the rest of the equation that only contains spatial-derivative, the entire equation will have the following multiplying factor.

$$\sum_r \sum_k (\bar{b}_{ij}^k)_{i_0 j_0}^r$$

Note that we can choose choose $(\bar{b}_{ij}^k)_{i_0 j_0}^r$ such that they form linearly independent vectors in the index r. For first order integration, for instance, these can be given by:

$$(\bar{b}_{ij}^k)_{i_0 j_0} = \begin{bmatrix} \frac{1}{\sqrt{2}} \\ \frac{1}{\sqrt{2}} \end{bmatrix}, (\bar{b}_{ij}^k)_{i_0 j_0} = \begin{bmatrix} \frac{1}{\sqrt{2}} \\ -\frac{1}{\sqrt{2}} \end{bmatrix}$$

This means that if we solve the partial-momentum equations to conserve $(\bar{m_k})_h^{i_0 j_0} h_r(t)$ for all such linearly-independent vectors, we can conserve all possible linear combinations of the partial-momenta. If this is possible, it would lead to the conservation of a large set of secondary variables. Of course, the implicit assumption here is that for different linearly-independent vector-fields, the partial-momenta solution will stay invariant which seems like a strong condition. This was not checked here, and this approach should be verified, and if successful, exploited in a future work.

Chapter 6

Results

In Chapter 5, a general framework for the discretization of incompressible Navier-Stokes equations was given. This framework was developed for the generalized-momentum conservation for which the continuous formulation is shown in Eq. (5-40).

$$\begin{aligned} &\frac{\partial \left\langle m^{(1,2)}, \boldsymbol{b} \right\rangle}{\partial t} + \mathrm{d}\left(\left\langle \mathcal{F}^{(1,1)}, \boldsymbol{b} \right\rangle + \left\langle \mathcal{H}^{(1,1)}, \boldsymbol{b} \right\rangle - \left\langle \mathcal{T}^{(1,1)}, \boldsymbol{b} \right\rangle \right) = \cdots \\ \cdots &\sum_i \left\langle m^{(1,2)}, \boldsymbol{\partial_i} \right\rangle \frac{\partial b^i}{\partial t} + \sum_i \left(\left\langle \mathcal{F}^{(1,1)}, \boldsymbol{\partial_i} \right\rangle + \left\langle \mathcal{H}^{(1,1)}, \boldsymbol{\partial_i} \right\rangle - \left\langle \mathcal{T}^{(1,1)}, \boldsymbol{\partial_i} \right\rangle \right) \wedge \mathrm{d}b^i \end{aligned} \tag{5-40}$$

In this work, the weighting vector-field used in Eq. (5-40) is simply a constant vector-field ($\boldsymbol{\partial_x}$ or $\boldsymbol{\partial_y}$). This gives the usual momentum conservation law, and is equivalent to Eq. (5-37).

$$\frac{\partial m_i^{(2)}}{\partial t} + \mathrm{d}(\mathcal{F}_i^{(1)} + \mathcal{H}_i^{(1)} - \mathcal{T}_i^{(1)}) = 0 \tag{5-37}$$

Thus, over here the only conservation law that is being tested is linear-momentum conservation, and the generalized conservation equation, Eq. (5-81), is left for future work.

This is applied to problems of Kovasznay flow, and the lid-driven cavity flow. This chapter presents results corresponding to these test cases, and brief analysis of their results. Before proceeding to the results, a brief setup of the mesh and the placement of unknowns is investigated.

6.1 Computational Mesh and Variable Placement

The setup of the computational mesh is described here first which is not specific to any problem, but to our method. This setup is explained for one spectral element, and the extension to multiple elements is straightforward.

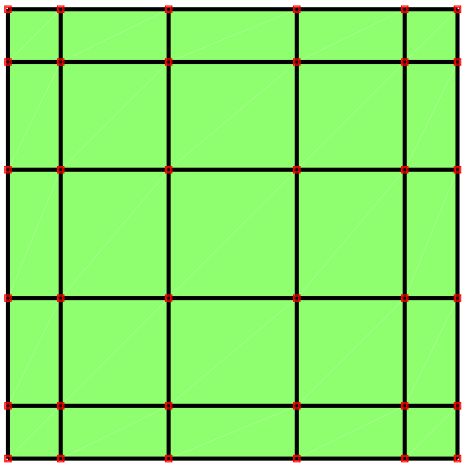

Figure 6-1: A 2D cell complex: (1) 0-Cells: ■ (2) 1-Cells: ▬ (3) 2-Cells: ■

Consider a spectral element of polynomial order N. This will be our primal, outer-oriented computational mesh, and is shown in Figure 6-1. The different *ingredients*, all outer-oriented, that build up this mesh are:

- $(N+1)^2$ Zero-cells
- $2N(N+1)$ One-cells
- N^2 Two-cells

Our primary variables, velocities and pressures, are discretized on this mesh as per their appropriate rank. We have already seen in Chapter 5 that velocity is discretized as vector-valued (inner-oriented) 0-forms,

$$\boldsymbol{v} = u\ \boldsymbol{\partial_x} + v\ \boldsymbol{\partial_y} \tag{6-1}$$

or as the 1-forms associated to this vector-field.

$$v^{(1)} = G_\rho(\boldsymbol{v}) = \rho u\ dx + \rho v\ dy \tag{6-2}$$

At the same time, we should also note that this was the appropriate discretization for an inner-oriented mesh. Hence, on our outer-oriented mesh, the duals of these forms of velocity need to be reduced. In this work, the reduction of $\star G_\rho(\boldsymbol{v})$ was chosen as the primary discretization. In a future work, the difference between the two approaches should be quantified. Hence, the velocity 1-form that was chosen for discretization in this work is,

$$v^{(1)} = \star G_\rho(\boldsymbol{v}) = \rho u\ dy - \rho v\ dx \tag{6-3}$$

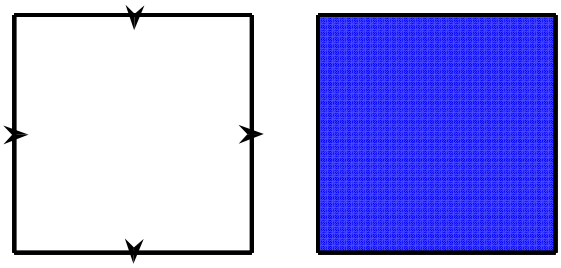

(a) $\bar{u}$ and $\bar{v}$ (b) $\bar{p}$

Figure 6-2: The velocities are discretized as mass-fluxes, and thus on 1-cells of this lowest-order mesh. Pressures on the other hand are discretized as 2-forms, and thus as a single integral value for this single-cell mesh.

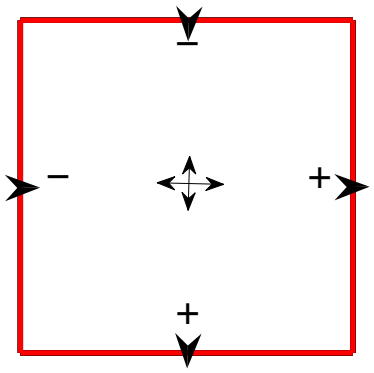

Figure 6-3: Once velocities have been discretized as mass-fluxes (Eq. (6-3)), calculation of divergence is simply taking a linear combination of mass-flux cochains with the appropriate weights.

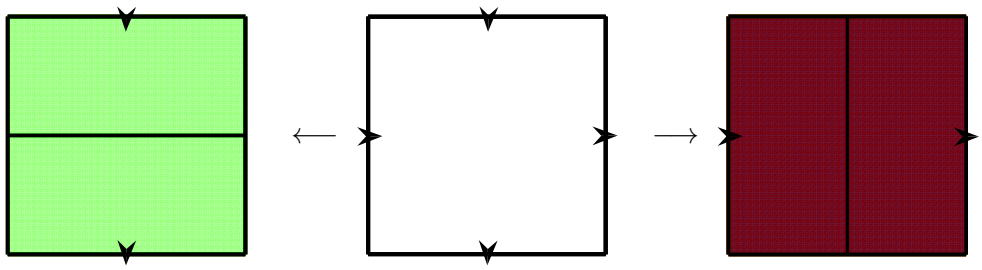

(a) Volumes for y-momenta, $\bar{m_y}$ (b) Primal 1-cells (c) Volumes for x-momenta, $\bar{m_x}$

Figure 6-4: A staggered-mesh system can be constructed from a single primal-cell as shown in this figure. There is a one-to-one relation between the number of 2-cells and the number of 1-cells for momenta and velocities, respectively.

This means that velocities are already being discretized as fluxes on the 1-cells (▬) of our mesh and the pressures are discretized as outer-oriented 2-forms on our 2-cells (■). Their respective finite-dimensional representations would be as below for pressures,

$$\begin{aligned} p_h^{(2)} &= \sum_{i=1}^{N}\sum_{j=1}^{N} \bar{p}_{ij} e_i(x) e_j(y) \\ &= \sum_{i=1}^{N}\sum_{j=1}^{N} \bar{p}_{ij} \epsilon_i(x) \epsilon_j(y)\ dxdy \end{aligned} \tag{6-4}$$

and for velocities as follows,

$$\begin{aligned} v_h^{(1)} &= \sum_{i=1}^{N}\sum_{j=0}^{N} \bar{v}_{ij}^x e_i(x) h_j(y) + \sum_{i=0}^{N}\sum_{j=1}^{N} \bar{v}_{ij}^y h_i(x) e_j(y) \\ &= \sum_{i=1}^{N}\sum_{j=0}^{N} \bar{v}_{ij}^x \epsilon_i(x) h_j(y)\ dx + \sum_{i=0}^{N}\sum_{j=1}^{N} \bar{v}_{ij}^y h_i(x) \epsilon_j(y)\ dy \end{aligned} \tag{6-5}$$

with the cochains being defined by the following equations,

$$\begin{aligned} \bar{p}_{ij} &= \int_{S_{ij}} p^{(2)} \\ \bar{v}_{ij}^x = \int_{C_{ij}^x} v^{(1)} \text{ and } \bar{v}_{ij}^y &= \int_{C_{ij}^y} v^{(1)} \end{aligned} \tag{6-6}$$

where S_{ij} is the ij^{th} 2-cell, and C_{ij}^k is the ij^{th} 1-cell in k^{th} direction.

To make things easier to understand and explain, consider the ij^{th} 2-cell of the above mesh along with its surrounding outer-oriented 1-cells as shown in Figure 6-2. The crossing-direction specified for these 1-chains implies their outer-orientation. The 2-cell is assigned a source-like orientation.

Let us say that we want to see how mass-conservation can be enforced for this cell (■). Recall that the 1-cochains, $\bar{v}_{ij}^x$ and $\bar{v}_{ij}^y$, discretized as above are mass fluxes through the edges

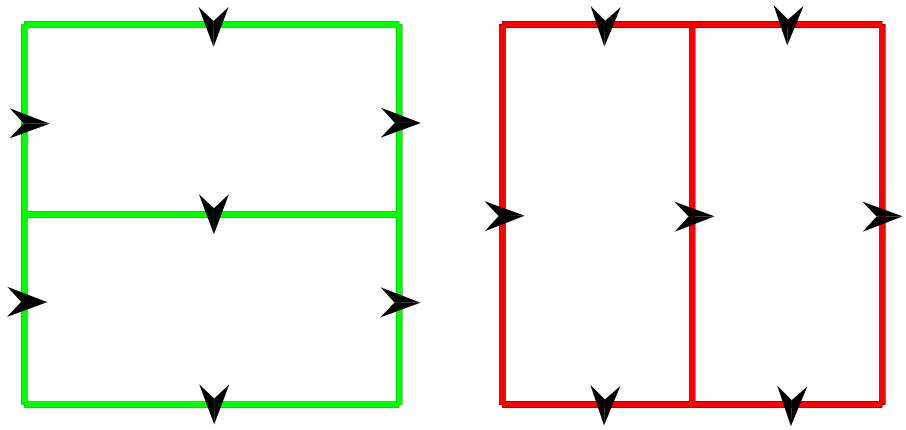

(a) $\bar{\zeta_y}, \bar{\lambda_y}, \bar{\tau_y}$ (b) $\bar{\zeta_x}, \bar{\lambda_x}, \bar{\tau_x}$

Figure 6-5: Momentum fluxes' are placed on the 1-cells surrounding the staggered-mesh volumes (shown in Figure 6-4).

of the cell. Hence, using the discrete representation of the exterior derivative, we see that the equation for mass-conservation for this cell is simply:

$$\bar{v}^x_{ij} + \bar{v}^y_{(i+1)j} - \bar{v}^x_{i(j+1)} - \bar{v}^y_{ij} = 0 \tag{6-7}$$

This operation is shown in Figure 6-3.

Mass conservation can be similarly applied to all cells, and the matrix representation of this operation will be as shown in Eq. (5-79).

The placement of our primary variables is thus complete. Now we can move on towards the derived variables and see where they go. Recall that we are weighting the momentum by constant vector-fields in either direction, $\boldsymbol{\partial_x}$ and $\boldsymbol{\partial_y}$, and so our momentum components are simply,

$$m^{(2)}_i = \left\langle m^{(1,2)}, \boldsymbol{\partial_i} \right\rangle, \qquad i = \{x, y\} \tag{6-8}$$

In order to maintain the one-to-one relation between momentum and velocities that has been stressed on in Chapter 5, we define two additional meshes which are also outer-oriented, and which have the correct number of 2-chains corresponding to our primal mesh's 1-chains. This automatically leads to a staggered-mesh setup, and is explained as follows.

In order to see the placement of our derived variables, consider the 1-cells surrounding a typical 2-cell on our primal mesh, and let us see what kind of mesh do we get corresponding to this 2-cell. In order to maintain the one-to-one relationship between momenta and velocities, we surround each 1-cell corresponding to i^{th} component of velocity by volumes that correspond to this component of momentum. This is shown in Figure 6-4.

Note that, as shown in Figure 6-4, the volumes surrounding 1-cells in x-direction are related to momentum in y-direction, and the volumes surrounding 1-cells in y-direction are related to momentum in x-direction. This is because of the outer-oriented nature of the velocities that we discretize, and can be easily deduced from the expression for $v^{(1)}$.

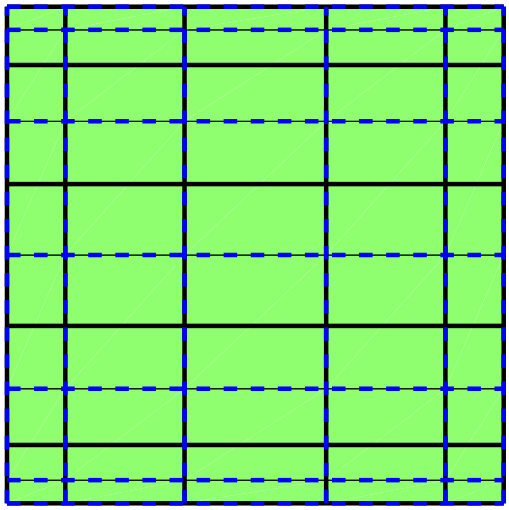

(a) Volumes surrounding 1-cells in X-direction

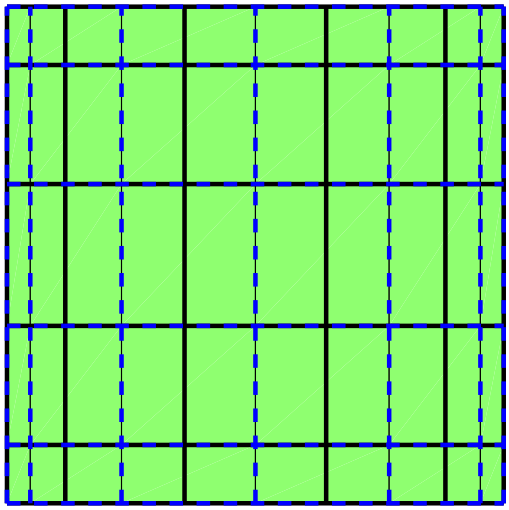

(b) Volumes surrounding 1-cells in Y-direction

Figure 6-6: A staggered-mesh can be constructed by straightforward extension of the single-cell approach shown in Figure 6-4. Primal mesh: (—); Staggered-mesh: (- -)

These new outer-oriented volumes on which x- and y-momentum equations are solved can be seen as the result of a different tesselation of our outer-oriented computational domain. The 1-cells corresponding to these meshes are shown in Figure 6-5. These are the one-cells where our pressure-forces ($\bar{\lambda}_i$), convective-momentum fluxes ($\bar{\zeta}_i$), and stresses ($\bar{\tau}_i$) *live*.

The above construction allows us to preserve our one-to-one relation between momentum by an equality of degrees of freedom. The actual calculation of momentum inside these volumes using $v_h^{(1)}$ was covered in Chapter 5. The fluxes corresponding to momenta in different directions can also be evaluated by following the procedure outlined in Chapter 5.

Once we have the momentum inside our staggered-mesh 2-cells and the momentum-fluxes corresponding to our staggered-mesh 1-cells, the change in momentum in time can be related to the divergence of these fluxes. This was shown in Eq. (5-81).

The construction of the staggered-mesh above was shown for a single 2-cell which can be thought of as a lowest-order mesh. This procedure can be carried out for a high-order mesh in an analogous way by surrounding each 1-cell (associated to a velocity cochain) by a corresponding 2-cell (associated to a momentum cochain) thus preserving the one-to-one relation between momentum and velocity. The resulting meshes are shown in Figure 6-6 This completes our section on the setup of a typical computational mesh, and now some results are presented.

6.2 Kovasznay Flow

Kovasznay flow is a steady-state, analytical solution available to the Navier-Stokes equations. The solution is similar to the flow behind a periodic array of circular cylinders. The analytical solution to this problem for velocity, (u, v), and pressures, p, is given as follows:

$$\begin{aligned} u &= 1 - e^{\lambda x} cos(2\pi y) \\ v &= \frac{\lambda}{2\pi} e^{\lambda x} sin(2\pi y) \\ p &= \frac{1}{2}(1 - e^{2\lambda x}) \end{aligned} \tag{6-9}$$

where

$$\lambda = \frac{1}{2\nu} - \sqrt{\frac{1}{4\nu^2} + 4\pi^2} \tag{6-10}$$

The kinematic-viscosity chosen for this flow was

$$\nu = \frac{\mu}{\rho} = \frac{1}{40} \tag{6-11}$$

and the computational domain considered was $\Omega = [-0.5\ 1] \times [-0.5\ -0.5]$.

The h, p-adaptivity plots for this problem are given in Figure 6-7 for pressures and in Figure 6-8 for velocities. It can be seen that the solutions converge spectrally. There is some stagnation

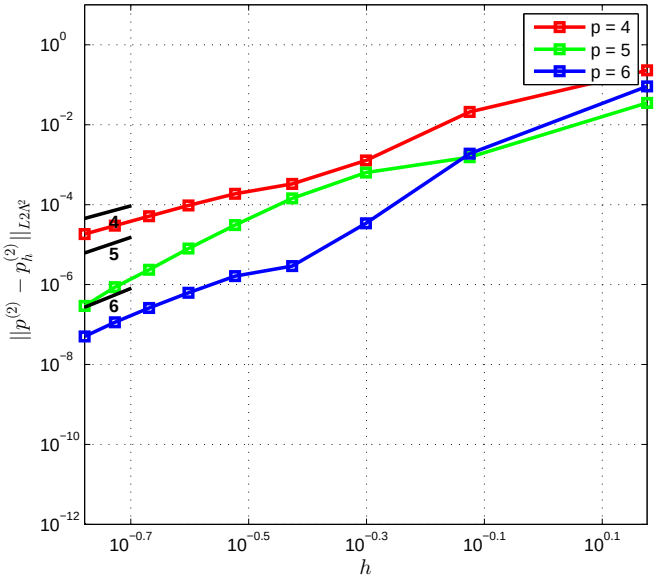

(a) h-refinement

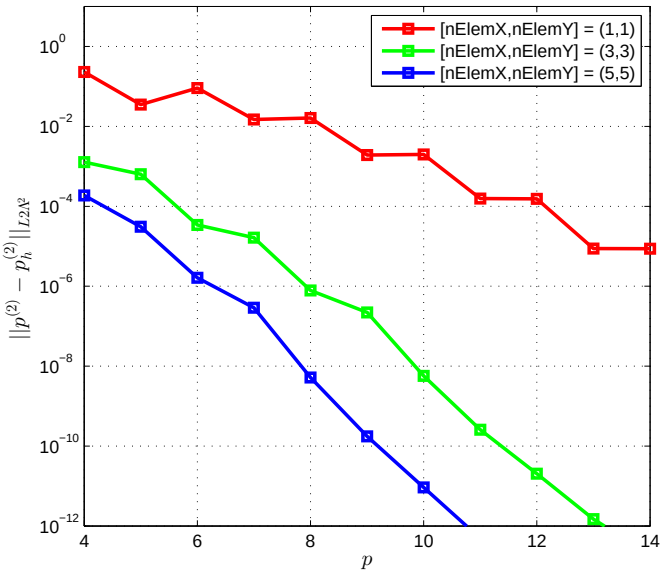

(b) p-refinement

Figure 6-7: The convergence analysis for the solution for pressures is as shown. The plots show that spectral convergence is obtained for the discretization scheme used.

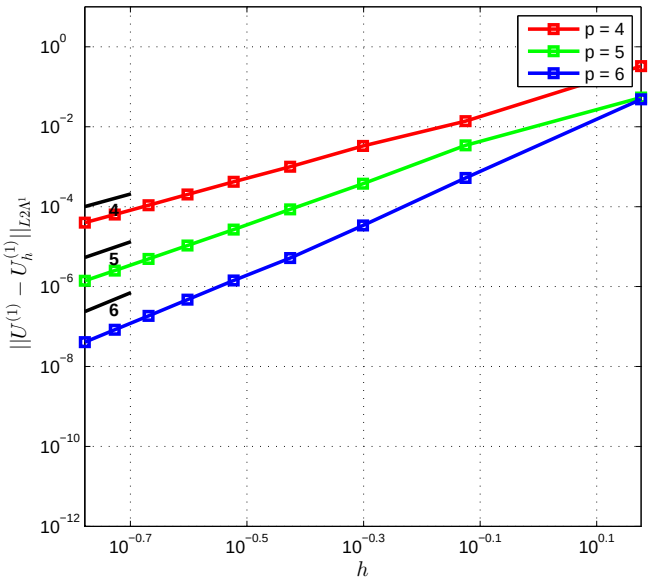

(a) h-refinement

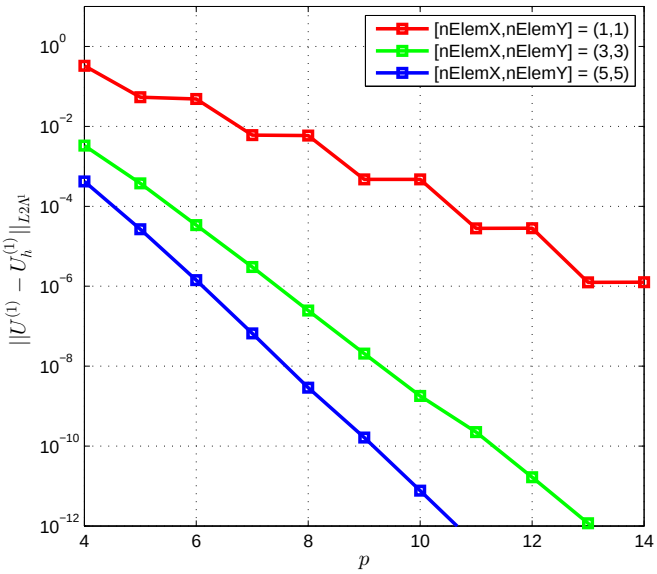

(b) p-refinement

Figure 6-8: The convergence analysis for the solution for velocities is as shown. These plots show spectral convergence as well, just like Figure 6-7.

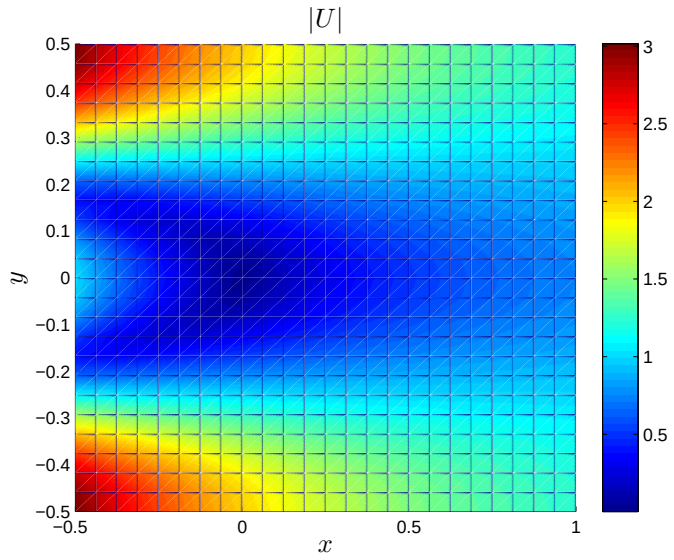

(a) Velocity magnitudes

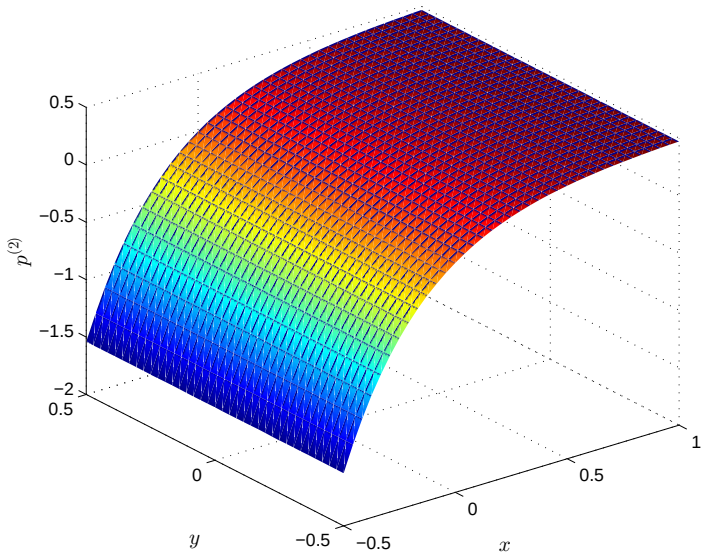

(b) Pressures

Figure 6-9: A sample solution of Kovasznay Flow for a mesh with a 4X4 mesh and elements of order 3.

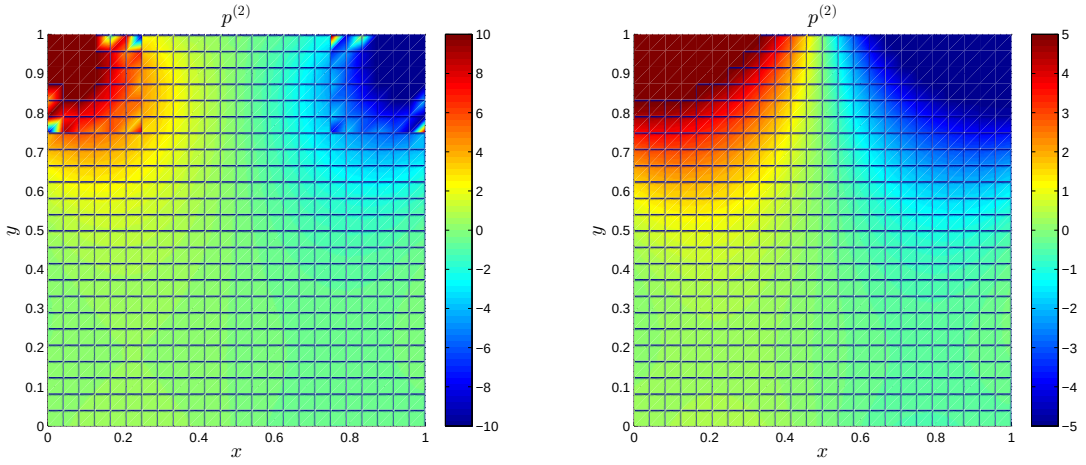

(a) With singularities

(b) Regularized

Figure 6-10: The initial pressure-field generated as a result of the solution of Stokes' flow is shown in this picture. The singularities at the top corners cause oscillations at the element boundaries. The solution is discontinuous at these boundaries because of the discontinuous nature of edge-functions between elements. Regularizing the lid-velocity (removing singularities) makes the solution better, however discontinuities between elements may still exist if the resolution is not high enough. Mesh size is 4X4 and made up of elements of order 6.

observed in convergence for a mesh with a single element, and this is attributed to the fact that our basis may not be capturing certain modes (even/odd). An example solution of the problem is seen in Figure 6-9 where we show the velocity magnitudes, and the pressure plot for a 4X4 mesh of order 3.

6.3 Lid-driven Cavity Flow

The momentum-conservation theory developed here was also applied to the problem of flow in a cavity with the help of a moving boundary. This is a shear driven flow, and the boundary conditions for this can be simply stated as follows for the velocities on a square domain, $\Omega = [0\ 1]^2$.

- Normal lid-driven cavity flow (with singularities) ([9]):

$$\begin{aligned} u(x,y) &= \begin{cases} -1, & y = 1 \\ 0, & \text{elsewhere on } \partial\Omega \end{cases} \\ v(x,y) &= 0 \text{ on } \partial\Omega \end{aligned} \tag{6-12}$$

- Regularized lid-driven cavity flow ([52]):

$$\begin{aligned} u(x,y) &= \begin{cases} -16x^2(1-x)^2, & y = 1 \\ 0, & \text{elsewhere on } \partial\Omega \end{cases} \\ v(x,y) &= 0 \text{ on } \partial\Omega \end{aligned} \tag{6-13}$$

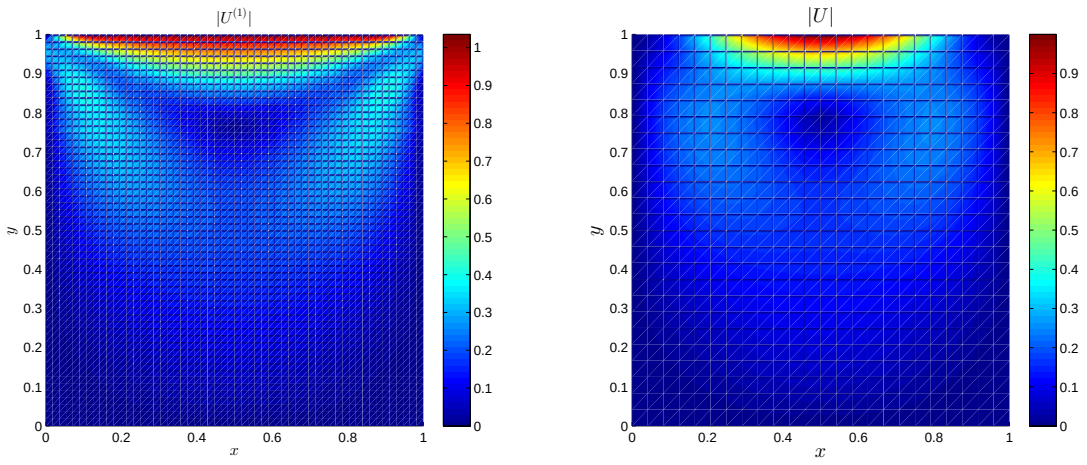

(a) With singularities

(b) Regularized

Figure 6-11: The magnitude of the initial velocity-field generated as a result of the solution of Stokes' flow is as shown for a mesh of 4X4 and made up of elements of order 6.

The simulations were run with the following kinematic-viscosity:

$$\nu = \frac{1}{1000} \tag{6-14}$$

This problem in its normal formulation has two top-corner singularities because of velocity discontinuities, and in many methods some form of correction needs to be done for this [9]. In our method, however, we have no variables placed exactly at the singularities. This is because in our velocity-stress-pressure formulation, all variables are either discretized on lines or surfaces. Some surfaces/lines may contain these singularities, and the integral values for these surfaces/lines will be very high, but no correction needs to be done for this.

6.3.1 Initial Solution: Stokes' Flow

For this problem, an initial solution was generated by solving a Stokes' problem in stress-velocity-pressure formulation. This was done by ignoring the time-derivative and convective terms in Eq. (5-37), and choosing $\nu = 1$. The equations thus solved were,

$$\begin{aligned} \mathrm{d}(\mathcal{H}_i^{(1)} - \mathcal{T}_i^{(1)}) &= 0 \\ \mathcal{L}_{\boldsymbol{v}} \sigma_\rho &= 0 \end{aligned} \tag{6-15}$$

The pressure and velocity-magnitude plots for this problem are shown in Figure 6-10 and Figure 6-11. As expected, the singularities at the top-corner points make the integral values close to the corner-points high. This is the reason that the polynomial interpolation of these high-gradient solutions seen in Figure 6-11 and Figure 6-10 for velocities and pressures is

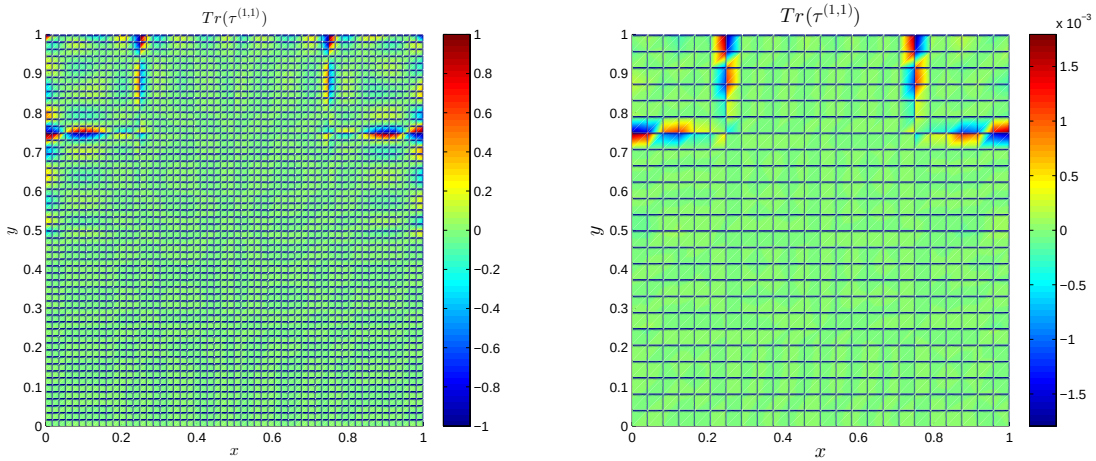

(a) With singularities (b) Regularized

Figure 6-12: Trace of the stress-tensor should be equal to the divergence of the velocity field, Eq. (6-16). This is plotted for the Stokes' flow solution. The global-value is found to be zero. The local value, however, is found to be non-zero. This is again attributed to the discontinuous basis-functions and their oscillatory nature. This can be checked by removing the singularities, as is seen in the regularized lid-driven cavity. However, higher resolution may be needed to make the trace pointwise zero. Mesh size is 4X4 and made up of elements of order 6.

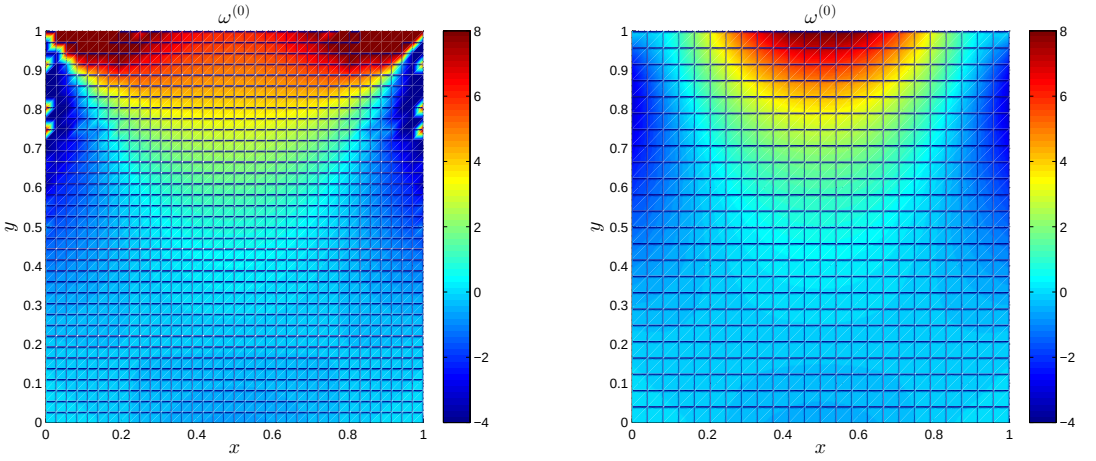

(a) With singularities (b) Regularized

Figure 6-13: The initial vorticity-field is shown in this figure where again numerical artifacts pertaining to the discontinuous solution are seen. These vanish when the singularities are removed by regularizing the lid-velocity. Mesh size is 4X4 and made up of elements of order 6.

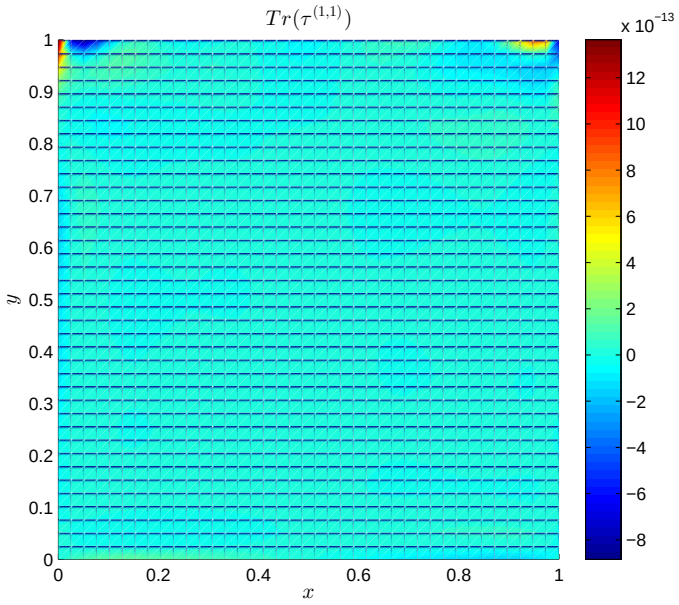

Figure 6-14: Trace of the stress-tensor for the Stokes' flow solution calculated on a single element is shown. This is found to be globally, as well as locally zero. Mesh size is 1X1 and the element is of order 10.

oscillatory in nature. At the element boundaries, because of the discontinuous nature of edge-basis functions, this oscillatory solution can thus become discontinuous. The discontinuities are clearly seen for the normal lid-driven cavity in Figure 6-10 and Figure 6-13.

The oscillations can be removed by removing the singularities as is seen in the regularized lid-driven cavity case. Even though visually the numerical artifact of discontinuity can be removed, it may still remain to some extent as is seen in the stress-tensor trace shown in Figure 6-12. Recall that the trace of the stress tensor is equal to the Lie-derivative of our density-weighted standard volume-form,

$$Tr(\mathcal{T}^{(1,1)}) = \frac{\mu}{\rho}\mathcal{L}_{\boldsymbol{v}}\sigma_\rho \tag{6-16}$$

We would of course like the above to be globally, as well as pointwise zero. Even though it is not seen to vanish completely even for the regularized lid-driven cavity flow, it becomes pointwise zero for a single-element mesh where no element discontinuities exist. This is shown in Figure 6-14

6.3.2 Steady-state solution to full Navier-Stokes problem

The solution for the full Navier-Stokes equation, proceeding from the Stokes' problem solution, is as shown in Figure 6-15 and Figure 6-16 for velocity-magnitudes corresponding to multiple-element meshes and single-element meshes, respectively. The discontinuities at element interfaces is seen to be more significant for normal lid-velocity case; increase in order

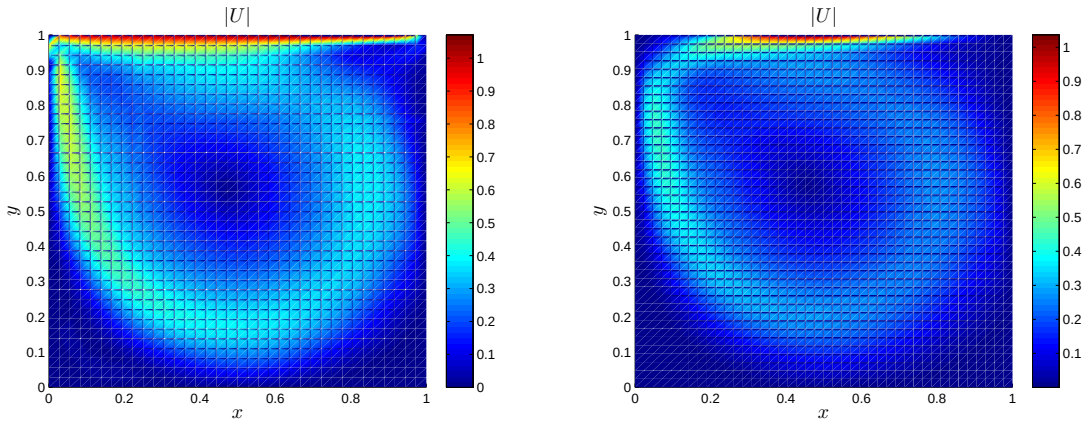

(a) With singularities (b) Regularized

Figure 6-15: Velocity magnitudes calculated for the lid-driven cavity are as shown. Mesh size for the flow with singularities is 4X4 with elements of order 7, while that for the regularized cavity is 3X3 and made up of elements of order 8. The discontinuities at the element interfaces is more prominent for the normal lid-velocity case. However, this is seen to reduce with increase of order, and completely disappears for single-element runs (see Figure 6-16)

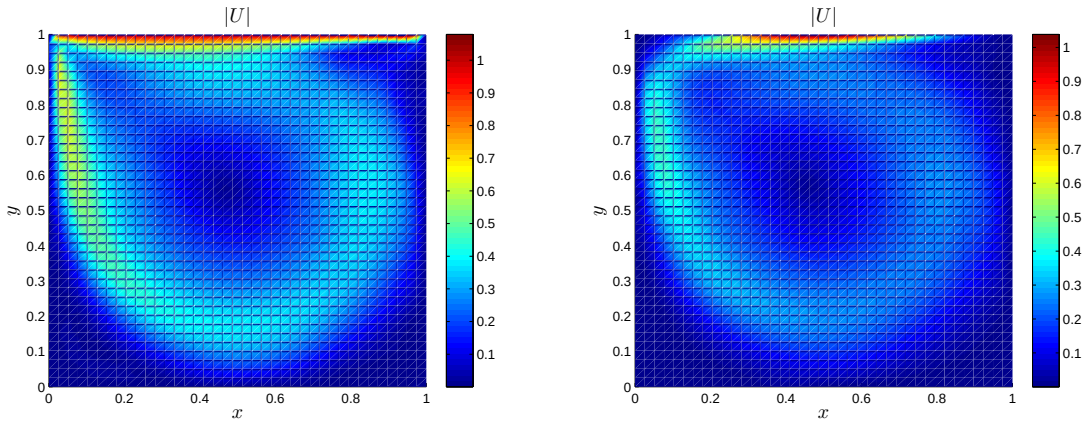

(a) With singularities (b) Regularized

Figure 6-16: Velocity magnitudes calculated for the lid-driven cavity are as shown. Mesh size is 1X1 and made up of elements of order 16. As can be seen, for a single element the solution is smooth with no spurious oscillations.

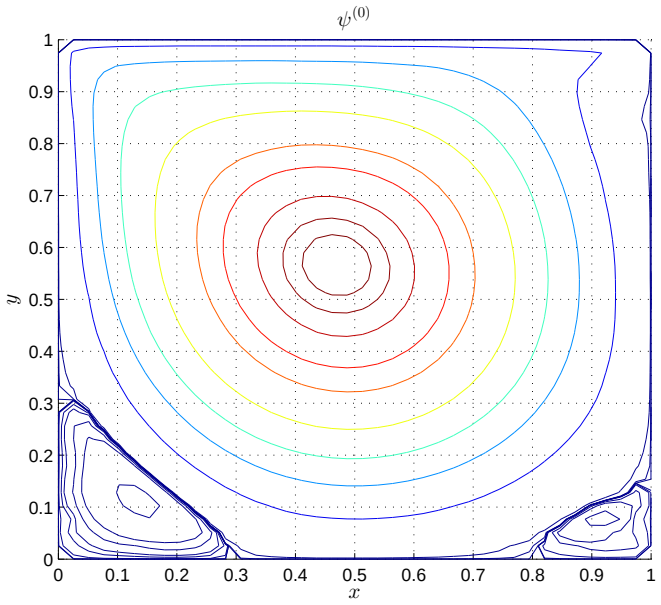

Figure 6-17: Stream-function contours plotted for the lid-driven cavity problem with a $Re = 1000$. The contours plotted are in accordance with the levels used in [9]. Mesh size is 1X1 and made up of elements of order 16.

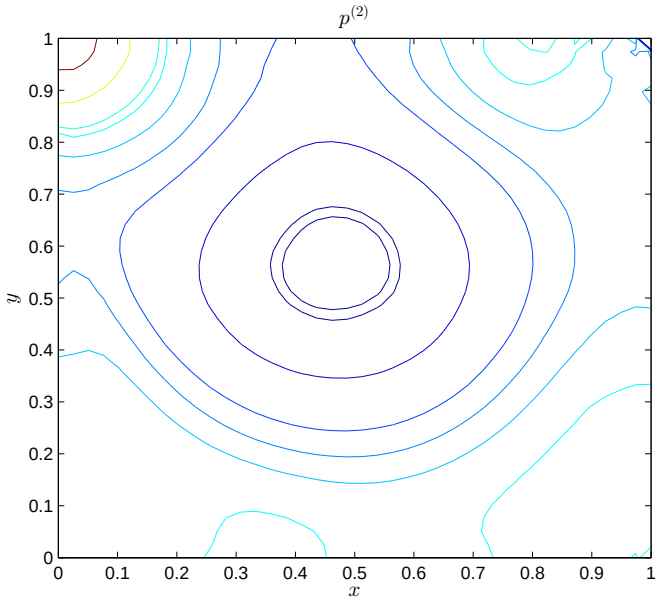

Figure 6-18: Pressure contours plotted for the lid-driven cavity problem with a $Re = 1000$. The contours plotted are in accordance with the levels used in [9]. Mesh size is 1X1 and made up of elements of order 16.

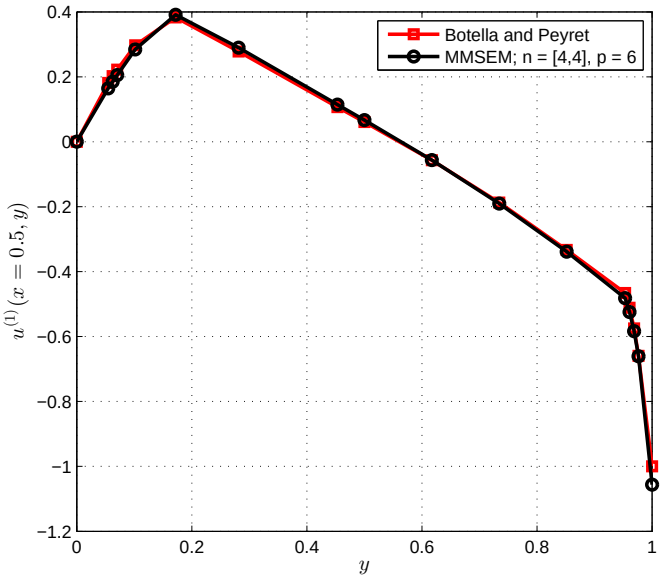

(a) Vertical-velocity for x = 0.5 plane

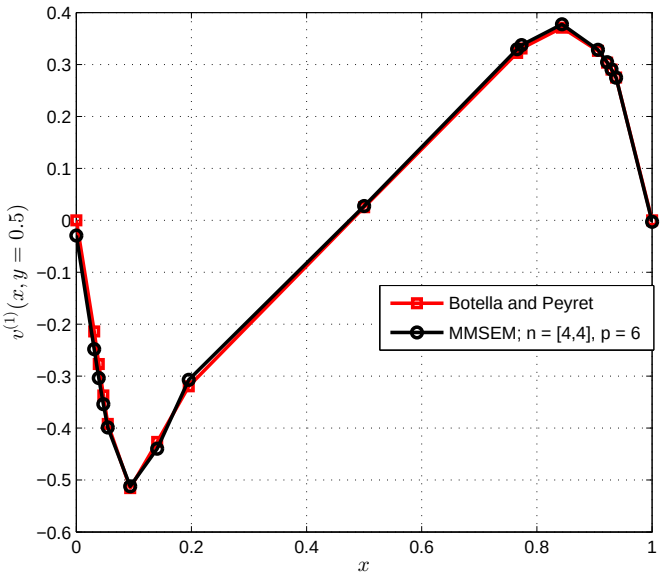

(b) Horizontal-velocity for y = 0.5 plane

Figure 6-19: Centerline velocities are plotted and compared with the solutions of [9], and the solutions are found to be reasonably close. Mesh size is 4X4 and made up of elements of order 6.

of elements is seen to alleviate this problem. Further analysis is done only for the normal-lid driven cavity flow.

Stream-function contour-levels									
-1.5E-3	-5E-4	-2.5E-4	-1E-4	-5E-5	-1E-5	-1E-6	0	1E-10	1E-5
1E-4	1E-2	3E-2	5E-2	7E-2	9E-2	1E-1	1.1E-1	1.15E-1	1.175E-1

Table 6-1: Contour-levels for stream-functions plotted in Figure 6-17 are taken from [9].

.

The contours corresponding to the streamfunctions and pressures can be seen in Figure 6-17 and Figure 6-18. These contours for stream-functions and pressures are plotted as per the contour-plots of [9], and the levels are shown in Table 6-1 and Table 6-2. As can be seen, the bottom-corner recirculation regions are captured, and a hint of the recirculation region in the top-right corner can also be seen. The bottom-corner recirculation regions appear to be slightly wobbly, and this is attributed to the Runge-effect of high-order polynomials.

Pressure contour-levels									
-2E-3	0	2E-2	5E-2	7E-2	9E-2	1.1E-1	1.2E-1	1.7E-1	3E-1

Table 6-2: Contour-levels for pressures plotted in Figure 6-18 are taken from [9].

.

The results are also compared to the results of [9], and these comparisons are shown in Figure 6-19. For these figures, a vertical cut, $x = 0.5$, was made for the u-velocities, and a horizontal-cute, $y = 0.5$, was made for the for the v-velocities. These results are compared to the data provided by [9] and our solution is seen to be in good agreement with theirs. While letting the flow-evolve to its steady-state from the initial conditions provided by Stokes' flow, momentum was conserved exactly.

Chapter 7

Conclusions and Recommendations

7.1 General Remarks

Time reversibility. Exact reversibility in time is seen to exist for the time-integration scheme, as is shown in Figure 4-7. This symmetry would be extremely important for simulations that should conserve energy exactly (Euler's equations, for instance), and should be exploited in the future. Time reversibility is going to be presented in detail in [8].

Applicability of the mimetic spectral element method. In Chapter 4, the mimetic spectral element method is applied to a host of physical field problems and the results obtained comply with important conservation laws (mass conservation, for instance), and are seen to give an edge over conventional discretization methods (2D Maxwell resonant cavity example, Section 4.1). This is achieved with the help of the framework outlined in [7].

7.2 Conclusions

Bundle-valued differential-forms. The concept of bundle-valued differential-forms is included in the context of [7], and their implementation is discussed in Chapter 5. Since integration for these forms is not well defined, a duality pairing is done with vector-fields in order to be able to use the familiar operators discretized in Chapter 3 in a discrete setting. subsequently it is shown how this idea can be used to develop a novel approach towards conservation of momentum.

Momentum conservation. In a previous formulation of the Stokes' problem, [50], it was noticed that momentum was not being conserved exactly. This work shows how this can be done by treating momentum as a covector-valued volume-form. Although the formulation

is given specifically for two-dimensional space, it can be easily extended to three-dimensions because the action of all the operators used in this work is well-known in higher-dimensions. The association of momentum with volumes, in addition to the properties of the edge-basis functions, helps in conserving this quantity exactly in a discrete setting. Moreover, a general conservation law was also derived in Chapter 5 which could help conserve a large set of secondary variables in addition to momentum. This needs to be verified numerically.

7.3 Recommendations

Extension to curvilinear grids. It should be noted that the formulation presented for momentum in Section 5.3 may not be unique and is only a first attempt towards the *geometrization* of conservation of momentum. A future work should include the extension to curvilinear grids, and should make sure that the equations transform properly by making use of the exterior covariant-differential shown in Eq. (2-48).

Convection of volume-forms. It was noticed throughout this work that the convection of volume-forms, in its present formulation, is not well suited for multi-element meshes. This was also seen in Figure 6-15. This problem is present because of the discontinuous nature of edge-basis functions between elements that yields different fluxes from both sides of the common boundary between elements. Presently, an *ad hoc* weighted-average is being done to calculate the common flux and in the future this could be handled differently, using [53] for instance, to see if better results are obtained.

Implementation of generalized-momentum conservation. Energy conservation is extremely important with regards to maritime applications. As an example, there is quite some interest in real-time prediction of waves that would reach the observer based on observations made of waves in a distance. In the absence of energy conservation, such predictions would be of limited use. The numerical implementation of Eq. (5-40) should be done to this effect to see if energy conservation is possible. An extension to model free-surfaces, as well, would make such numerical experiments possible.

Bibliography

[1] E. Tonti and G. nazionale per la fisica matematica, *On the formal structure of physical theories*. Istituto de matematica, Politecnico, 1975.

[2] W. Burke, *Applied differential geometry*. 1985.

[3] C. Mattiussi, "The finite volume, finite element, and finite difference methods as numerical methods for physical field problems," *Advances in Imaging and electron physics*, 2000.

[4] A. Bossavit, "On the geometry of electromagnetism," *Journal of Japanese Society of Applied Electromagnetism and Mechanics*, 1998.

[5] P. Bochev and J. Hyman, "Principles of mimetic discretizations of differential operators," *Compatible spatial discretizations*, pp. 89–119, 2006.

[6] M. Desbrun and A. Hirani, "Discrete exterior calculus," *Arxiv preprint*, 2005.

[7] J. Kreeft, A. Palha, and M. Gerritsma, "Mimetic framework on curvilinear quadrilaterals of arbitrary order," p. 69, Nov. 2011.

[8] A. Palha, *In preparation*. PhD thesis, Delft University of Technology, 2012.

[9] O. Botella and R. Peyret, "Benchmark spectral results on the lid-driven cavity flow," *Computers & Fluids*, vol. 27, no. 4, pp. 421–433, 1998.

[10] J. Hanc, S. Tuleja, and M. Hancova, "Symmetries and conservation laws: Consequences of NoetherâĂŹs theorem," *American Journal of Physics*, vol. 72, no. 4, p. 428, 2004.

[11] I. Newton, "The Principia," 1995.

[12] J. Maxwell, "Remarks on the mathematical classification of physical quantities," *Proceedings of the London Mathematical Society*, 1871.

[13] R. Feynman, "Lecture notes in physics," *Vol*, vol. 3, pp. 1–1, 1964.

[14] E. Tonti, "A classification diagram for physical variables," 2003.

[15] C. Mattiussi, "A reference discretization strategy for the numerical solution of physical field problems," *Advances in imaging and electron physics*, 2002.

[16] T. Frankel, *The geometry of physics: an introduction*. 2011.

[17] J. Perot, "Discrete conservation properties of unstructured mesh schemes," *Annual Review of Fluid Mechanics*, 2011.

[18] M. Desbrun, "Discrete differential forms for computational modeling," *Discrete differential geometry*, 2008.

[19] A. Hirani, "Discrete exterior calculus," 2003.

[20] S. Elcott, Y. Tong, E. Kanso, P. Schröder, and M. Desbrun, "Stable, circulation-preserving, simplicial fluids," *ACM Transactions on Graphics (TOG)*, vol. 26, no. 1, p. 4, 2007.

[21] P. Mullen, A. McKenzie, and D. Pavlov, "Discrete Lie Advection of Differential Forms," *Arxiv preprint*, 2009.

[22] D. Pavlov, P. Mullen, and Y. Tong, "Structure-preserving discretization of incompressible fluids," *Arxiv preprint*, 2009.

[23] E. Kanso, M. Arroyo, and Y. Tong, "On the geometric character of stress in continuum mechanics," *Mathematik und Physik*, 2007.

[24] A. Yavari, "On geometric discretization of elasticity," *Journal of Mathematical Physics*, 2008.

[25] D. Arnold, "Finite element exterior calculus, homological techniques, and applications," *Acta numerica*, 2006.

[26] A. Gillette and M. Holst, "Finite Element Exterior Calculus for Evolution Problems," p. 24, Feb. 2012.

[27] A. N. Hirani, K. B. Nakshatrala, and J. H. Chaudhry, "Numerical method for Darcy flow derived using Discrete Exterior Calculus," *Arxiv preprint arXiv:0810.3434*, 2008.

[28] J. Perot and V. Subramanian, "Discrete calculus methods for diffusion," *Journal of Computational Physics*, vol. 224, no. 1, pp. 59–81, 2007.

[29] M. Gerritsma, "Edge functions for spectral element methods," *Spectral and High Order Methods for Partial Differential Equations*, 2011.

[30] M. Gerritsma, "An Introduction to a Compatible Spectral Discretization Method," *Mechanics of Advanced Materials and Structures*, 2012.

[31] G. Oud, "Discrete Differential Geometry," 2011.

[32] J. Kreeft, A. Palha, and M. Gerritsma, "Mimetic Spectral Element Method For Generalized Convection-Diffusion Problems." 2010.

[33] G. Oud, "Discrete Differential Geometry," Master's thesis, Delft University of Technology, 2011.

[34] J. Kreeft, *In preparation.* PhD thesis, Delft University of Technology, 2012.

[35] R. Hiemstra, "Isogeometric Mimetic Methods," Master's thesis, Delft University of Technology, 2011.

[36] P. Rebelo, "Physically accurate advection with the discrete representation of the Lie derivative," Master's thesis, Delft University of Technology, 2011.

[37] P. Kuystermans, "Mimetic Mesh Refinement," Master's thesis, Delft University of Technology, 2012.

[38] R. Darling, *Differential forms and connections.* 1994.

[39] H. Flanders, "Differential forms," 1963.

[40] D. Holm, *Geometric mechanics: Dynamics and symmetry.* 2008.

[41] M. Labbi, "Double forms, curvature structures and the (p, q)-curvatures," *Transactions of the American Mathematical Society*, 2005.

[42] R. Kulkarni, "On the Bianchi identities," *Mathematische Annalen*, 1972.

[43] N. Robidoux, "Polynomial histopolation, superconvergent degrees of freedom, and pseudospectral discrete hodge operators,"

[44] R. Hiemstra, R. Huijsmans, and M. Gerritsma, "Compatible Nurbs," 2012.

[45] J. Kreeft, A. Palha, and M. Gerritsma, "Mimetic Spectral Element Method for elliptic problems," 2010.

[46] D. Boffi, "Finite element approximation of eigenvalue problems," *Acta Numerica*, vol. 19, no. 1, pp. 1–120, 2010.

[47] T. J. R. Hughes, A. Masud, and J. Wan, "A stabilized mixed discontinuous Galerkin method for Darcy flow," *Computer Methods in Applied Mechanics and Engineering*, vol. 195, no. 25-28, pp. 3347–3381, 2006.

[48] A. Palha, P. Rebelo, J. Kreeft, and M. Gerritsma, "Physically accurate advection with the discrete representation of the Lie derivative," 2011.

[49] J. Anderson, *Fundamentals of aerodynamics.* 2001.

[50] J. Kreeft and M. Gerritsma, "Mixed Mimetic Spectral Element Method for Stokes Flow: A Pointwise Divergence-Free Solution," Jan. 2012.

[51] A. Bossavit, "Force-related nuts and bolts in the discretization toolkit for electromagnetics," *Magnetics, IEEE Transactions on*, 2008.

[52] J. Shen, "Hopf bifurcation of the unsteady regularized driven cavity flow," *Journal of Computational Physics*, 1991.

[53] P. Castonguay, P. E. Vincent, and A. Jameson, "A New Class of High-Order Energy Stable Flux Reconstruction Schemes for Triangular Elements," *Journal of Scientific Computing*, vol. 51, pp. 224–256, June 2011.